50 2/6 a Distr Formal

No Stock

GEAP-10066
AEC RESEARCH AND
DEVELOPMENT REPORT
JULY 1969

MASTER

MECHANICAL PROPERTIES EVALUATION OF AUSTENITIC STAINLESS STEELS IRRADIATED IN EBR-II

T. LAURITZEN
A. WITHOP
G.P. FERGUSON

U.S. ATOMIC ENERGY COMMISSION
CONTRACT AT(04-3)-189
PROJECT AGREEMENT 10

P4161

BREEDER REACTOR DEVELOPMENT OPERATION
GENERAL ELECTRIC
SUNNYVALE, CALIFORNIA

GEAP-10066
AEC Research and
Development Report
July 1969

MECHANICAL PROPERTIES EVALUATION OF AUSTENITIC STAINLESS STEELS IRRADIATED IN EBR-II

T. Lauritzen
A. Withop
G.P. Ferguson

Approved: E. L. Zebroski
E. L. Zebroski, Manager
Sodium Reactor Technology

Approved: W. E. Baily
W. E. Baily, Project Engineer
Fast Ceramic Reactor Development Program

Prepared for the
U. S. Atomic Energy Commission
Under Contract Number AT(04-3)-189
Project Agreement 10

Printed in U. S. A. Available from the
Clearing House for Federal Scientific and Technical Information
National Bureau of Standards, U. S. Department of Commerce
Springfield, Virginia
Price: $3.00 per copy

BREEDER REACTOR DEVELOPMENT OPERATION
GENERAL ELECTRIC
SUNNYVALE, CALIFORNIA

DISTRIBUTION OF THIS DOCUMENT IS UNLIMITED

LEGAL NOTICE

TABLE OF CONTENTS

LIST OF ILLUSTRATIONS

LIST OF ILLUSTRATIONS (Continued)

LIST OF ILLUSTRATIONS (Continued)

LIST OF ILLUSTRATIONS (Continued)

LIST OF TABLES

ABSTRACT

Tensile coupons of five austenitic materials (Types 304, 316, 321, 347 and Incoloy-800) prepared from thin-wall tubing were irradiated in EBR-II. The maximum accumulated neutron exposure was 3.4 × 10^{22} n/cm², total, at temperatures ranging from 1000 to 1300°F. The mechanical properties of the irradiated coupons were determined; the results are reported here. Post-irradiation mechanical testing included uniaxial tensile and burst (biaxial) tests at temperatures ranging from 900 to 1500°F. Light optical and electron metallography studies were conducted to characterize the mode of failure.

Heat treatment for Type-304 stainless steel to produce a "carbide agglomerated" state was found to promote increased residual ductilities after reactor exposure. This observation, which needs confirmation, is in contrast to larger reductions in ductility (measured by percent elongation) found for all five commercial austenitic alloys used in these experiments in the as-received or mill-annealed condition.

1. SUMMARY

This report describes the first phase of a comprehensive experimental program directed toward the characterization of the effects of irradiation on austenitic stainless steels. This work complements the irradiation testing of fuel pins in that it permits assessment of a greater number of variables—as well as isolation of some variables—than pin testing. The ultimate objective of this work is the selection of the most appropriate austenitic alloy for use in a sodium-cooled fast breeder reactor as cladding for mixed urania-plutonia fuel. Of particular importance in this application is the degradation in mechanical properties due to long-term exposure to high fast-neutron fluxes at elevated temperatures. The work discussed here was designed to establish the magnitude of damage incurred under these conditions.

Five austenitic alloys—Types 304, 316, 321, 347 and Incoloy-800—were irradiated as tubular and sheet tensile specimens in EBR-II. Two microstructures were investigated: Annealed (pre-irradiation microstructure free of intergranular carbides), and carbide-agglomerated (pre-irradiation microstructure consisting of large discrete intergranular carbides). The capsules containing these specimens accumulated maximum fluences ranging from 1.7 to 3.4 × 10^{22} n/cm² (E_{Total}) at temperatures as high as 1300°F. Post-irradiation examination of these specimens included metallography to establish the effect of irradiation on alloy microstructure, and uniaxial and biaxial mechanical properties tests to assess the magnitude of damage.

Tensile test results showed that, within the neutron fluence range investigated, all annealed materials exhibited decreases in total strain with increasing fluence and decreasing strain rate. For Types 304 and 316L, total strains recorded were in the range of 3.6 to 7.7%, while those for Types 321, 347, and Incoloy-800 were 1.0 to 5.8%. Total strain values for all unirradiated materials in the annealed condition were 30 to 44% at 1300°F. In the carbide agglomerated condition, Type-304 stainless steel exhibits an increase in fracture strain. Although this observation is encouraging, it needs further confirmation before it acquires enough significance to be considered in the selection of an appropriate fuel cladding.

Significant increases in yield strength were noted for all materials with the strengthening effect increasing with fluence, except for Incoloy-800 which remains relatively constant. The degree of strengthening decreased with test temperature, with recovery occurring at 1500 to 1600°F for all alloys.

Elevated temperature bursting of tubular specimens revealed substantial increases in burst strength and reductions in circumferential ductility with irradiation. At a test temperature of 1300°F, the core and blanket specimens exhibited increases in burst strength to 40% and 17%, respectively, relative to unirradiated annealed specimens. This disparity diminishes with increasing test temperature, and indicates complete recovery at approximately 1600°F.

The effects of carbide morphology and distribution on the embrittlement of Type 304 during irradiation was also investigated. In the annealed (unirradiated) condition, the alloy was free of grain-boundary carbides, but exhibited a continuous grain-boundary precipitation after irradiation. In the carbide-agglomerated condition, the microstructure consisted of large, discrete intergranular carbides both before and after irradiation. Post-irradiation results at 1300°F indicate that specimens in both structural conditions were embrittled; however, the carbide-agglomerated material showed a lower degree of embrittlement.

2. CONCLUSIONS

Specimens of five austenitic alloys (304, 316, 321, 347, and Incoloy-800) were irradiated in EBR-II to accumulated fluences of up to 3.4×10^{22} n/cm^2 (total) and peak temperatures as high as 1300°F. Post-irradiation examination of both strip tensile and tubular specimens yielded the following results:

a. Embrittlements ranging from 70 to 98%, as monitored by reduction in total tensile strain, were measured on all alloys investigated.

b. Intergranular carbides of the morphology and distribution found in carbide-agglomerated materials caused an increase in total tensile elongation of irradiated Type-304 stainless steel. (This observation, however, requires further confirmation before carbide agglomeration can be considered as a specification for LMFBR cladding.)

c. Except for Incoloy-800, all alloys tested after irradiation exhibited increases in yield strength. The degree of strengthening was reduced by post-irradiation annealing, with full recovery occurring between 1500 and 1600°F. However, most of the embrittlement remained.

d. The yield strengths of all irradiated alloys were observed to vary with the strain rate used in tensile testing. A reduction in strain rate caused a corresponding reduction in yield.

3. INTRODUCTION

Current fuel cladding designs for a Liquid Metal Fast Breeder Reactor (LMFBR) call for cladding to operate with (a) fast-neutron fluxes near 10^{16} n/cm^2-sec, (b) total fluences over 10^{23} n/cm^2, (c) peak cladding temperatures up to 1300°F, (d) a variety of stress systems arising from fuel swelling, clad swelling, fission-gas pressure, thermal gradients, and power and temperature cycling, and (e) close contact with fuel and flowing sodium.

Thus far, the austenitic stainless steels are considered to be the most promising cladding materials for the first generation of LMFBR's. Those alloys receiving attention in this program are Type 304, Type 316, Type 321, Type 347, and Incoloy-800. The objective of this report is to describe the irradiation history and the post-irradiation mechanical and physical properties of these alloys, exposed as tensile specimens in the Experimental Breeder Reactor No. II (EBR-II).

4. EXPERIMENTAL PROCEDURE

4.1 MATERIALS

These experiments comprised three subassemblies irradiated in EBR-II. A total of 12 materials capsules were incorporated into these subassemblies. Series L-2′ contained five capsules, one each of five commercial alloys of austenitic stainless steel: Types 304, 316L, 321, 347, and Incoloy-800. Type 316 was used exclusively in the two capsules of series L-4. The five materials capsules irradiated in series L-4′ were fabricated from Incoloy-800 (2 capsules), and Types 304, 321, and 347 (one capsule of each). All alloys were purchased as welded and drawn tubing. The chemical compositions of the six alloys used in this investigation are listed in Table 4-1.

The test section material was irradiated in two configurations: thin-wall tubing and thin-sheet tensile coupons. Two structural conditions were studied: mill annealed and carbide agglomerated. The mill-annealed structure is defined as the as-received condition; the carbide-agglomerated structure was developed by heat-treating as-received material at 1650°F for 24 hours in a helium atmosphere. The heat-treatment schedule for tensile coupons is shown in Figure 4-1. Tensile coupons were fabricated from flattened tubing and stamped out to conform to the dimensions shown in Figure 4-2. Microstructure of the materials prior to irradiation are shown in Figures 4-3 through 4-12. Transverse sections of tubular samples and longitudinal sections of tensile coupons were selected to show the material structure in the direction corresponding to the direction of principal stress during subsequent mechanical testing.

Type 304 microstructures are seen in Figures 4-3 (mill-annealed) and 4-4 (carbide-agglomerated). The grain size is ASTM 7 to 8. Slight grain growth occurred in the tensile coupon, resulting from the 1800°F anneal given to the coupon after flattening and stamping.

The mill-annealed Type 316L (Figure 4-5) has a grain size of ASTM 7; the grain size in the weld region is somewhat finer (not fully recrystallized). A duplex grain

TABLE 4-1
CHEMICAL COMPOSITION OF TEST MATERIALS

Alloy	Heat No.	Ni	Cr	Fe	C	Mn	Si	Cu	Mo	P	S	B*	N*	Other
Type 304	125653	9.15	18.42	Balance	0.06	1.55	0.41	0.27	0.50	0.025	0.010	16	540	
Type 316	850145	13.16	17.63	Balance	0.04	1.90	0.52	0.16	2.81	0.021	0.006	7.8	630	
Type 316L	133310	13.31	17.39	Balance	0.02	1.80	0.66	0.07	2.20	0.017	0.008	9.5	500	
Type 321	800738	9.53	17.13	Balance	0.05	1.35	0.64	0.16	0.29	0.019	0.011	18.5	110	0.53 Ti
Type 347	99973	9.32	18.20	Balance	0.05	1.16	0.72	0.20	0.14	0.023	0.009	12.0	560	0.91 Cb+Ta
Incoloy-800	4167	32.00	20.44	46.09	0.05	0.99	0.25	0.33	N.D.	N.D.	0.007	12	930	0.51 Ti+0.40 Al

* Impurities in ppm.

TABLE 4-2
IN-PILE STRESS PARAMETERS AT 1200°F

Test Material	In-Pile Stress Level (psi)
Type 304	8,000
Type 316L	9,000
Type 316	13,000
Type 321	10,000
Type 347	12,000
Incoloy-800	12,000

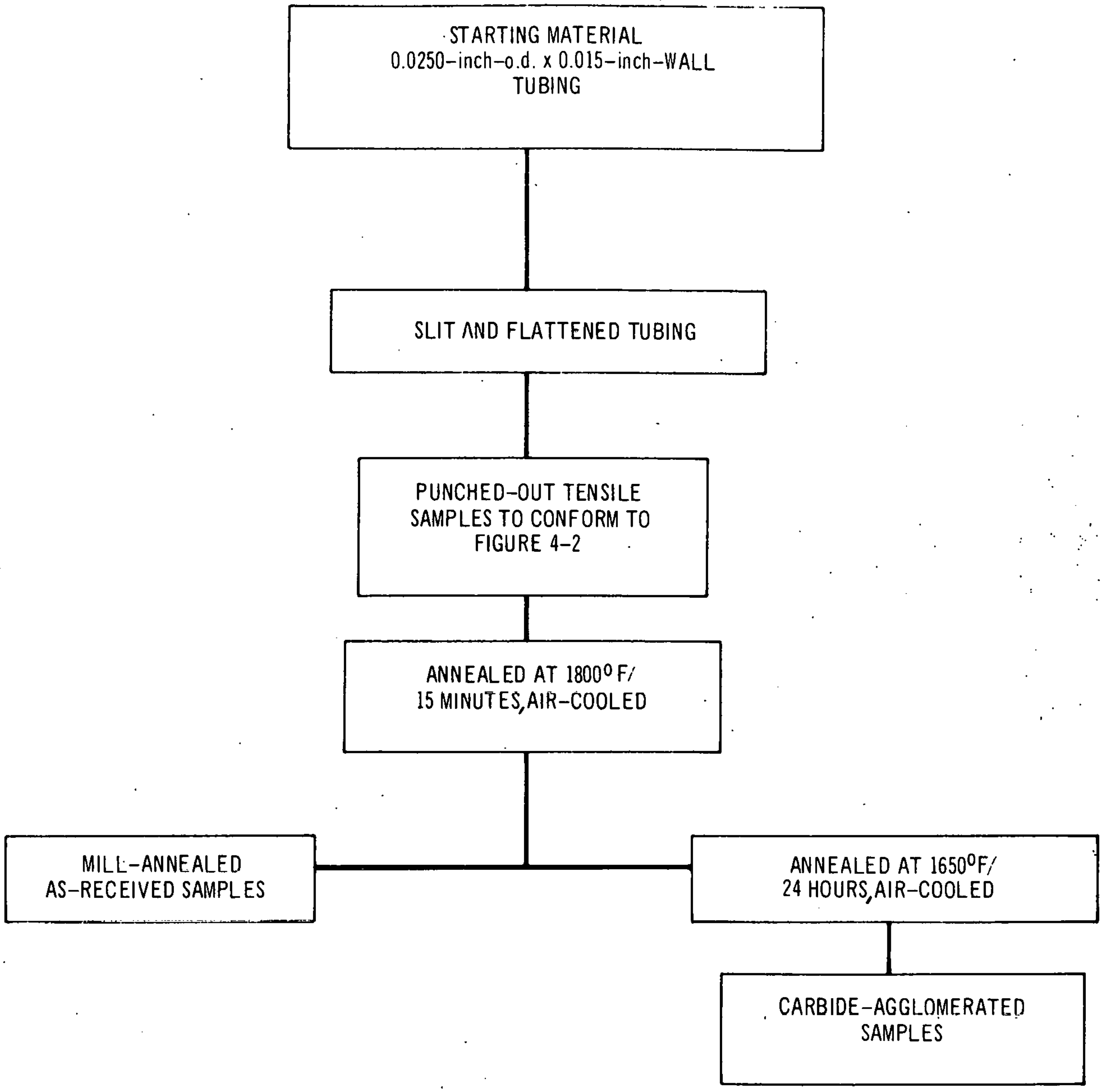

Figure 4-1. Flow Diagram for Fabrication of Tensile Samples from Commercial Tube

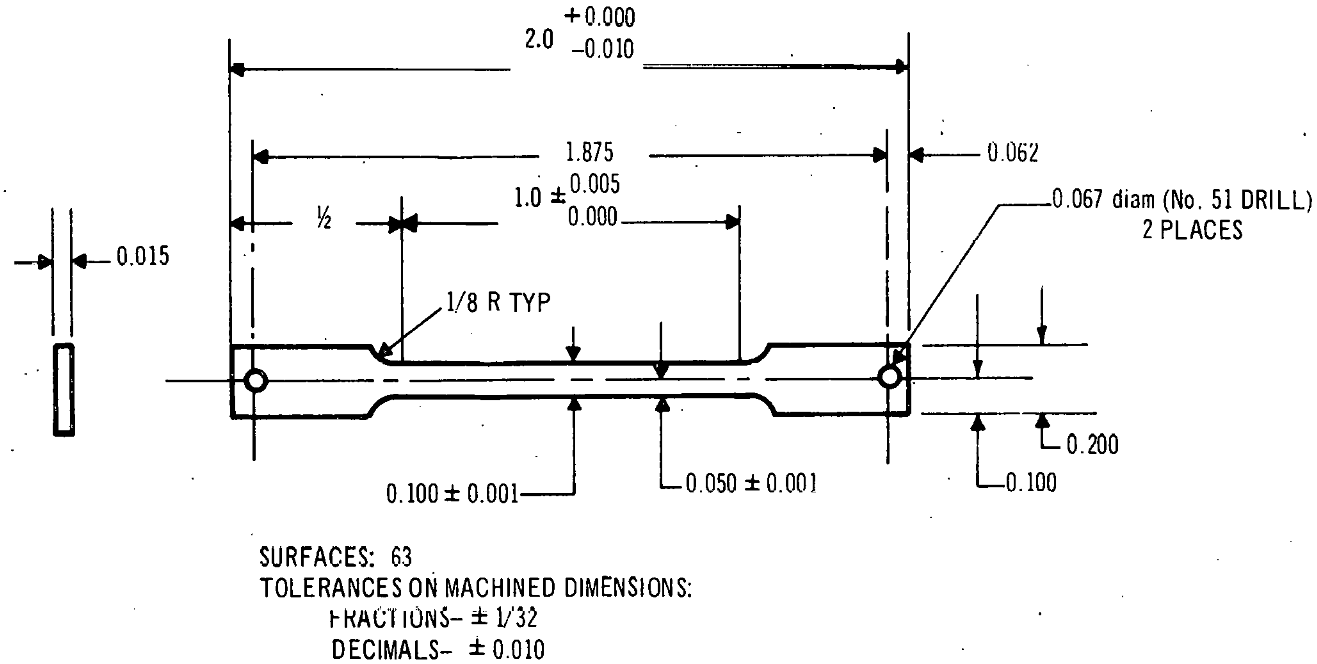

Figure 4-2. Tensile Coupon

TUBULAR COUPON

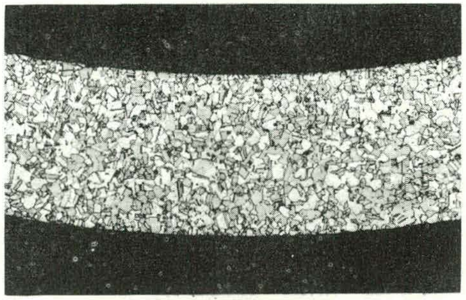

SECTION: TRANSVERSE
MAGNIFICATION: 100X
ATSM GRAIN SIZE NO. 7

TUBULAR COUPON

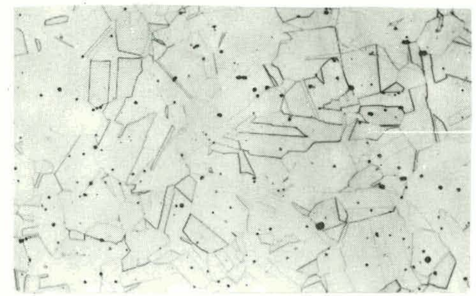

SECTION: TRANSVERSE
MAGNIFICATION: 500X

TUBULAR COUPON
WELD ZONE

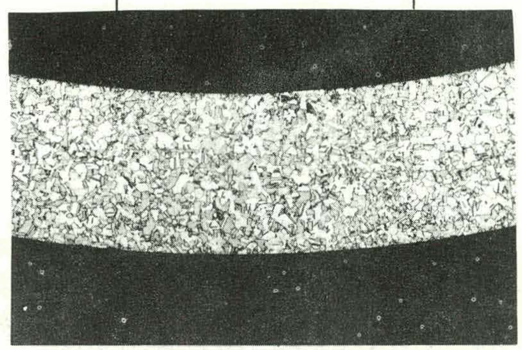

SECTION: TRANSVERSE-WELD AREA
MAGNIFICATION: 100X

TENSILE COUPON

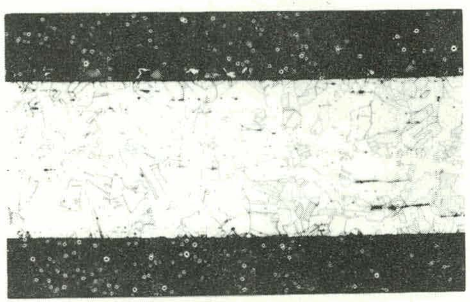

SECTION: LONGITUDINAL
MAGNIFICATION: 100X
ATSM GRAIN SIZE NO. 6

TENSILE COUPON

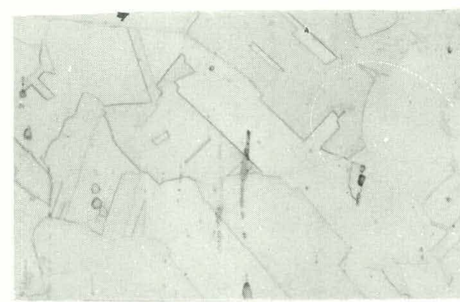

SECTION: LONGITUDINAL
MAGNIFICATION: 500X

Figure 4-3. Microstructure of Type-304 Stainless Steel, Mill Annealed. Etchant: HCl + H_2O_2 (Reduced to ~ 75% for reproduction purposes)

TUBULAR COUPON

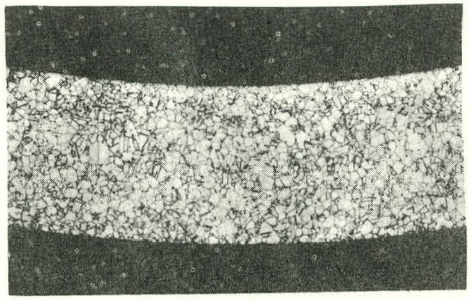

SECTION: TRANSVERSE
MAGNIFICATION: 100X
ASTSM GRAIN SIZE NO. 8

TENSILE COUPON

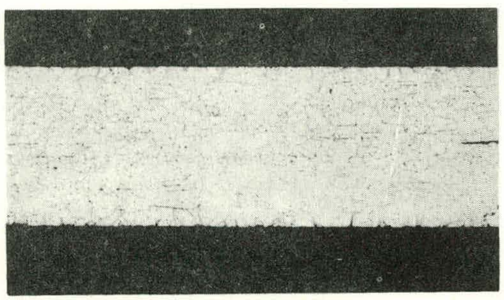

SECTION: LONGITUDINAL
MAGNIFICATION: 100X
ATSM GRAIN SIZE NO. 7

TUBULAR COUPON
WELD ZONE

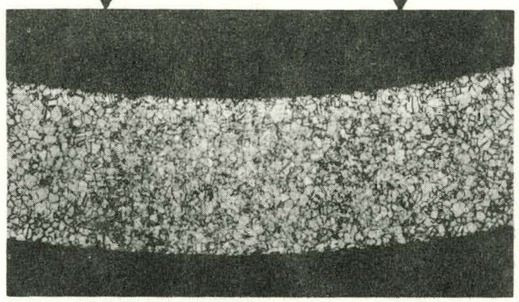

SECTION: TRANSVERSE-WELD AREA
MAGNIFICATION: 100X

TUBULAR COUPON

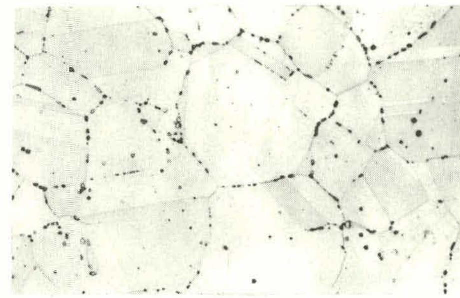

SECTION: TRANSVERSE
MAGNIFICATION: 500X

TENSILE COUPON

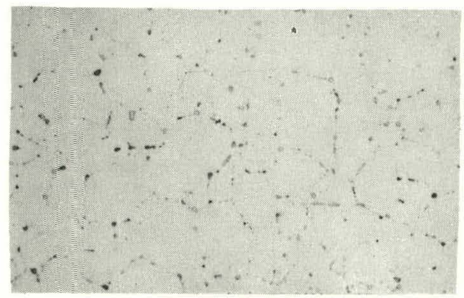

SECTION: LONGITUDINAL
MAGNIFICATION: 500X

Figure 4-4. Microstructure of Type-304 Stainless Steel, Carbide Agglomerated. Etchant: Modified Glyceregia (Reduced to ~ 75% for reproduction purposes)

TUBULAR COUPON

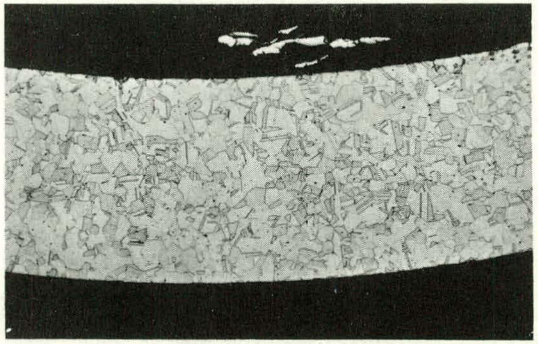

SECTION: TRANSVERSE
MAGNIFICATION: 100X
ATSM GRAIN SIZE No. 7

TENSILE COUPON

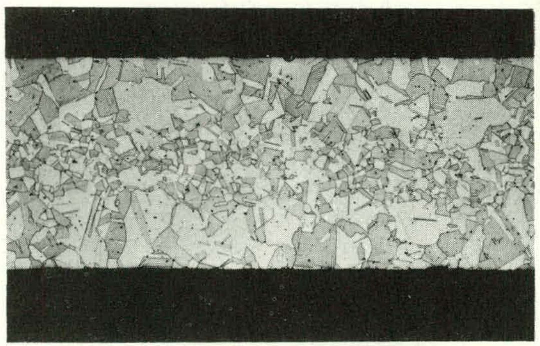

SECTION: LONGITUDINAL
MAGNIFICATION: 100X

DUPLEX GRAIN SIZE

TUBULAR COUPON
WELD ZONE

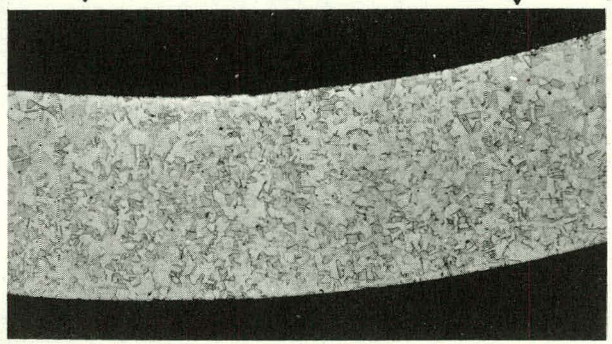

SECTION: TRANSVERSE–WELD AREA
MAGNIFICATION: 100X

TUBULAR COUPON

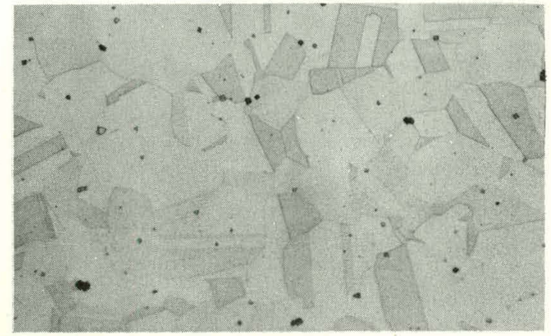

SECTION: TRANSVERSE
MAGNIFICATION: 500X

TENSILE COUPON

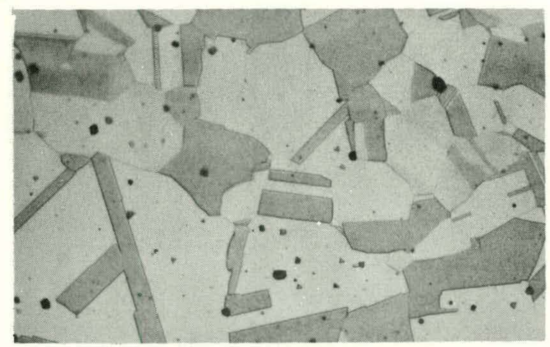

SECTION: LONGITUDINAL
MAGNIFICATION: 500X

Figure 4-5. Microstructure of Type-316L Stainless Steel, Mill Annealed. Etchant: $HCl + H_2O_2$ (Reduced to ~ 75% for reproduction purposes)

TUBULAR COUPON

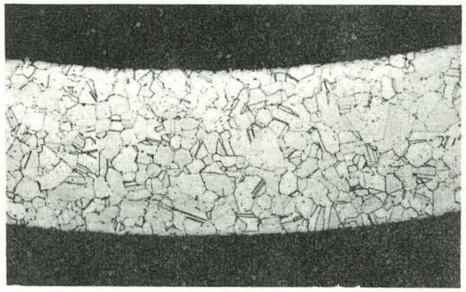

SECTION: TRANSVERSE
MAGNIFICATION: 100X
ATSM GRAIN SIZE NO. 6

TENSILE COUPON

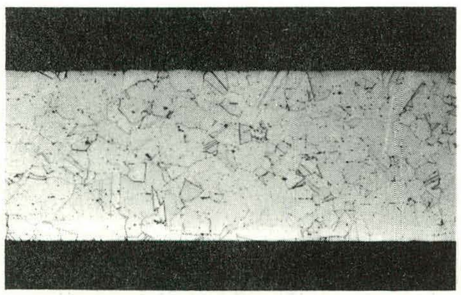

SECTION: LONGITUDINAL
MAGNIFICATION: 100X
ATSM GRAIN SIZE NO. 6

TUBULAR COUPON

WELD ZONE

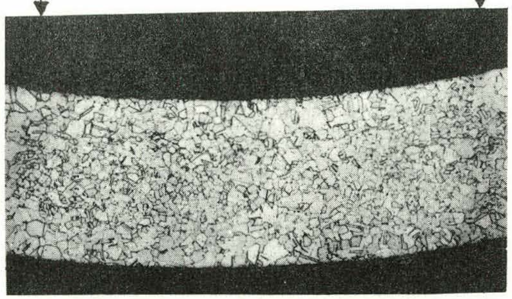

SECTION: TRANSVERSE-WELD AREA
MAGNIFICATION: 100X

TUBULAR COUPON

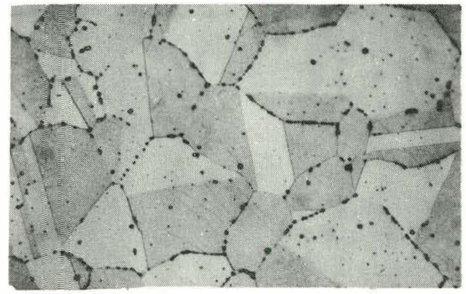

SECTION: TRANSVERSE
MAGNIFICATION: 500X

TENSILE COUPON

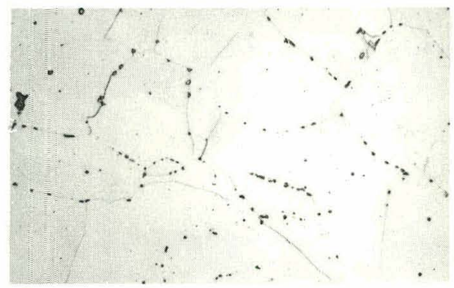

SECTION: LONGITUDINAL
MAGNIFICATION: 500X

Figure 4-6. Microstructure of Type-316 Stainless Steel, Carbide Agglomerated. Etchant: Modified Glyceregia (Reduced to ~ 75% for reproduction purposes)

TUBULAR COUPON

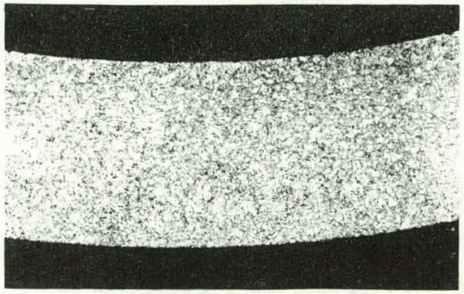

SECTION: TRANSVERSE
MAGNIFICATION: 100X
ATSM GRAIN SIZE NO. 10

TENSILE COUPON

WELD ZONE

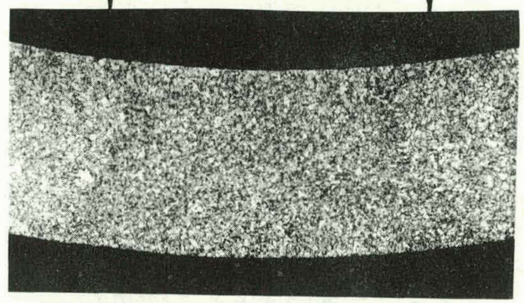

SECTION: TRANSVERSE-WELD AREA
MAGNIFICATION: 100X

TUBULAR COUPON

SECTION: TRANSVERSE
MAGNIFICATION: 500X

TENSILE COUPON

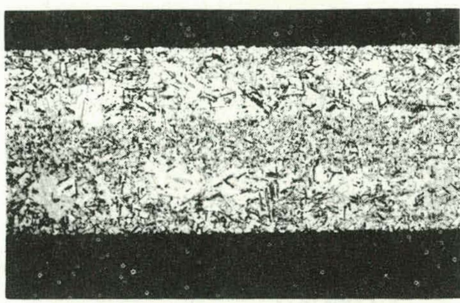

DUPLEX GRAIN SIZE

SECTION: LONGITUDINAL
MAGNIFICATION: 100X

TENSILE COUPON

SECTION: LONGITUDINAL
MAGNIFICATION: 500X

Figure 4-7. Microstructure of Type-321 Stainless Steel, Mill Annealed. Etchant: HCl + H_2O_2 (Reduced to ~ 75% for reproduction purposes)

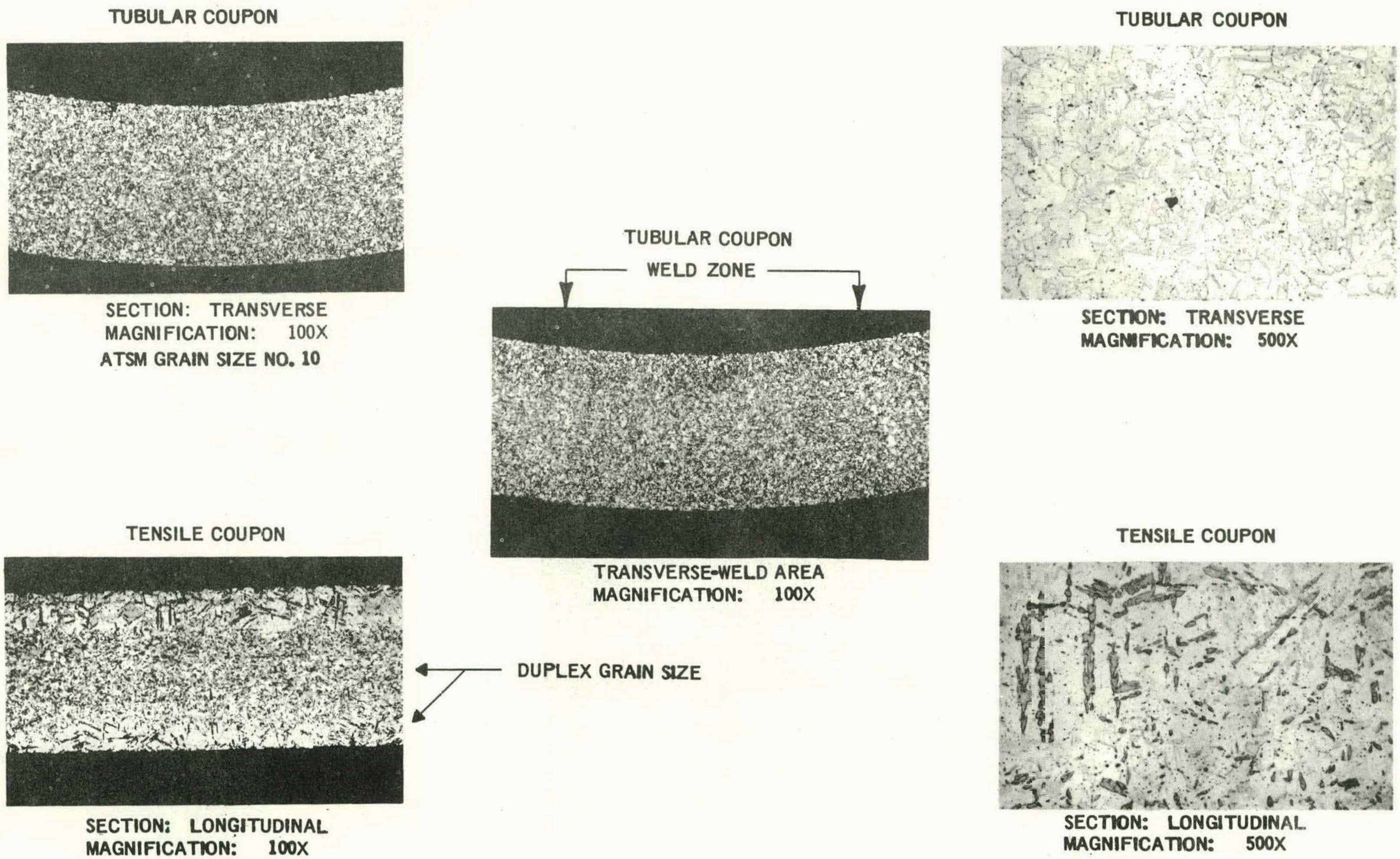

Figure 4-8. Microstructure of Type-321 Stainless Steel, Carbide Agglomerated. Etchant: Modified Glyceregia (Reduced to ~ 75% for reproduction purposes)

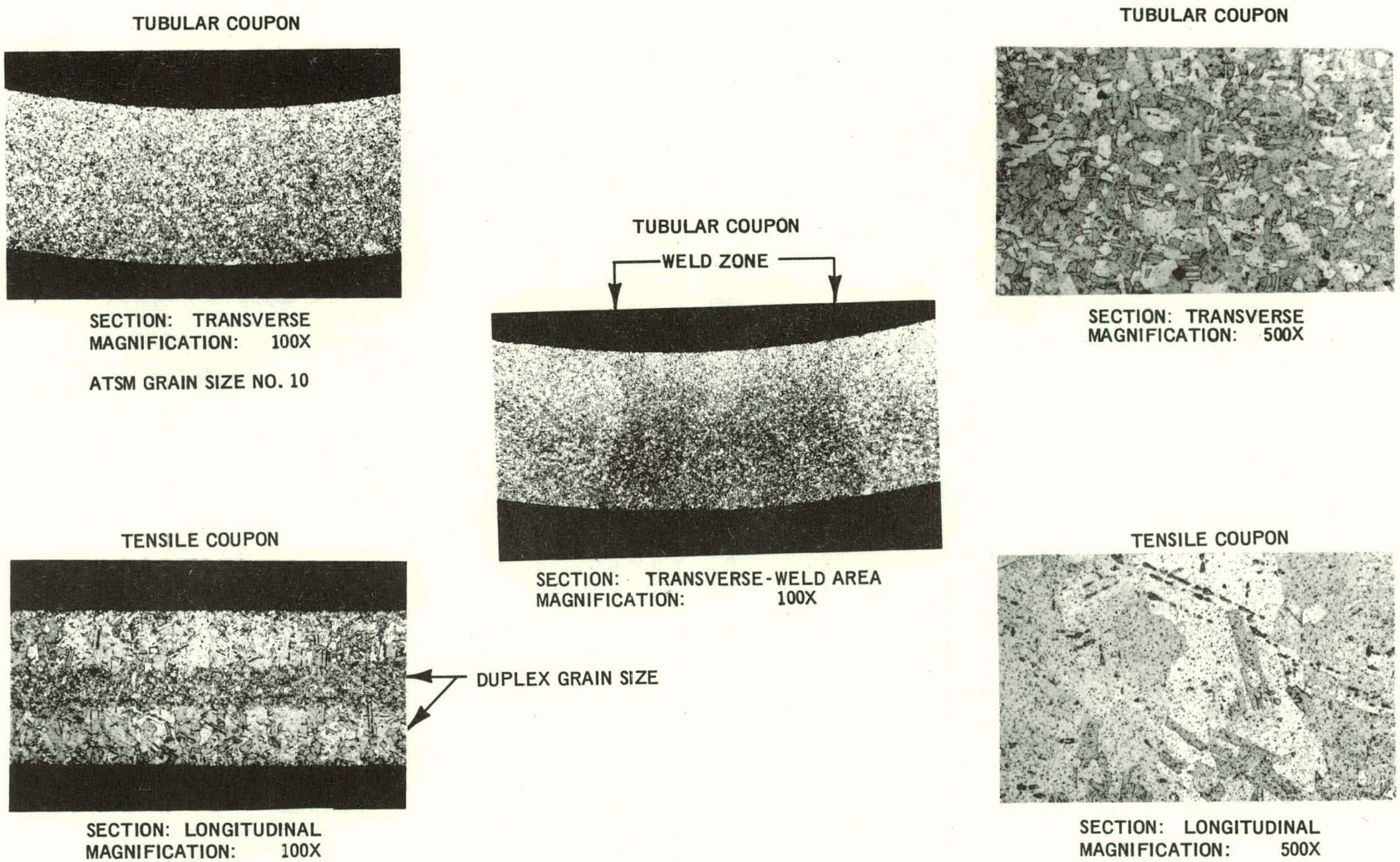

Figure 4-9. Microstructure of Type-347 Stainless Steel, Mill Annealed. Etchant: HCl + H_2O_2 (Reduced to ~ 75% for reproduction purposes)

TUBULAR COUPON

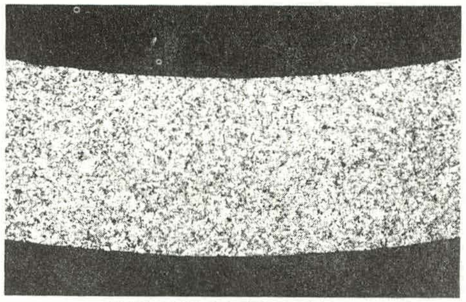

SECTION: TRANSVERSE
MAGNIFICATION: 100X

ATSM GRAIN SIZE NO. 10

TUBULAR COUPON
WELD ZONE

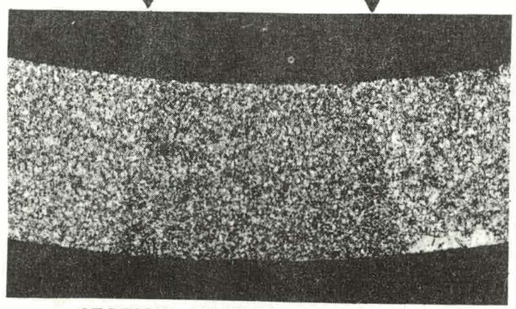

SECTION: TRANSVERSE—WELD AREA
MAGNIFICATION: 100X

TUBULAR COUPON

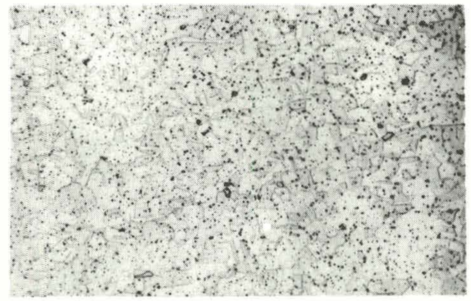

SECTION: TRANSVERSE
MAGNIFICATION: 500X

TENSILE COUPON

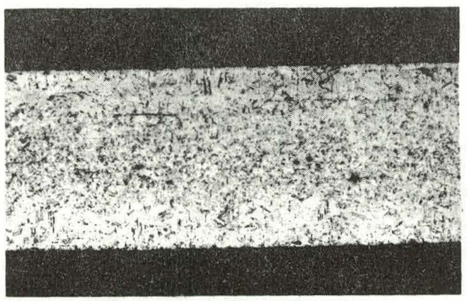

DUPLEX GRAIN SIZE

SECTION: LONGITUDINAL
MAGNIFICATION: 100X

TENSILE COUPON

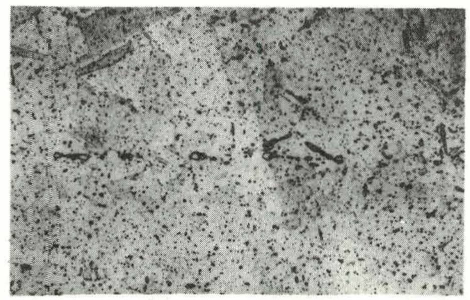

SECTION: LONGITUDINAL
MAGNIFICATION: 500X

Figure 4-10. Microstructure of Type-347 Stainless Steel, Carbide Agglomerated. Etchant: Modified Glyceregia (Reduced to ~ 75% for reproduction purposes)

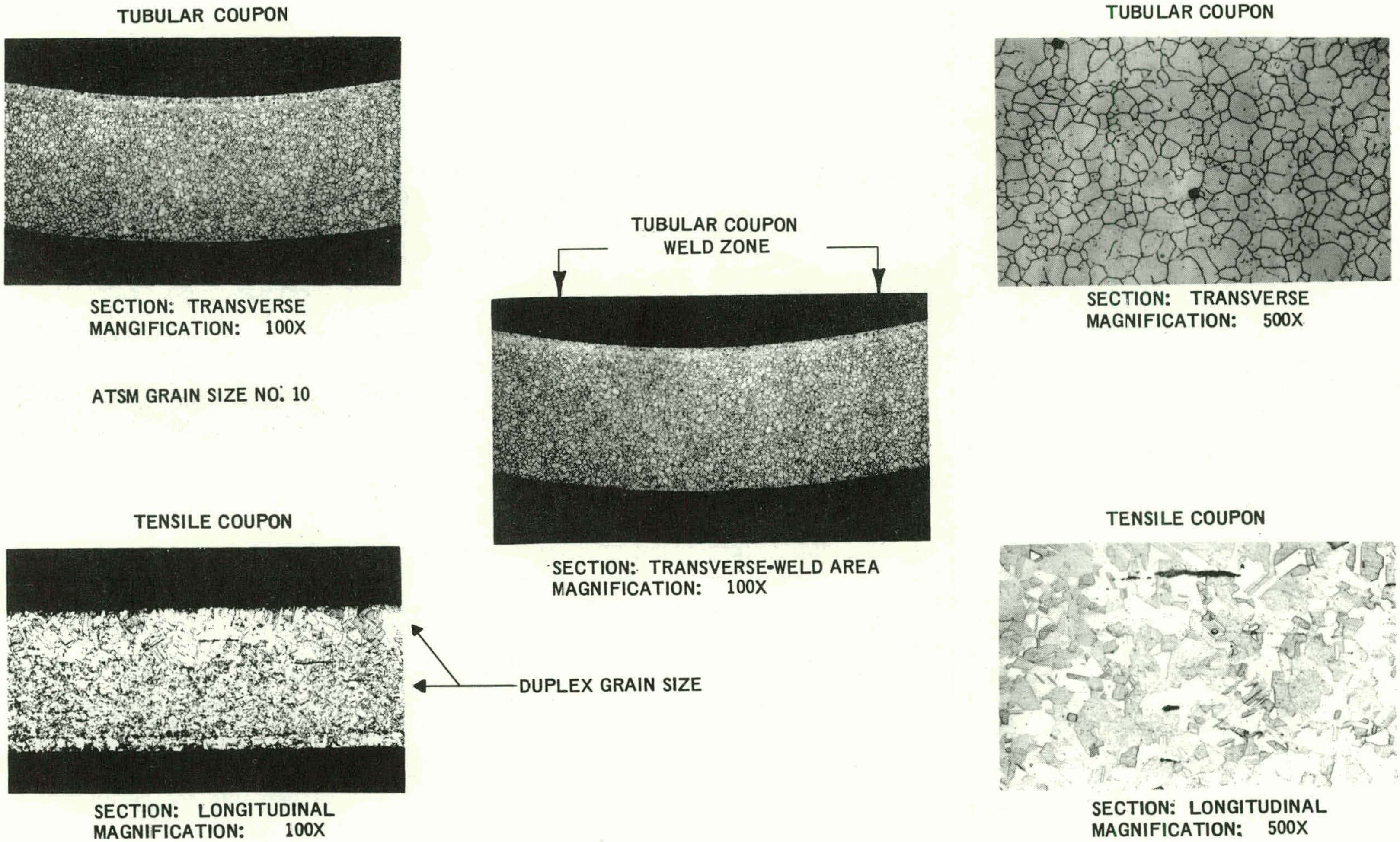

Figure 4-11. Microstructure of Incoloy-800, Mill Annealed. Etchant: 10% Oxalic Acid–Tubular Coupon, HCl + H_2O_2, Tensile Coupon (Reduced to ~ 75% for reproduction purposes)

TUBULAR COUPON

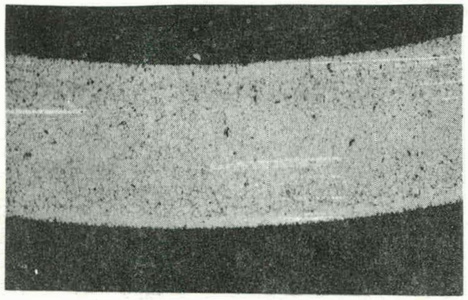

SECTION: TRANSVERSE
MAGNIFICATION: 100X
ATSM GRAIN SIZE NO.9

TUBULAR COUPON

SECTION: TRANSVERSE
MAGNIFICATION: 500X

NOTE: WELD WAS FULLY RECRYSTALLIZED; THUS, NO SEAM-WELD COULD BE LOCATED.

TENSILE COUPON

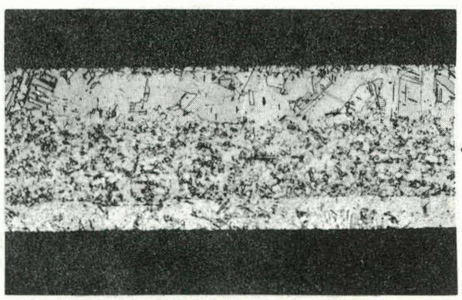

DUPLEX GRAIN SIZE

SECTION: LONGITUDINAL
MAGNIFICATION: 100X

TENSILE COUPON

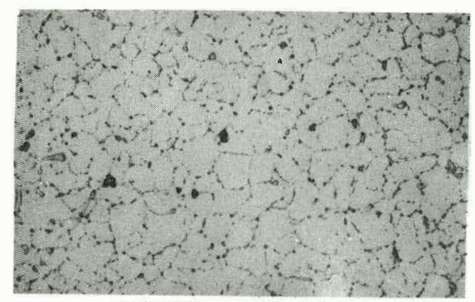

SECTION: LONGITUDINAL
MAGNIFICATION: 500X

Figure 4-12. Microstructure of Incoloy-800, Carbide Agglomerated. Etchant: 10% Oxalic Acid (Reduced to ~ 75% for reproduction purposes) structure is apparent in the tensile coupon section. This structure also appears in tensile coupons of Types 321 (Figure 4-7 and 4-8), 347 (Figures 4-9 and 4-10), and Incoloy-800 (Figures 4-11 and 4-12). Consistently large grains are at the outer surfaces, with a fine-grain structure near the centroid. The outer and inner fibers are regions of maximum strain (during the flattening and stamping operation), and the middle region is one of minimum deformation. It is possible, therefore, that the 1800°F anneal caused recrystallization and grain growth to occur at the regions of maximum strain. The center region was unaffected because of the lack of appreciable cold work.

The carbide-agglomerated Type 316 is shown in Figure 4-6. The structure is similar to mill-annealed Type 316L, except that carbide precipitation is now evident at grain boundaries in discrete locations—somewhat comparable to the carbide-agglomerated Type 304.

A very fine grain size (ASTM 10) was observed in both structural conditions of Type 321 (Figures 4-7 and 4-8), and the weld region was fully recrystallized. Type 347, in both the mill-annealed (Figure 4-9) and carbide-agglomerated (Figure 4-10) structures, was nearly identical in grain size to Type 321. The weld area in Type 347, however, was not fully recrystallized. Types 321 and 347 did not respond to the carbide-agglomeration heat-treatment to the extent shown by Types 304 and 316. In these specimens, stabilized carbides were uniformly distributed throughout the structure.

Mill-annealed Incoloy-800 (Figure 4-11) has a grain size of ASTM 10, and the carbide-agglomerated structure (Figure 4-12) is about ASTM 9. The weld region was not easily observed in the mill-annealed material and could not be located in the material which was heat-treated for agglomeration of carbides. That this heat treatment was partially successful in forming discrete intergranular carbides is illustrated in Figure 4-12, but continuous grain-boundary precipitates are also in evidence.

4.2 IRRADIATION CAPSULE

The capsule configuration used in all three subassemblies consisted of several tubular test sections axially strung together in a "piggy-back" fashion. Series L-2′ (Figures 4-13 through 4-15) contained three test sections per capsule; series L-4 and L-4′ each had five (Figures 4-16 through 4-18). The test section consisted of a 0.250-inch-o.d. by 0.220-inch-i.d. tube which encased several tensile coupons, a tungsten holder for gamma heating, a thermometer capsule containing fusible metal rods to provide indications of temperature of irradiation, and sodium to promote axial and radial heat transfer from the tungsten to the tubular test section.

By balancing the heat generated by gamma heating of all metal components in the capsule with the heat loss across an argon-filled annulus, the capsule was designed to operate at 1200°F. Since no external instrumentation was possible on these capsules, approximate indications of temperatures attained were provided by fusible metal thermometry. This technique is based on the judicious selection of metals or alloys with well-established melting points in the temperature range of interest. Meltdown of the alloys is then observed by radiography or, when recovery of the thermometer is possible, by direct observation.

Internal pressure at temperature was provided as follows: The assembled test sections and sodium reservoir were flushed with helium prior to sodium filling, to purge the system of air. Liquid sodium was then allowed to fill the test sections from the capsule bottom to a set level in the sodium reservoir, and then solidified. The level of solid sodium in the reservoir was then measured with an eddy-current probe. The test coupon assembly was then filled with helium gas to a preselected pressure level associated with the measured sodium level. This initial pressure is designed to increase to a higher pressure level during reactor operation due to the temperature increase and volume decrease of the gas (caused by the expanding sodium). This higher pressure level was selected to produce a hoop stress in the tubular test section of approximately 80% of the reported 10,000-hour stress-rupture value at 1200°F. These target stress levels are listed in Table 4-2.

4.3 HISTORY OF IRRADIATION

4.3.1 EBR-II History

Capsule series L-2′ was loaded into EBR-II (S/A XG06) on September 3, 1965, and removed on February 20, 1967. During its residence in the reactor (Runs 9 through 24), the subassembly occupied position 4E2 (Row 4) and accumulated 9317 megawatt days (MWD). This corresponds to a fluence (based on reactor physics calculations)* of 3.4×10^{22} n/cm², total, at the core midplane—approximately 207 effective full-power days (EFPD).

Series L-4 (S/A X009) was inserted into the core at the beginning of Run 15 (March 24, 1966), and was removed at the completion of Run 22 (November 14, 1966). The subassembly occupied position 4A2 (Row 4) for 119 EFPD and reached an exposure of 5355 MWD or 1.9×10^{22} n/cm², total.

A Row-2 core position (2D1) was used to irradiate series L-4′ (S/A X014). Loaded on July 17, 1966, and removed on April 10, 1967, the L-4′ capsules were exposed in the reactor for Runs 20 to 24. The total neutron fluence was 1.7×10^{22} n/cm² (3674 MWD) at 82 EFPD.

* The accumulated exposure based on reactor physics calculations is reported on a quarterly basis in the EBR-II Operations Report; also is mentioned in Reference 6 of this report.

The EBR-II grid loading pattern for these three experiments is shown in Figure 4-19. The location of each of the capsules within each subassembly is presented in Figures 4-20, 4-21, and 4-22 for series L-2′, L-4, and L-4′, respectively.

4.3.2 Dosimetry

Fast-neutron damage to austenitic stainless steels at elevated temperatures is thought to be associated with the production of helium gas and cavities (Ref. 1–4). Although mechanisms regarding the formation of cavities are still subject to question, it is generally agreed that they are the result of a combination of two discrete phenomena: gas producing neutronic reactions [(n,α) reactions] with alloy constituents, and vacancy-producing displacement collisions.

Lattice displacements begin to occur at neutron energies around 10 keV (Ref. 5), and helium production is believed to have a threshold reaction at about 6 MeV. Thus, knowledge of the total flux, as well as the high-energy region of the neutron spectrum in an experimental fast reactor, is necessary in order to assess the degree of fast-neutron damage in austenitic stainless steels.

Materials irradiation experiments in the EBR-II have used flux wires as a means for determining the flux spectra during reactor exposure. In this experiment, the integrated fast-neutron exposure was monitored by the reaction Fe^{54} (n,p) Mn^{54}, which has a half-life of 303 days, and Ni^{58} (n,p) Co^{58} with a half-life of 71 days. The dosimetry results from the three-capsule series were reported previously (Ref. 6) and are summarized in Figure 4-23. Subassemblies XG06 (L-2′), X009 (L-4) and X014 (L-4′) were irradiated to fast fluences (En > 1 MeV) of 6.7×10^{21}, 3.9×10^{21}, and 3.0×10^{21}, n/cm^2, respectively, as determined by flux wire analysis.*

4.3.3 Evaluation of Temperature During Exposure

As discussed in subsection 4.2, each materials test section contained a temperature monitor consisting of fusible metal alloys (sentinels) which have well established melting points in the temperature range of interest. The configurations of the two types of monitors used are illustrated in Figures 4-15 and 4-18.

All L-2′ pins contained three monitors, equally spaced along the pin (approximately 5½ inches apart) as shown in Figure 4-13. Each monitor contained three sentinels capped with stainless steel discs. In both the upper and middle monitor (test sections 1 and 2) the sentinels consisted of the following materials:

Pure aluminum (MP = 1220°F)
Al–11.7Si (MP = 1070°F)
Al–33Cu (MP = 1018°F)

Of the five pins discussed here, four contained a monitor in the lower test section in which the Al-Si sensor was replaced by the low-temperature eutectic Ag-4.5Sb (MP = 903°F).

All L4 and L4′ pins contained five monitors, spaced approximately 3-½ inches along the pin (Figure 4-16). Each monitor contained three sentinels capped with stainless steel spherical balls. The sentinels consisted of the same materials as were used in test sections 1 and 2 of the L2′ pins.

The detailed evaluation of each alloy sentinel (or indicator disc) used in the L2′, L-4, and L4′ series of materials capsules is listed in Table 4-3. Also shown are the maximum temperatures attained in each test section. A typical temperature distribution curve (from the data of L4B) is shown in Figure 4-24.

The uncertainties associated with this technique are related primarily to uncertainty in the axial heat transfer from test section to temperature monitors, and the lack of adequate sensitivity during the post-irradiation measurement. Several kinds of events are suspected that can invalidate occasional measurements. Indicator hangup or melting of the fusible alloy during fabrication welding are two possibilities.

To confirm the nondestructive readout of temperature monitors, post-irradiation metallography was also conducted on selected sentinels. The results showed that all sensors positioned in the core region had undergone melting, indicating that a temperature greater than 1200°F was attained. Monitors in the upper blanket region (test section No. 1 for the L2′ series), on the other hand, showed that only the Al-33Cu sentinel melted, indicating that a temperature greater than 1018°F (548°C) but less than 1070°F (577°C) was reached in this position. A schematic of a representative monitor, a neutron radiograph and metallographic cross sections of the monitors used in test sections L4F-4 and L20-2 are shown in Figures 4-25 and 4-26.

Although the fusible metal thermometers used in these test capsules provided valuable information on the temperature of irradiation, the uncertainties mentioned above emphasize the need for direct monitoring of temperature—a need that can be satisfied only by using externally instrumented capsules.

* This method for determining neutron fluence in EBR-II yields total fluence values for row 2 and row 4 locations that are 60% and 40% lower, respectively, than those values based on the power normalization method used by ANL.[6]

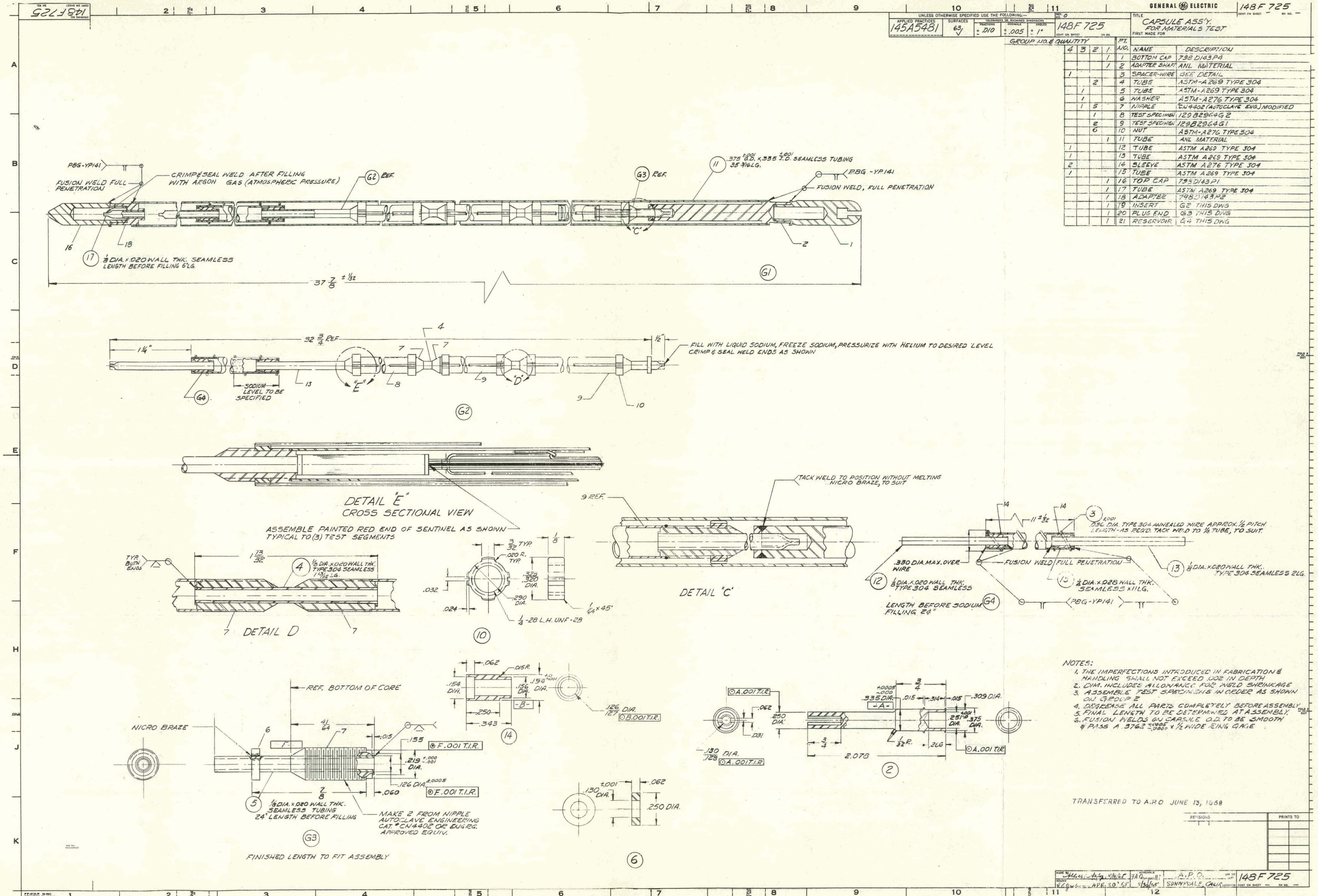

GROUP NO. & QUANTITY 4	3	2	1	PT. NO.	NAME	DESCRIPTION
			1	1	BOTTOM CAP	798D143P4
			1	2	ADAPTER SHAFT	ANL MATERIAL
1				3	SPACER-WIRE	SEE DETAIL
		2		4	TUBE	ASTM-A269 TYPE 304
	1			5	TUBE	ASTM-A269 TYPE 304
	1			6	WASHER	ASTM-A276 TYPE 304
	1	5		7	NIPPLE	#CN4402 (AUTOCLAVE ENG.) MODIFIED
		1		8	TEST SPECIMEN	129B2964G2
		2		9	TEST SPECIMEN	129B2964G1
		6		10	NUT	ASTM-A276 TYPE 304
			1	11	TUBE	ANL MATERIAL
1				12	TUBE	ASTM A269 TYPE 304
1				13	TUBE	ASTM A269 TYPE 304
2				14	SLEEVE	ASTM A276 TYPE 304
1				15	TUBE	ASTM A269 TYPE 304
			1	16	TOP CAP	798D143P1
			1	17	TUBE	ASTM A269 TYPE 304
			1	18	ADAPTER	798D143P2
			1	19	INSERT	G2 THIS DWG
			1	20	PLUG END	G3 THIS DWG
			1	21	RESERVOIR	G4 THIS DWG

Figure 4-13. Series L-2' Irradiation Capsule: Assembly

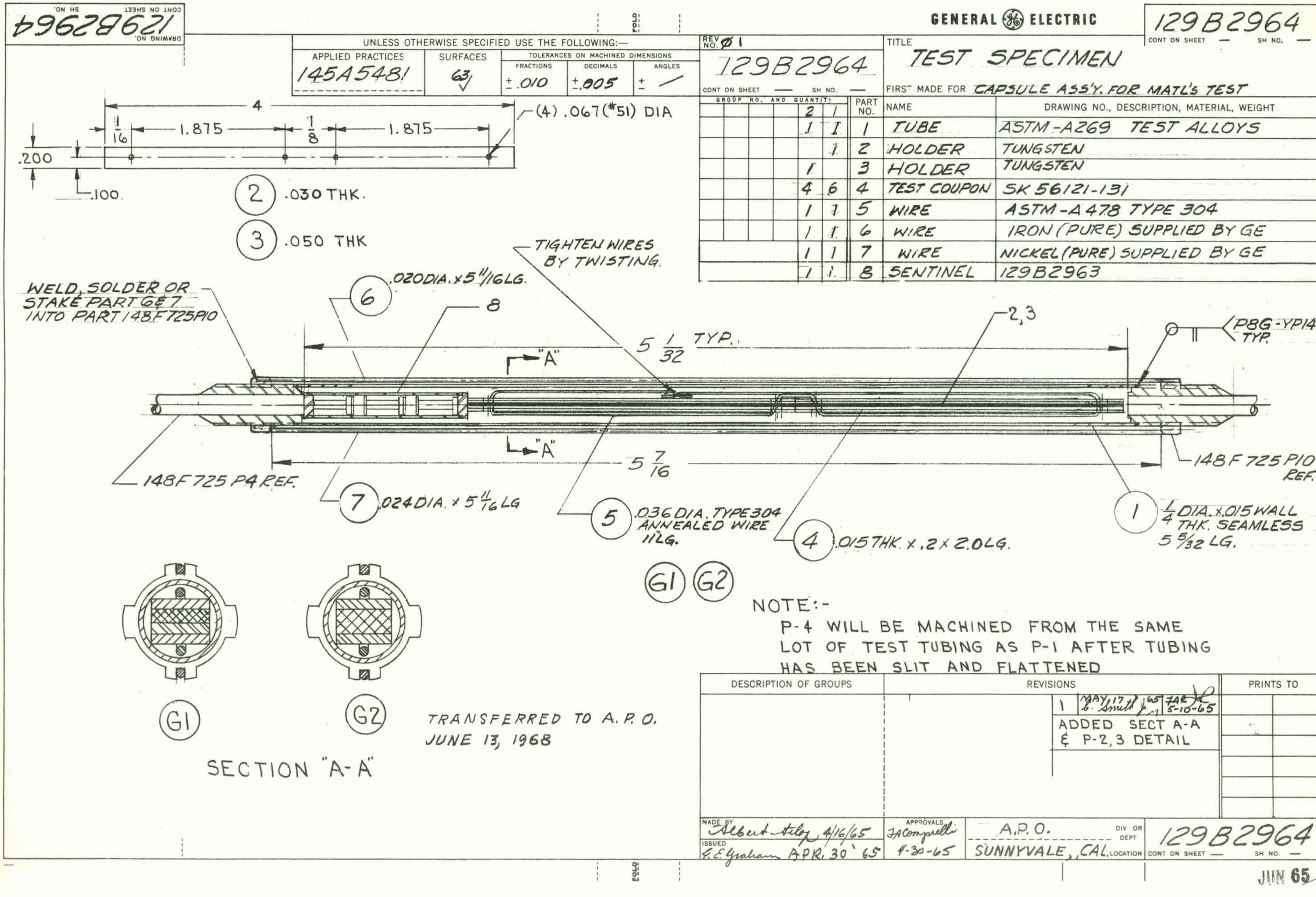

Figure 4-14. Series L-2' Irradiation Capsule: Test Specimen

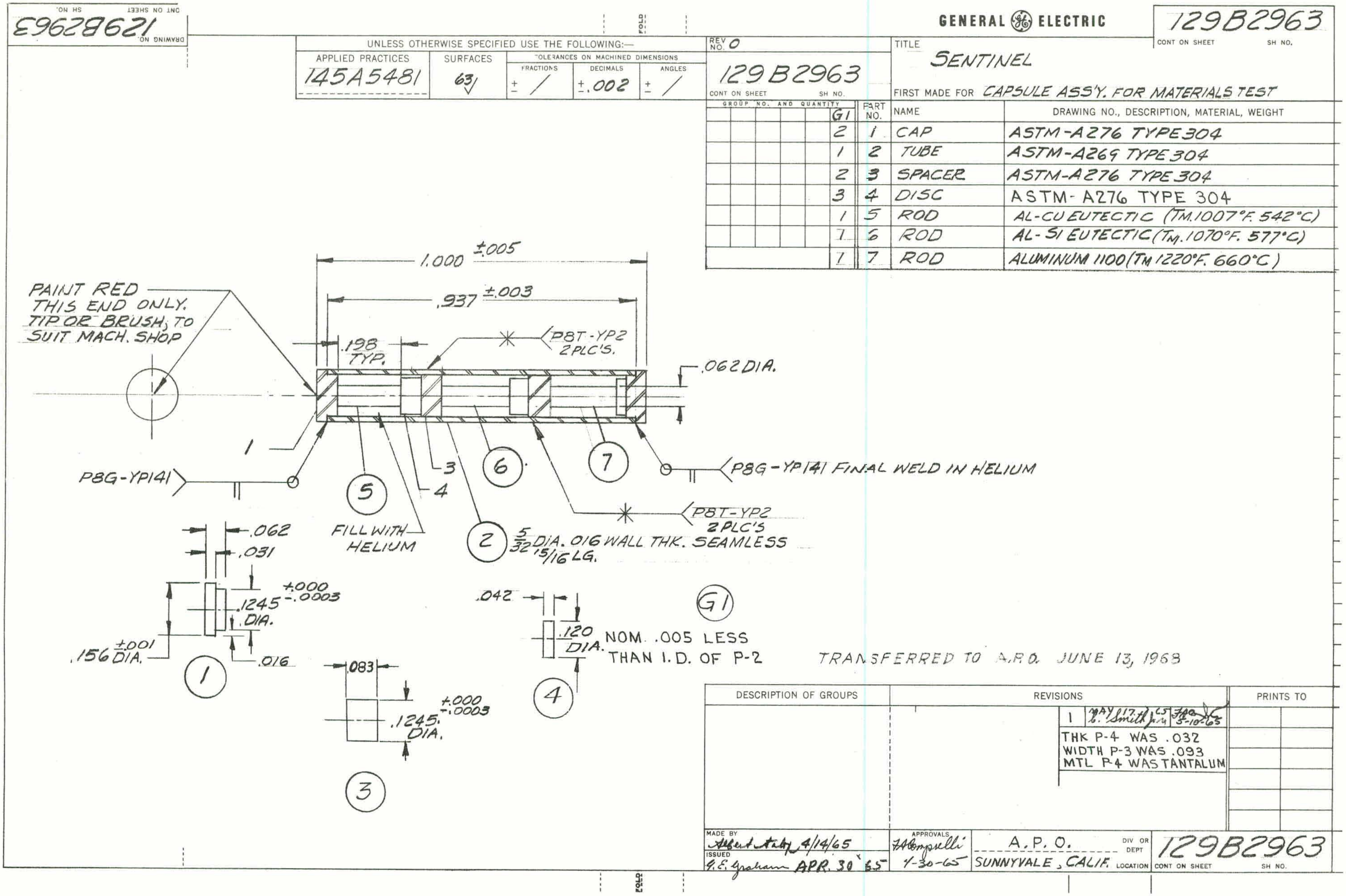

Figure 4-15. Series L-2' Irradiation Capsule: Sentinel

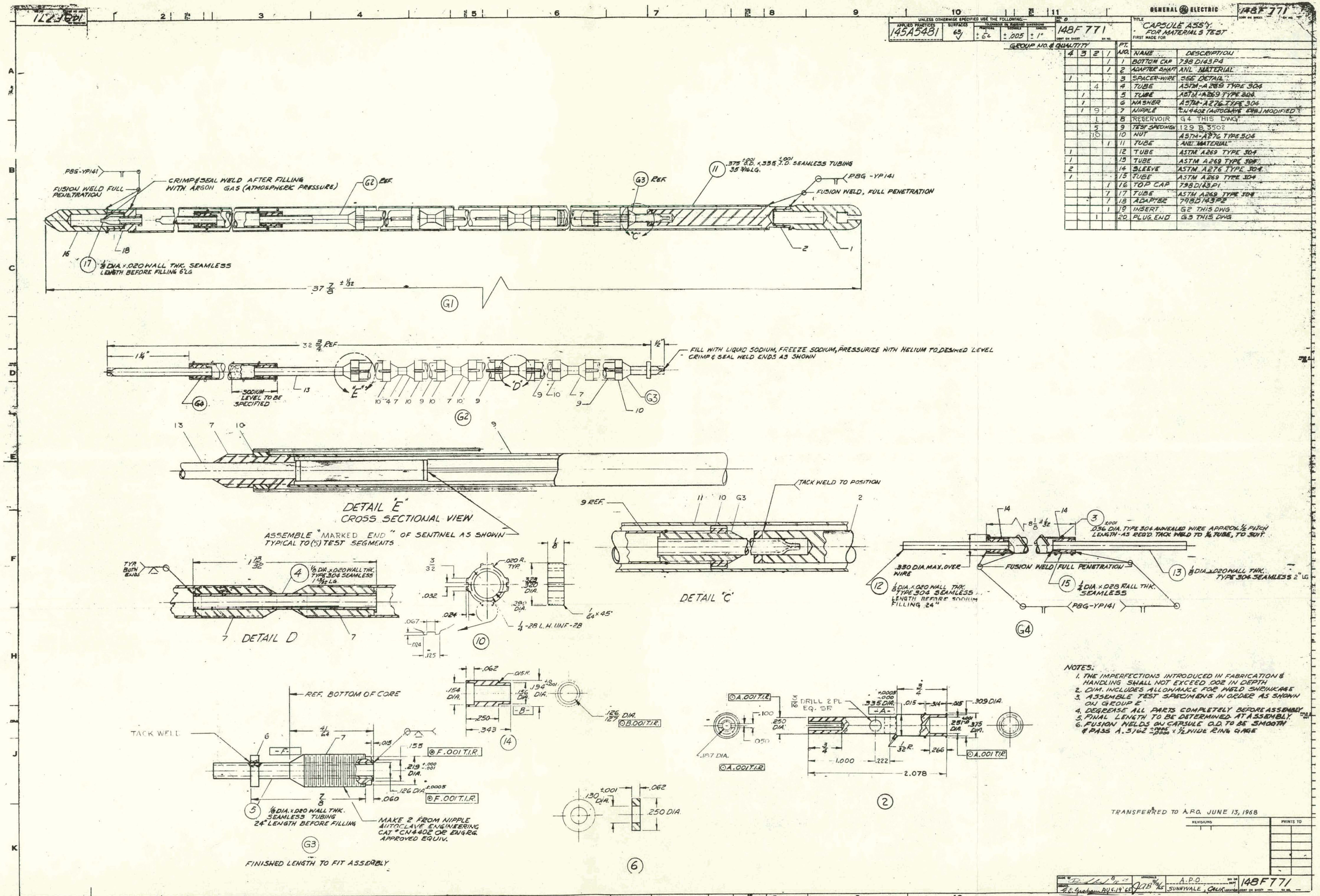

Figure 4-16. Series L-4/L-4' Irradiation Capsule: Assembly

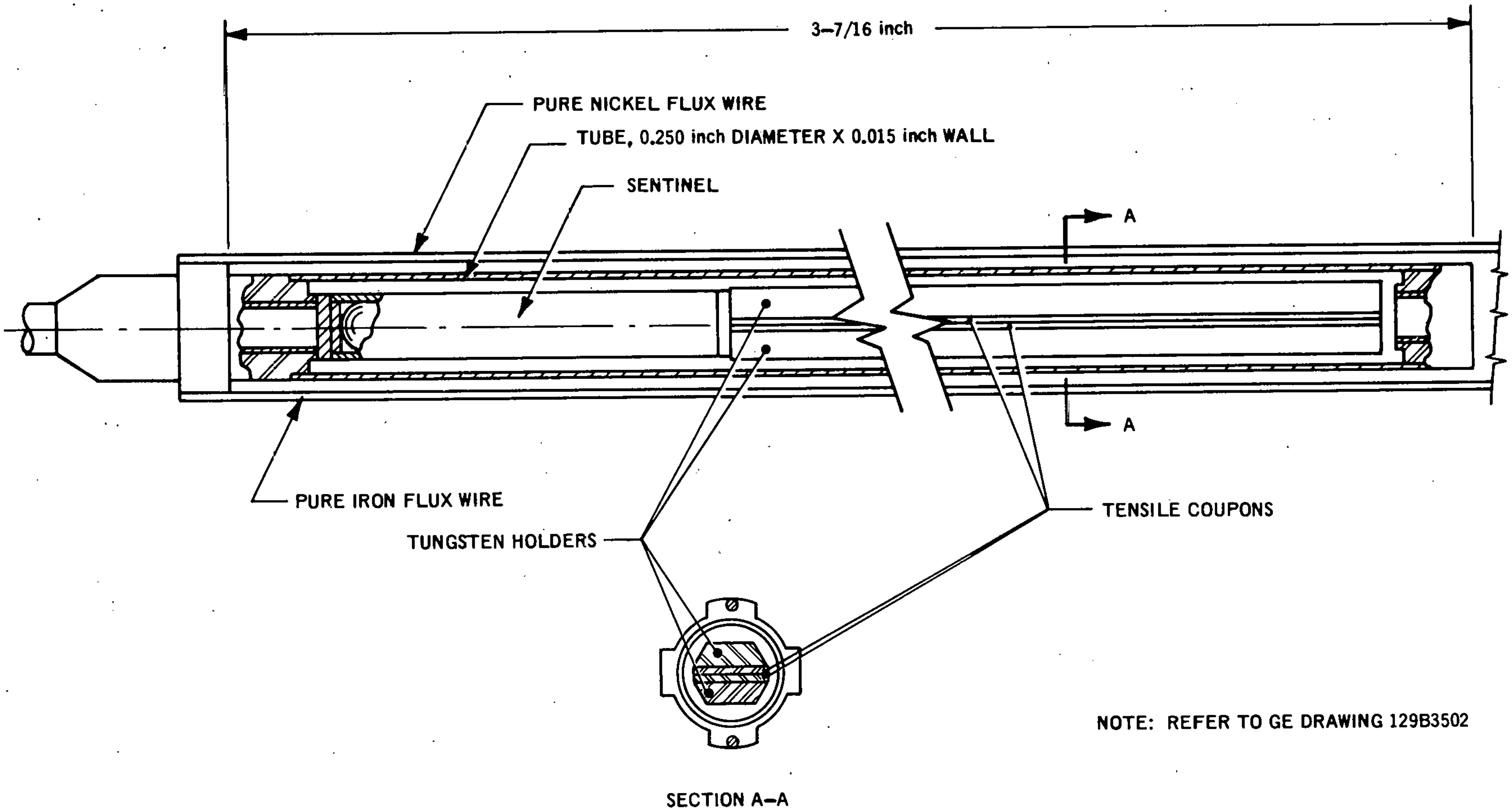

Figure 4-17. Series L-4/L-4′ Irradiation Capsule: Test Specimen

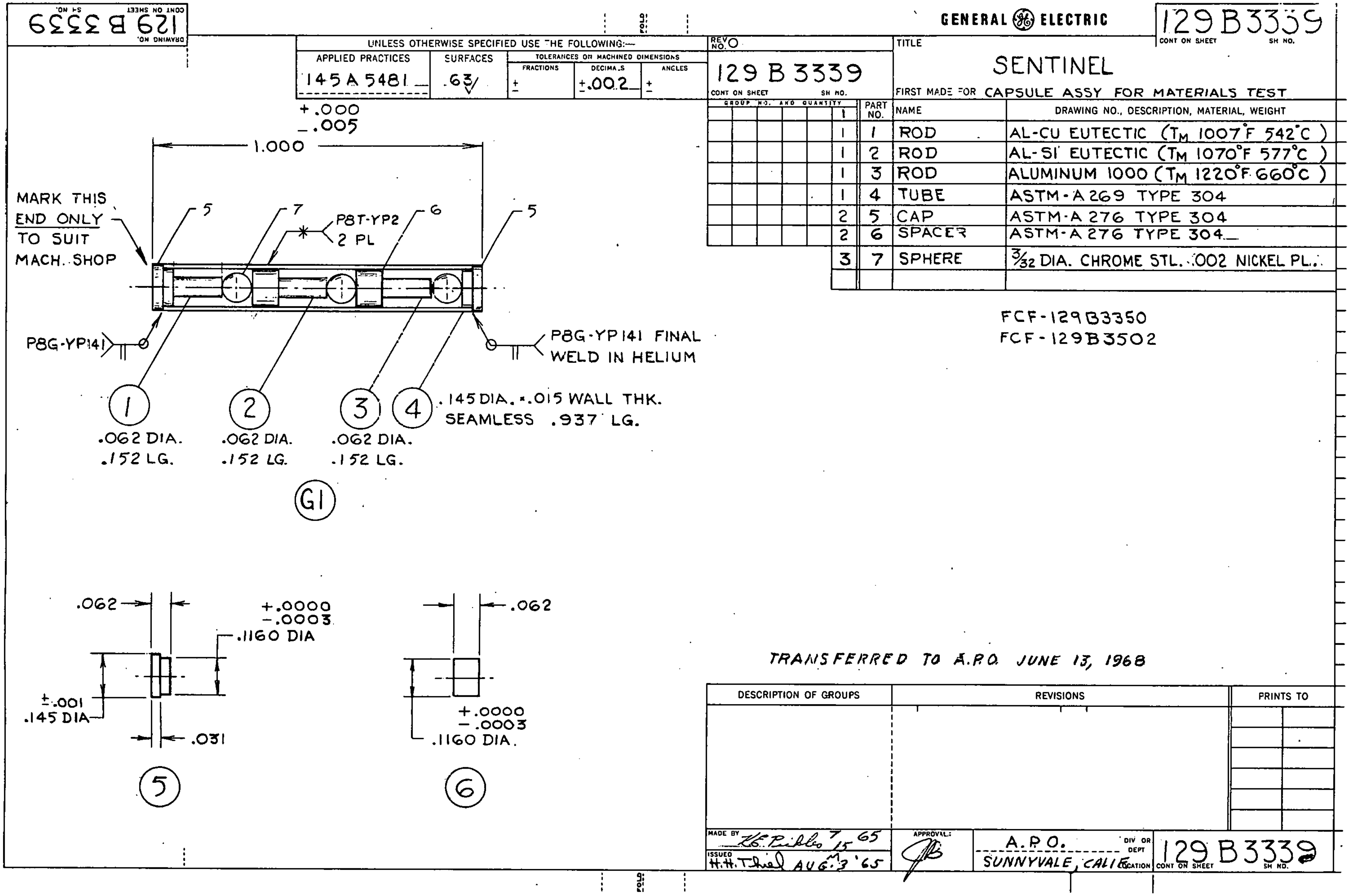

Group No. and Quantity	Part No.	Name	Drawing No., Description, Material, Weight
1	1	ROD	AL-CU EUTECTIC (T_M 1007°F 542°C)
1	2	ROD	AL-SI EUTECTIC (T_M 1070°F 577°C)
1	3	ROD	ALUMINUM 1000 (T_M 1220°F 660°C)
1	4	TUBE	ASTM-A 269 TYPE 304
2	5	CAP	ASTM-A 276 TYPE 304
2	6	SPACER	ASTM-A 276 TYPE 304
3	7	SPHERE	3/32 DIA. CHROME STL. .002 NICKEL PL.

Figure 4-18. Series L-4/L-4' Irradiation Capsule: Sentinel

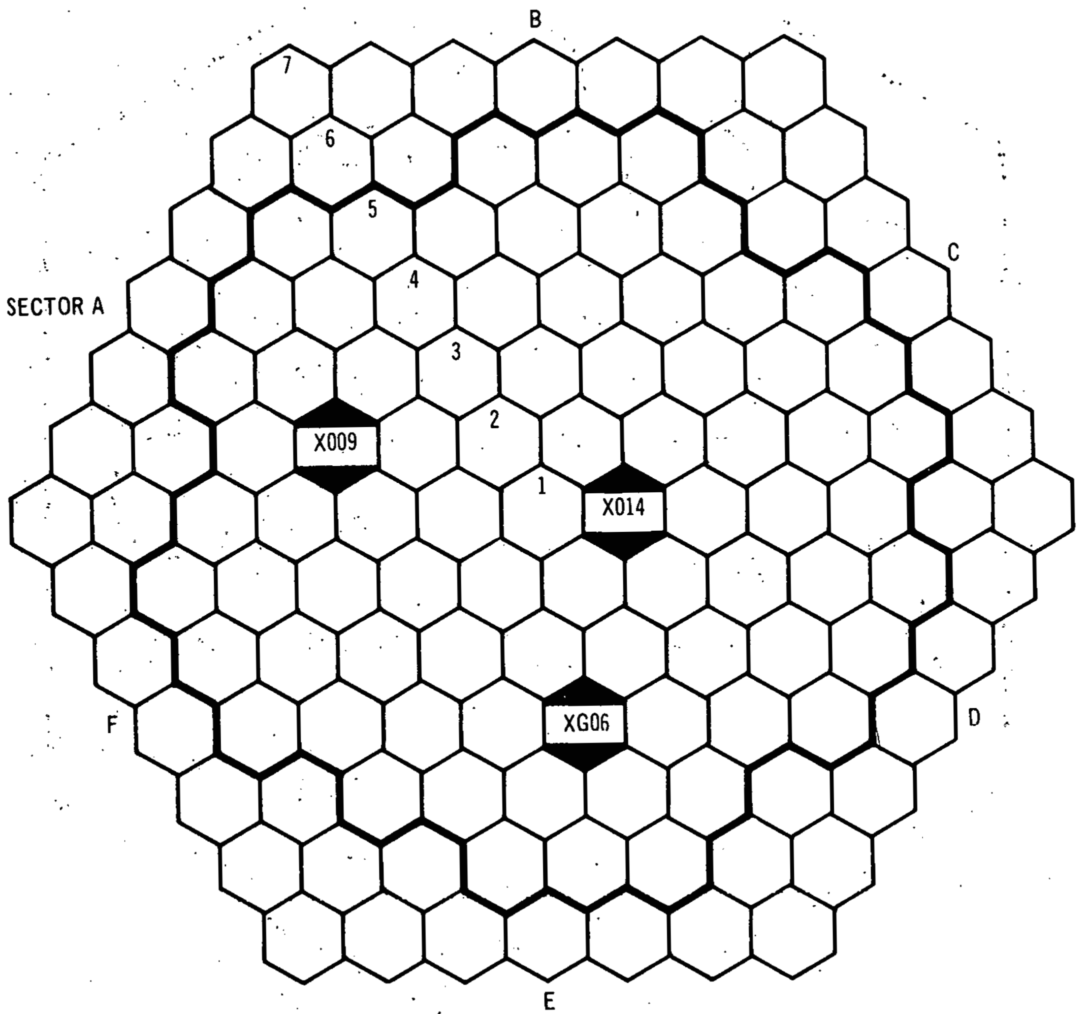

Figure 4-19. EBR-II Loading Pattern.

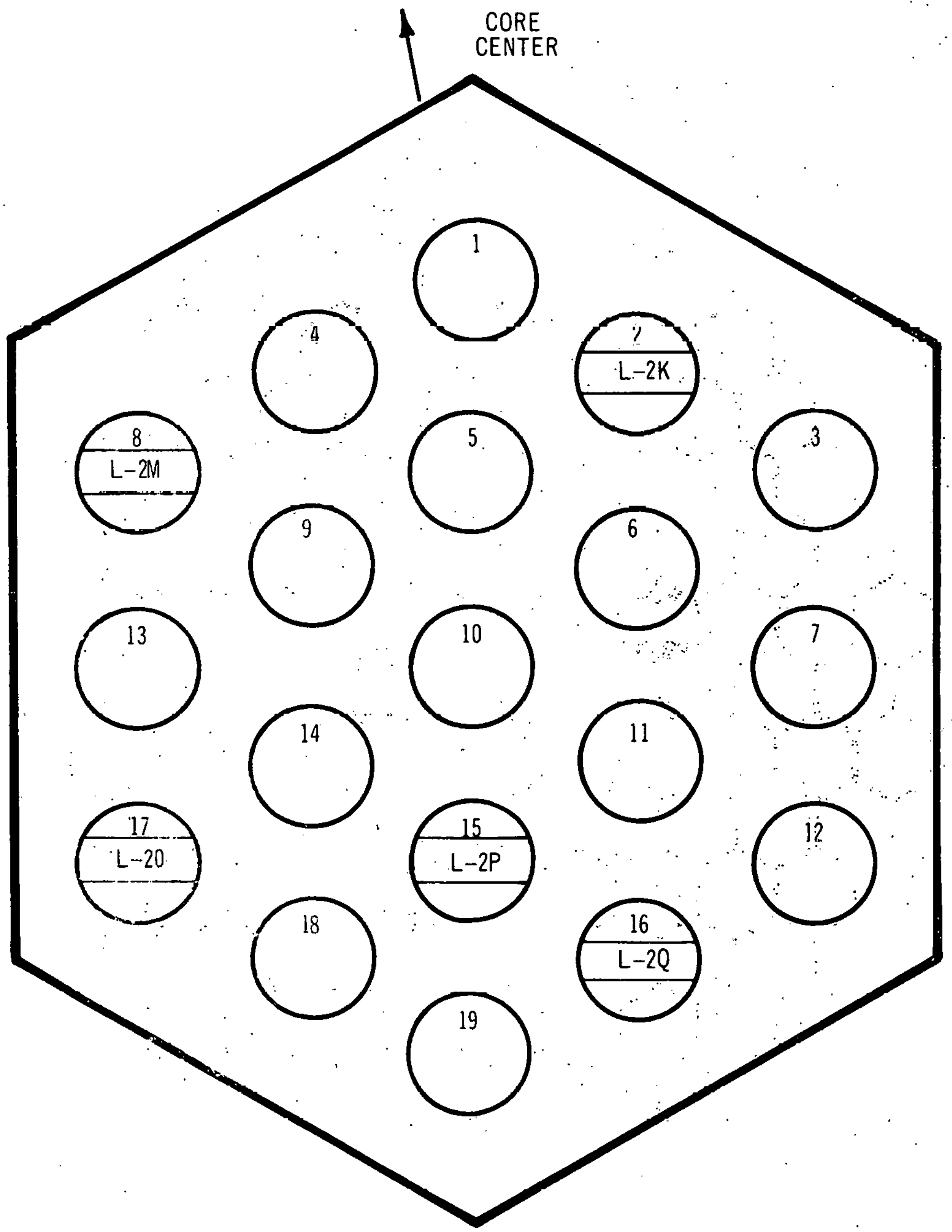

SUBASSEMBLY NO. XG06
CORE LOCATION 4E2

Figure 4-20. Subassembly Diagram, XG06

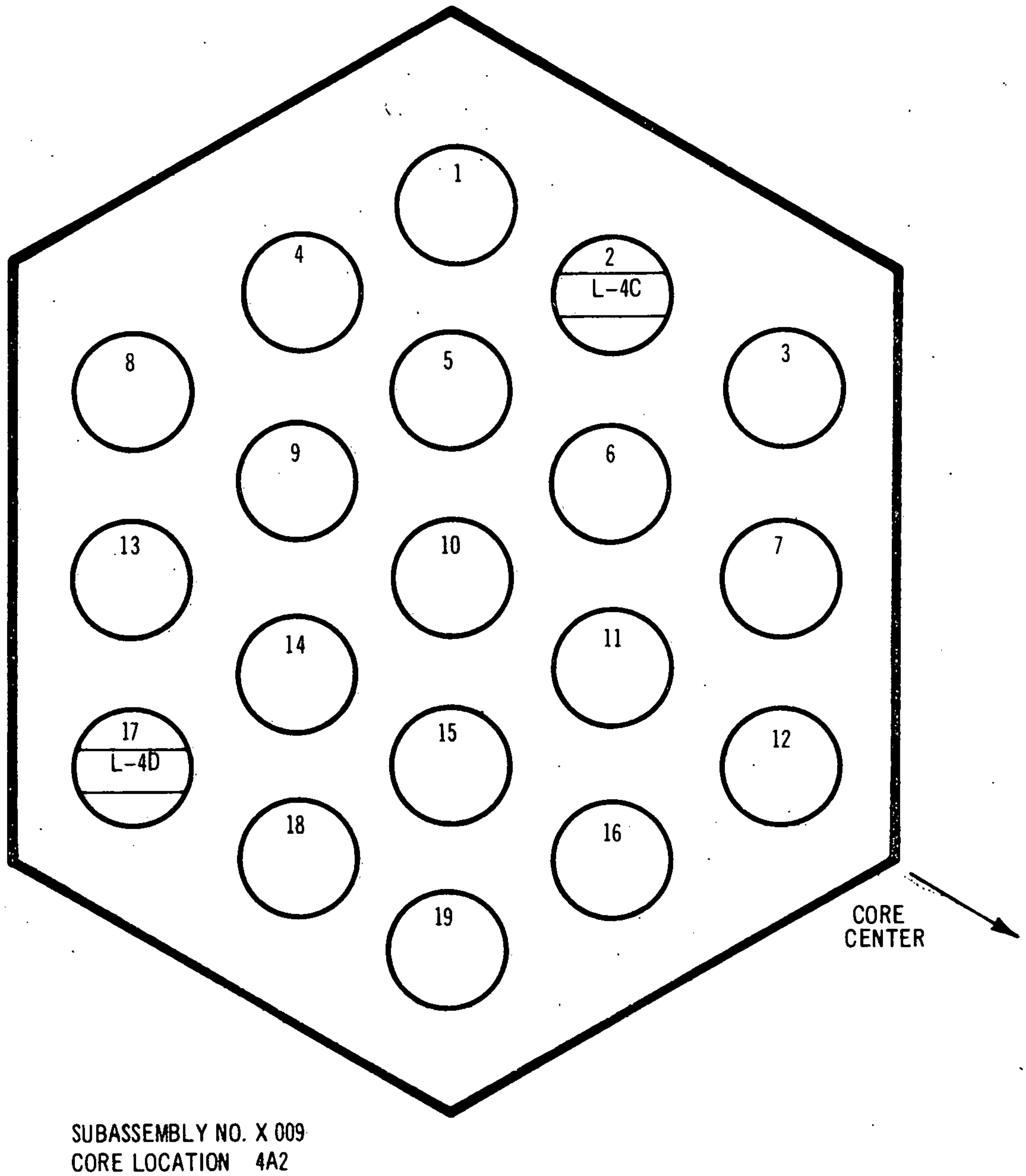

Figure 4-21. Subassembly Diagram, XO09

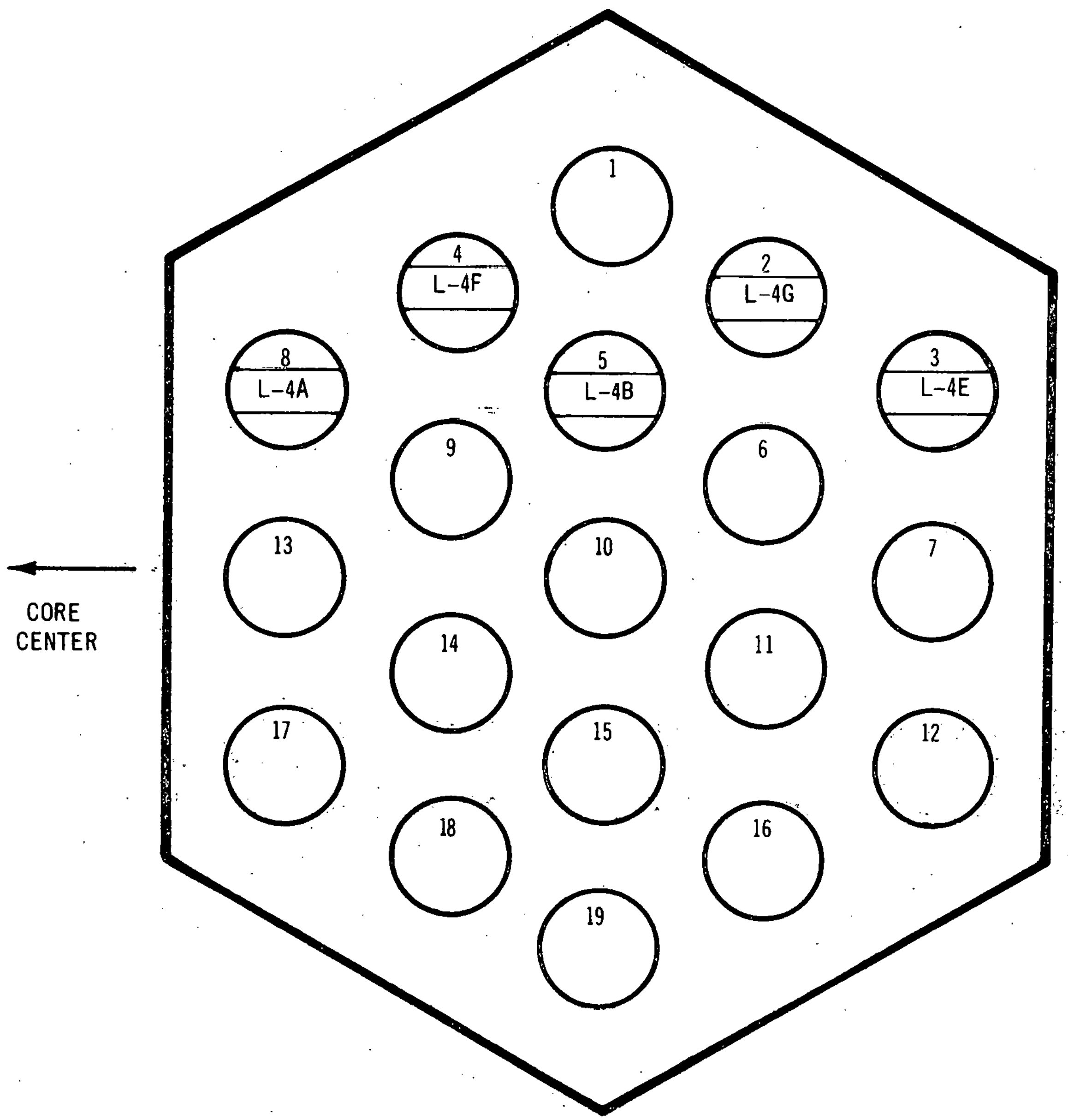

SUBASSEMBLY NO. X014
CORE LOCATION 2D1

Figure 4-22. Subassembly Diagram, X014

TABLE 4-3
SUMMARY OF TEMPERATURE MONITOR DATA

Pin Number	Region	Maximum Temperature Attained (°F)	Pin Maximum Temperature (°F)
L2K	No portion of pin attained a temperature as high as the lowest melting sentinel, Al–33Cu (MP = 1018°F)		< 1018
L2M	Upper 1/3	< 1018	
	Middle 1/3	1070>T>1018	1220>T>1018
	Lower 1/3	1220>T>1018	
L2O	Upper 1/3	1070>T>1018	
	Middle 1/3	1070>T>1018	1070>T>1018
	Lower 1/3	1018>T> 903	
L2P	Upper 1/3	1070>T>1018	
	Middle 1/3	1070>T>1018	> 1220
	Lower 1/3	> 1220	
L2Q	Upper 1/3	1070>T>1018	
	Middle 1/3	1070>T>1018	1070>T>1018
	Lower 1/3	1018>T> 903	
L4C	Upper 1/5	< 1018	
	Second 1/5	1220>T>1070	
	Middle 1/5	> 1220	> 1220
	Fourth 1/5	> 1018	
	Lower 1/5	1070>T>1018	
L4D	Upper 1/5	< 1018	
	Second 1/5	1220>T>1070	
	Middle 1/5	1220>T>1070	> 1220
	Fourth 1/5	1220>T>1070	
	Lower 1/5	> 1220	

NOTE
Since there is evidence to suggest that the aluminum sentinel had melted on a number of L4 monitors during welding, the apparent indication of melting in the lower L4D monitor and the middle L4C monitor should be disregarded. The probable pin temperature should be considered to be 1220>T>1070.

Pin Number	Region	Maximum Temperature Attained (°F)
L4A	Upper test section	< 1018
	Second test section	< 1018
	Middle test section	> 1220
	Fourth test section	> 1220
	Lower test section	> 1220

TABLE 4-3 (Continued)

Pin Number	Region	Maximum Temperature Attained (°F)
L4B	Upper test section	< 1018
	Second test section	< 1018
	Middle test section	1018–1070
	Fourth test section	> 1220
	Lower test section	> 1220
L4E	Upper test section	< 1018
	Second test section	1070–1220
	Middle test section	1070–1220
	Fourth test section	> 1220
	Lower test section	> 1220
L4F	Upper test section	< 1018
	Second test section	> 1220
	Middle test section	> 1220
	Fourth test section	> 1220
	Lower test section	1018–1070
L4G	All test sections	< 1018

Significant Observations

a. The maximum temperature attained in all pins except L4G was in excess of 1220°F.

b. The positions of the lower three monitors bracketed the highest temperature region of the core position.

c. The maximum temperature attained in L4G was below the minimum melting temperature of 1018°F.

d. The temperature of the region occupied by the upper monitor was below the minimum detectable temperature in all pins.

e. The effective temperature during irradiation can be estimated to ± 50°F with a reasonable degree of confidence.

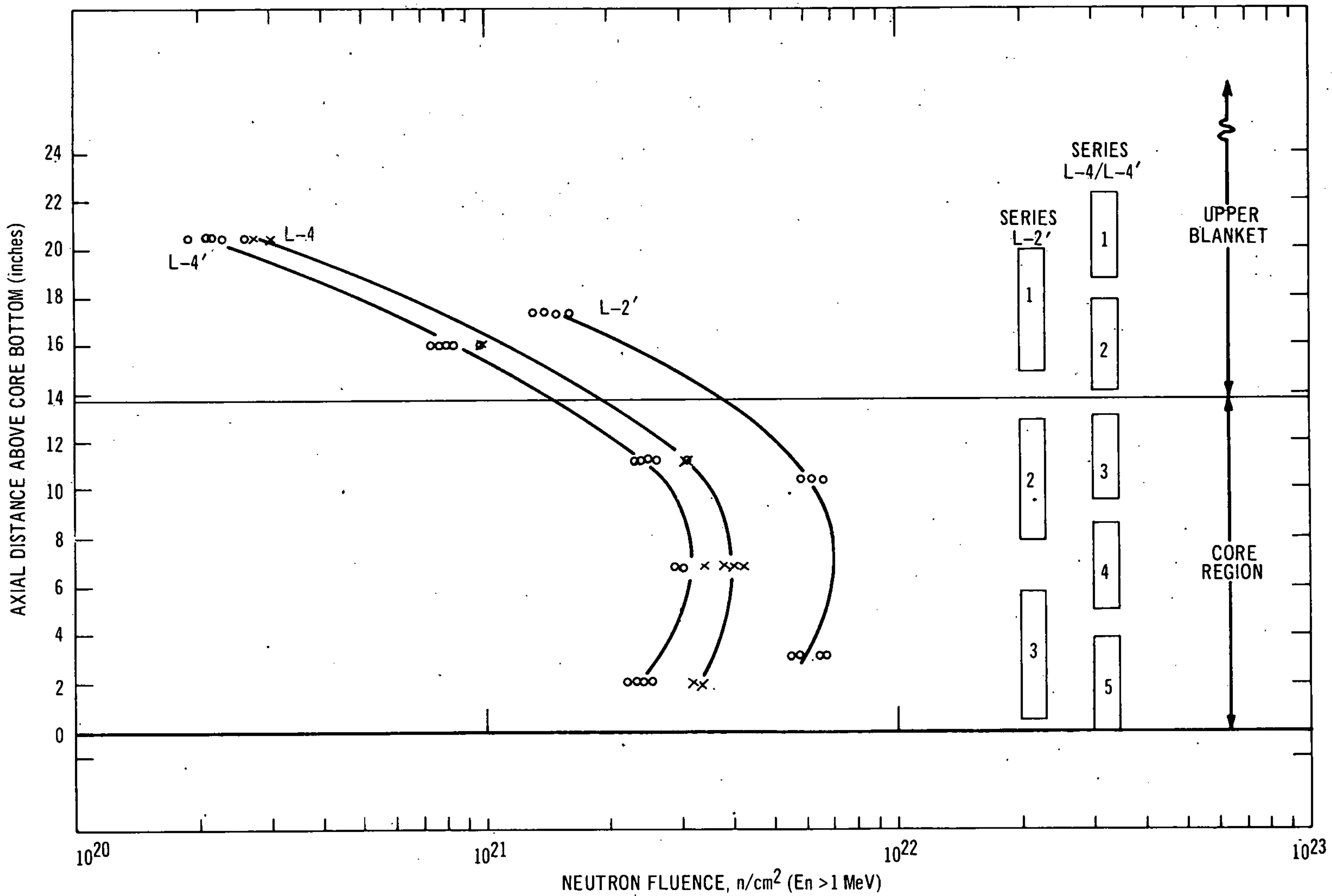

Figure 4-23. EBR-II Neutron Fluence Distribution for Capsule Series L-2, L-4, and L-4 ′

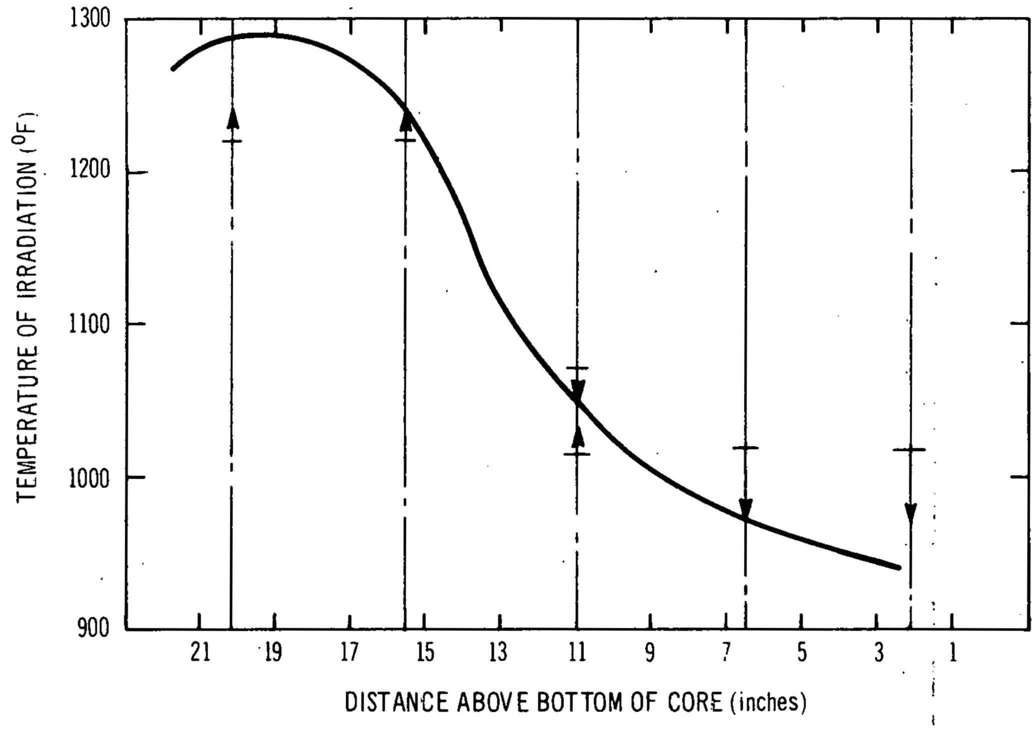

Figure 4-24. Temperature Distribution in Materials Capsule L4B

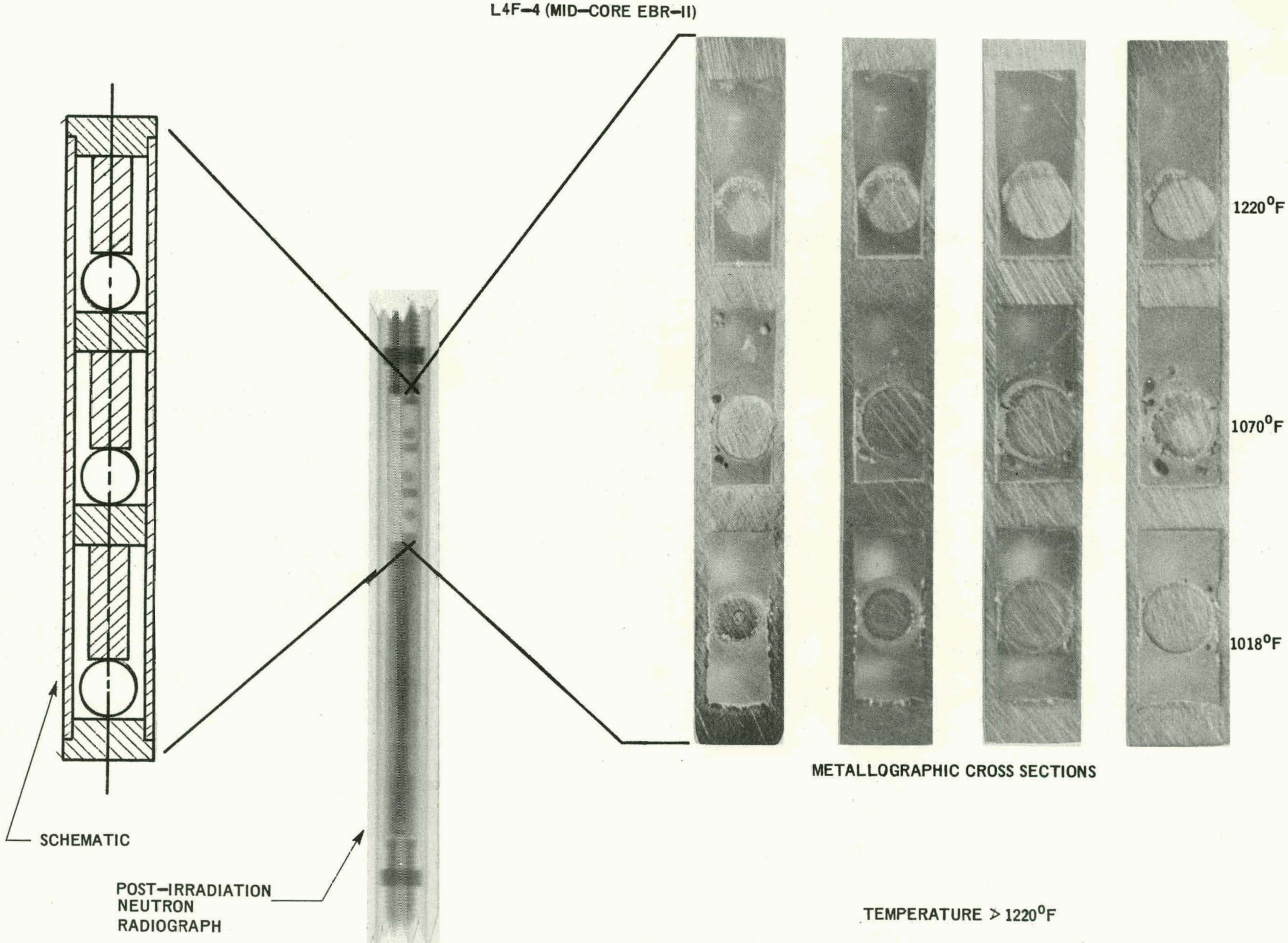

Figure 4-25. Metallographic Cross Section, L4F-4

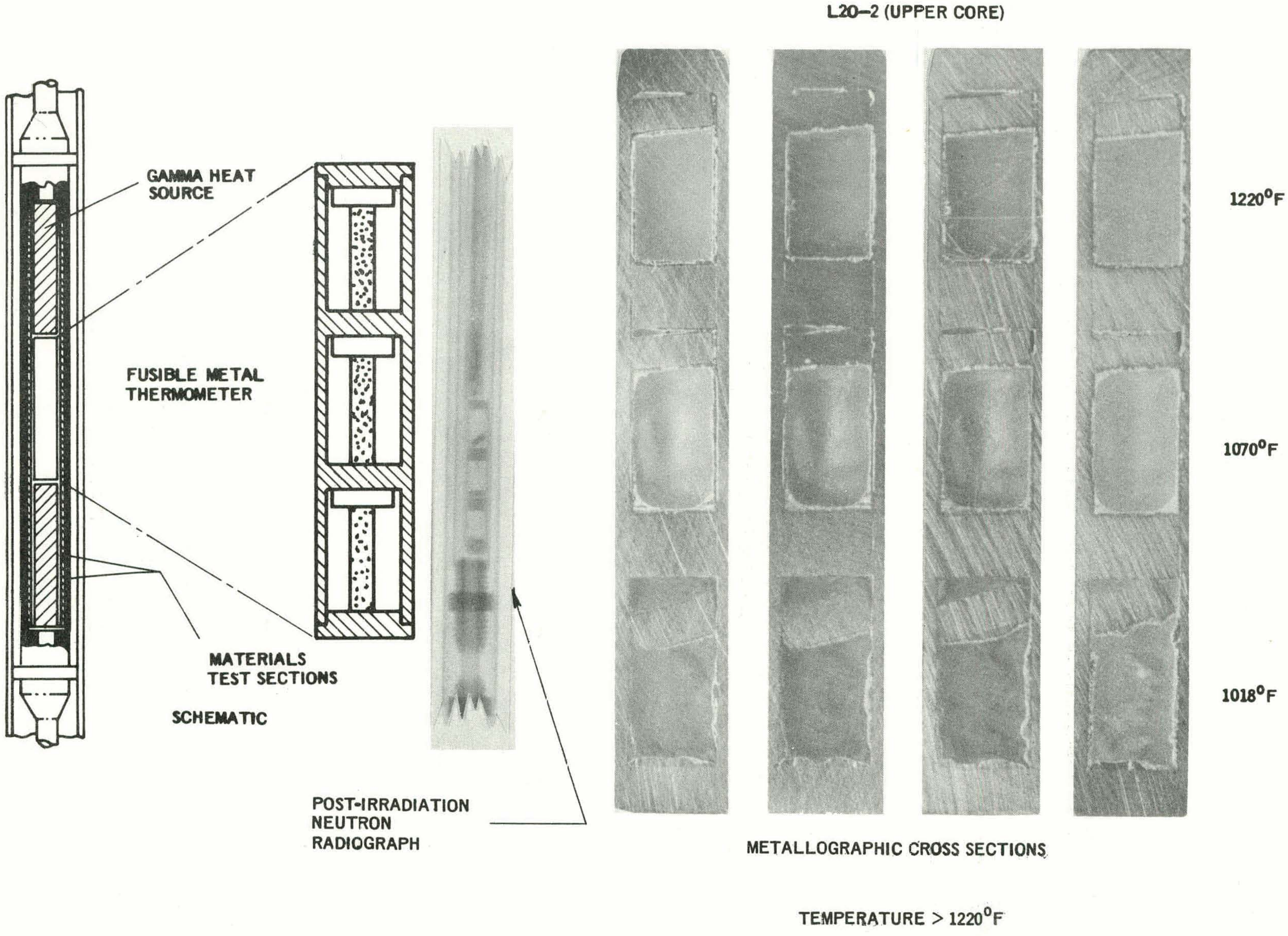

Figure 4-26. Metallographic Cross Section, L2O-2

5. RESULTS

Mechanical properties data were obtained from post-irradiation tensile (uniaxial) and burst (biaxial) tests, performed at temperatures from 900 to 1500°F. Optical and electron metallographic techniques were used to support or interpret the results.

5.1 IN-REACTOR DEFORMATION

Considerable difficulty was experienced in removing several test section arrays from the capsule assembly. Subsequent examination showed the presence of sodium in the annulus between the test sections and the capsule assembly tube, which prior to irradiation was filled only with argon gas. This indicated that some of the walls of the sodium-filled tubular sections had been breached during irradiation.

An attempt was made to locate the failure regions by pressurizing the test sections and helium leak-checking at room temperature. Several were located in either a weld joint or in the test section wall. This information is summarized in Tables 5-1 and 5-2. Only eight failures were observed; however, it is believed that, since all capsule assemblies showed evidence of sodium leakage, other test sections had through-cracks which were open only at elevated temperatures.

Micrometer and profilometer measurements were performed on the outside diameter of each of the tubular test sections to determine the extent of deformation that occurred during the reactor exposure. These measurements are listed in Tables 5-1 and 5-2 for capsule series L-2′ and L-4/L-4′, respectively. In general, the diametral growth resulting from pre-pressurization was either substantial and localized, or was negligible. Maximum diametral change usually was associated with the in-core test sections, which experienced the highest exposure temperatures. Figure 5-1 shows a profilometer trace for an Incoloy-800 test section from series L-4′, which was located in the upper blanket of the EBR-II. No deformation was observed. However, a profilometer trace from a similar Incoloy-800 test section, located in the core region (Figure 5-2), shows localized deformation and substantial diametral increase (15%).

A metallographic examination was made in an effort to establish the failure mode for those specimens that showed through-cracks. Test section L4C-4 (carbide-agglomerated Type 316) was selected because a breach in the tube wall had been located in this section using helium-leak detection methods. The resulting photomicrographs are shown in Figure 5-3. Cracking was observed throughout the section. The failure was intergranular, with many voids located at triple points and at grain boundaries. It appears that discrete voids grow and link together to form cracks. As would be expected, these voids and cracks were nearly perpendicular to the principal stress direction. Also evident was substantial sigma formation at triple points and carbides at grain boundaries. Localized necking and intergranular cracking were observed in the seam weld of this test section (Figure 5-4).

Because of the unusual deformation observed in the test sections, an effort was made to recalculate the pre-irradiation stress conditions and estimate the causes of the in-reactor deformation. It was concluded that the large amounts of deformation observed were due mainly to a higher temperature of irradiation than that used in the initial stress analysis.

The relatively high incidence of cracks in the weld zone of these tubes suggests that welded and drawn tubing may not perform satisfactorily under conditions of internal pressure and low deformation rates. If the weld zone is the weakest area in the material, the applicability of the in-core diametral growth changes is limited as an estimate of in-core creep behavior. However, if diametral strains are small, the specimens are useful for post-irradiation testing (uniaxial and biaxial) at medium-range strain rates.

5.2 BURST TESTS ON EBR-II CAPSULE TUBES

The tubes used in the encapsulation of all materials and fuel pins irradiated in EBR-II are welded and drawn Type-304 stainless steel, with nominal dimensions of 0.375 inch o.d. and 0.020-inch wall. The material utilized in the tests discussed here had an average ASTM grain size 8, and chemical composition as shown in Table 5-3. The tubing was irradiated in the as-received (solution-annealed) condition.

The irradiation history of the capsule tubes is identical to that of the L-2′ materials capsules, as discussed in subsection 4.3. A representative axial temperature profile and its relation to the fluence profile are shown in Figure 5-5 for capsule tubing containing fuel pins. Post-irradiation metallographic examination of a typical capsule tube revealed that

a. The tube is lightly sensitized throughout the cross section;
b. The grain structure is uniform, with an average grain size of ASTM 7;
c. Neither the outer tube surface, exposed to flowing sodium, nor the inner tube surface, exposed to static sodium, shows any evidence of attack, compositional disturbance, or unusual precipitation behavior.

The as-received material, in comparison, shows austenitic grains with numerous annealing twins, typical of a fully-annealed austenitic stainless steel, and a grain size of ASTM 8. When it is realized that the two tubing sections are not directly comparable except in heat number, the difference in grain size between as-received and irradiated material is not considered significant. Representative microstructures of as-received and irradiated materials are shown in Figure 5-6.

TABLE 5-1
DIAMETRAL GROWTH OF TUBULAR TEST SECTIONS FROM SERIES L-2′

Test Section[c] Designation	Material[d]	Maximum Diametral Growth (%)	Neutron Exposure[f] (En > 1 MeV) n/cm² $\times 10^{21}$
L-2K-1	Incoloy-800	None	1.3
L-2K-2	Incoloy-800	0.8[e]	6.7
L-2K-3[a]	Incoloy-800	1.0[e]	6.2
L-2M-1	Type 316L	None	1.3
L-2M-2	Type 316L	14.4	6.7
L-2M-3	Type 316L	3.6	6.2
L-2O-1	Type 347	1.0[e]	1.3
L-2O-2[b]	Type 347	9.6[e]	6.7
L-2O-3	Type 347	6.4	6.2
L-2P-1	Type 321	1.6	1.3
L-2P-2	Type 321	14.8	6.7
L-2P-3	Type 321	14.8[e]	6.2
L-2Q-1	Type 304	0.4[e]	1.3
L-2Q-2	Type 304	12.4	6.7
L-2Q-3	Type 304	8.0	6.3

(a) Failure located in weld zone between autoclave nipple and tube.

(b) Failure in test section; location unidentified.

(c) (-1) indicates top test section (upper blanket region).
(-2) indicates middle test section (in core).
(-3) indicates bottom test section (in core).

(d) Material was in as-received condition (mill annealed).

(e) Measurements made with micrometer; all other measurements were performed with a profilometer.

(f) The L-2′ series of materials capsules have 207 effective full-power days (EFPD) in the EBR-II.

TABLE 5-2
DIAMETRAL GROWTH OF TUBULAR TEST SECTIONS FROM SERIES L-4 AND L-4′

Test Section[c] Designation	Material[d]	Maximum Diametral Growth (%)	Neutron Exposure[g] (En > 1 MeV) n/cm² × 10²¹
L-4A-1	Incoloy-800	None	0.22
L-4A-2	Incoloy-800	None	0.76
L-4A-3	Incoloy-800	3.6	2.4
L-4A-4[a]	Incoloy-800	15.2	3.0
L-4A-5	Incoloy-800	10.0	2.5
L-4B-1	Incoloy-800	None	0.22
L-4B-2	Incoloy-800	None	0.76
L-4B-3[a]	Incoloy-800	8.8	2.4
L-4B-4[a]	Incoloy-800	7.2	3.0
L-4B-5[a]	Incoloy-800	2.8	2.5
L-4C-1	Type 316	None	0.3
L-4C-2	Type 316	None[f]	0.96
L-4C-3	Type 316	1.0[e]	3.1
L-4C-4	Type 316	5.2[e]	3.9
L-4C-5	Type 316	2.0[f]	3.3
L-4D-1	Type 316	None[f]	0.3
L-4D-2	Type 316	None[e]	0.96
L-4D-3	Type 316	—[f]	3.1
L-4D-4	Type 316	None[f]	3.9
L-4D-5	Type 316	—[f]	3.3
L-4E-1	Type 347	None	0.22
L-4E-2	Type 347	None	0.76
L-4E-3	Type 347	16.8[f]	2.4
L-4E-4	Type 347	20.8	3.0
L-4E-5	Type 347	16.8[f]	2.5
L-4F-1	Type 304	—[g]	0.22
L-4F-2	Type 304	None	0.76
L-4F-3	Type 304	None	2.4
L-4F-4	Type 304	None	3.0
L-4F-5	Type 304	None	2.5
L-4G-1[2]	Type 321	1.2	0.22
L-4G-2	Type 321	1.2	0.76
L-4G-3	Type 321	1.2	2.4
L-4G-4	Type 321	1.2	3.0
L-4G-5	Type 321	1.2	2.5

(a) Failure located in tube wall.
(b) Failure located in weld zone between autoclave nipple and tube.
(c) (-1) indicates top test section (upper blanket region).
(-2) indicates second test section (upper blanket region).
(-3) indicates middle test section (in core).
(-4) indicates fourth test section (in core).
(-5) indicates bottom test section (in core).
(d) Material is in carbide-agglomerated condition (1650F-24 hours).
(e) Measurements made with micrometer; all other measurements were performed with a profilometer.
(f) Test section was scratched and possibly deformed during disassembly.
(g) All materials capsules have 81.6 effective full power days (EFPD) in EBR-II except Type 316 (L-4C and L-4D) which have 119 EFPD.

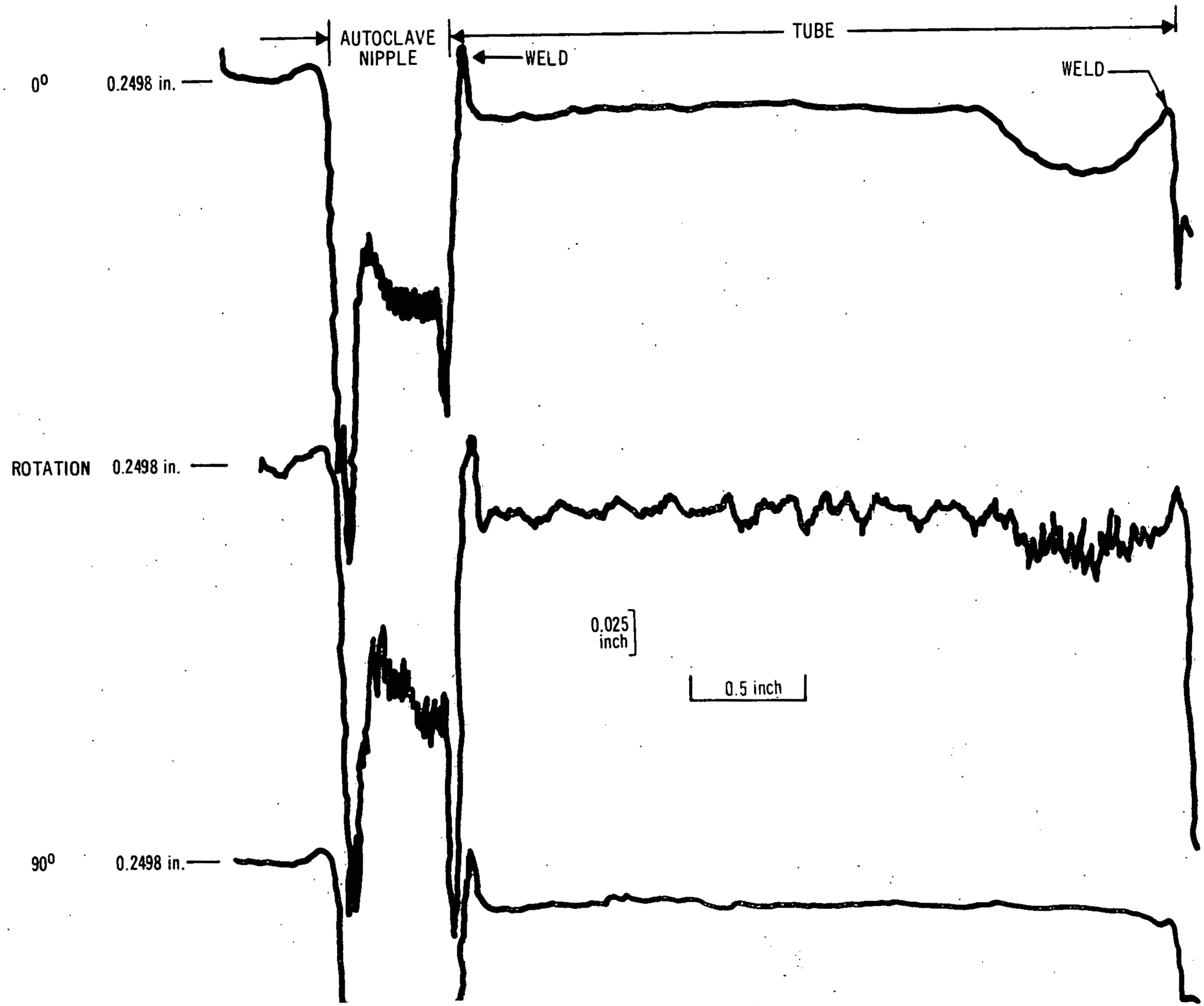

Figure 5-1. Post-Irradiation Profilometer Trace for Tubular Test Section L-4A-1 (Incoloy-800)

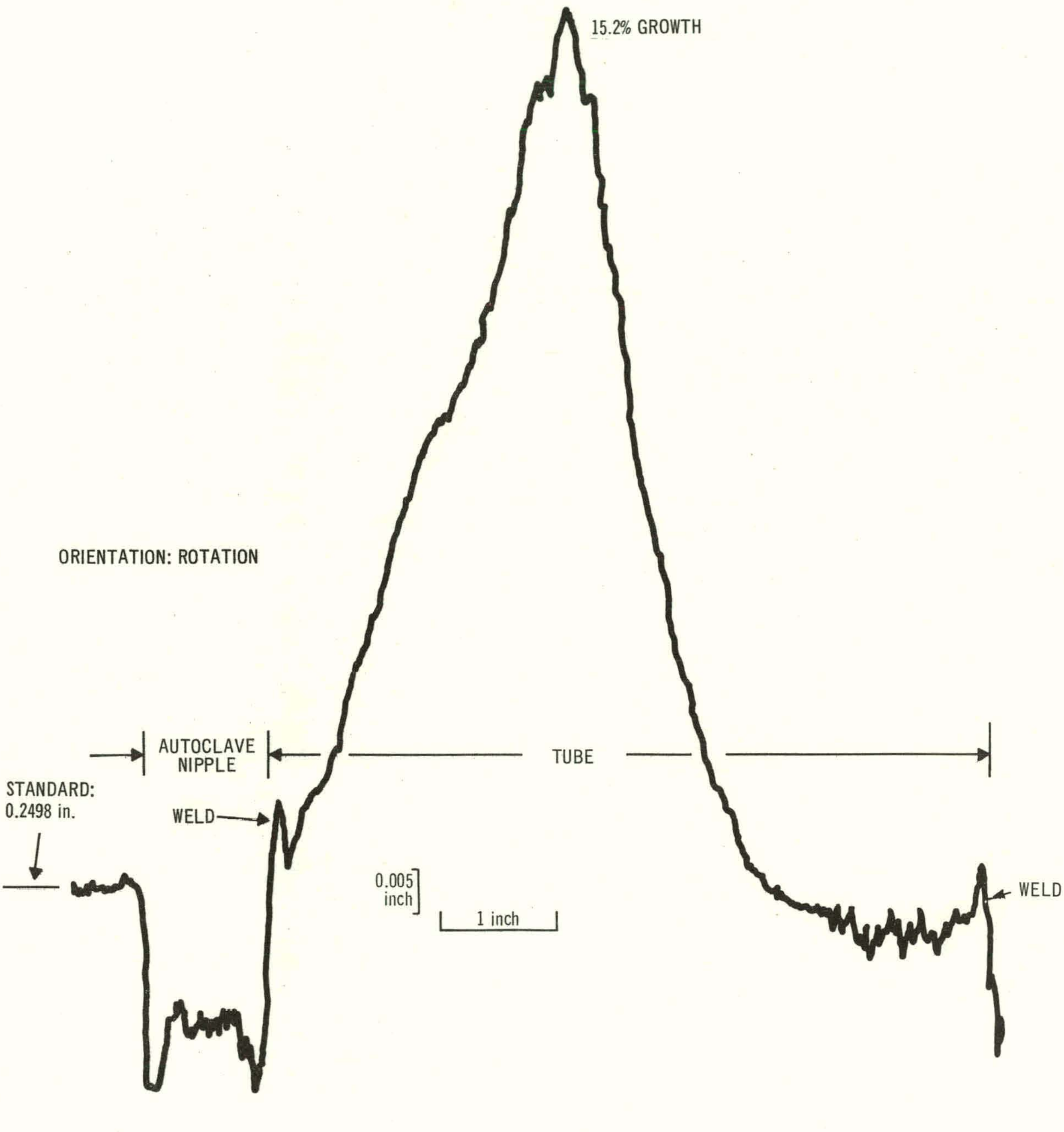

Figure 5-2. Post-Irradiation Profilometer Trace for Tubular Test Section L-4A-4 (Incoloy-800)

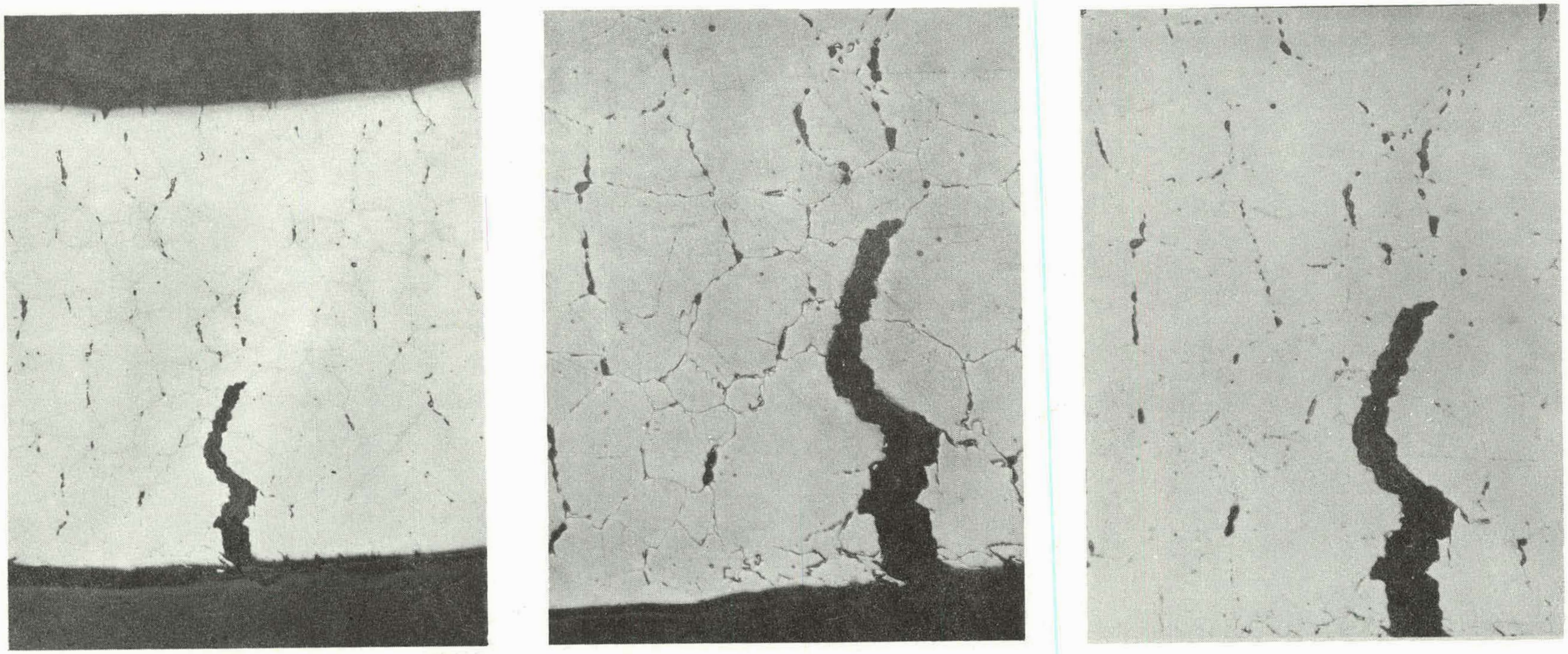

(a) ETCH: VILELLA 250X

(b) ETCH: VILELLA 500X

(c) ETCH: MURAKAMI 500X

Figure 5-3. Photomicrographs of Failed Tubular Test Section L-4C-4 (Type 316) Transverse Section

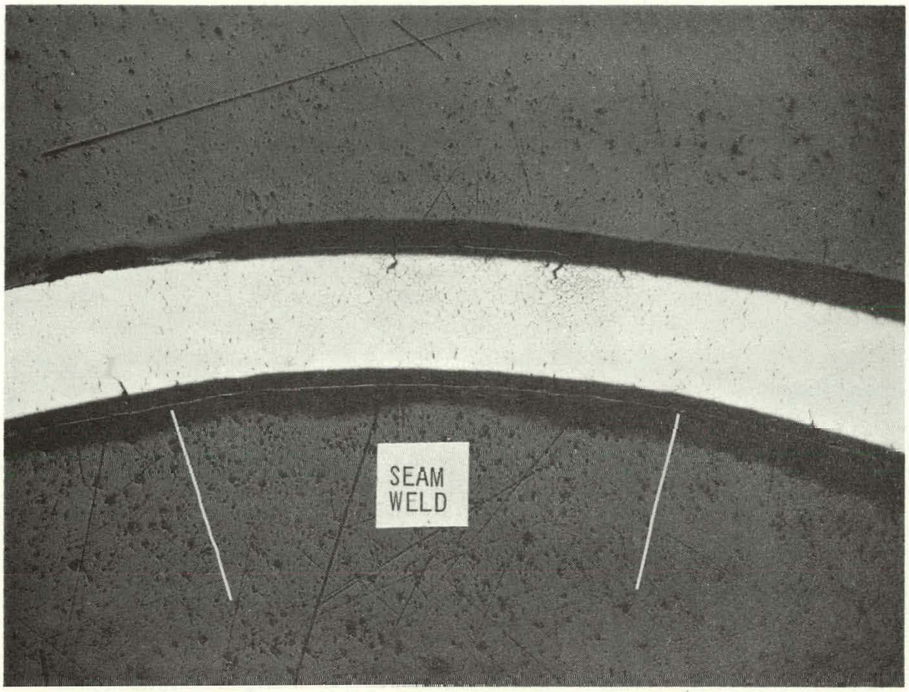

(a) ETCH: VILELLA 50X

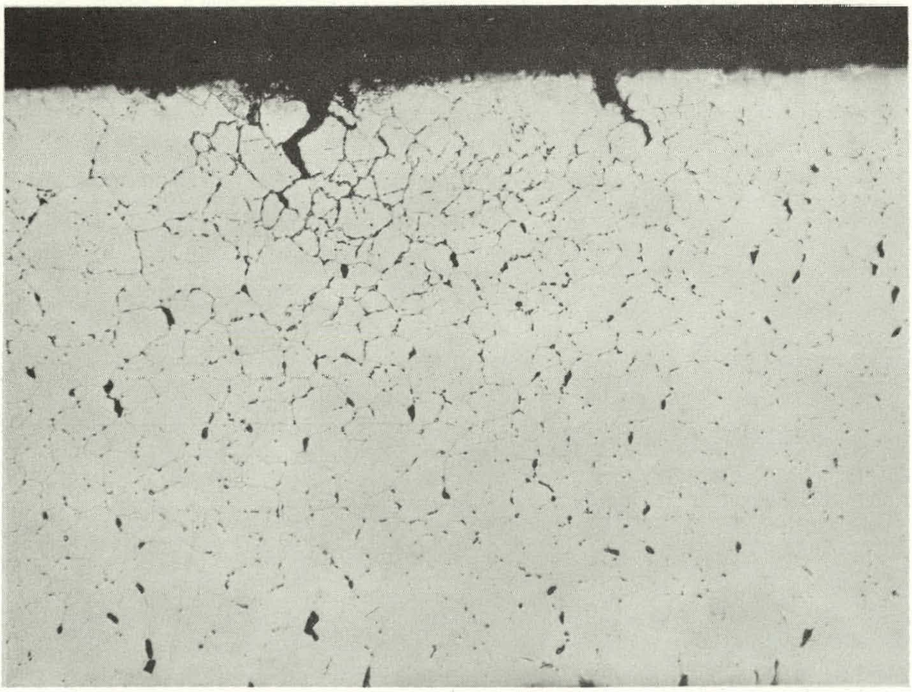

(b) ETCH: VILELLA 250X

Figure 5-4. Transverse Section of Tubular Test Section L-4C-4 (Type 316) Seam Weld Region

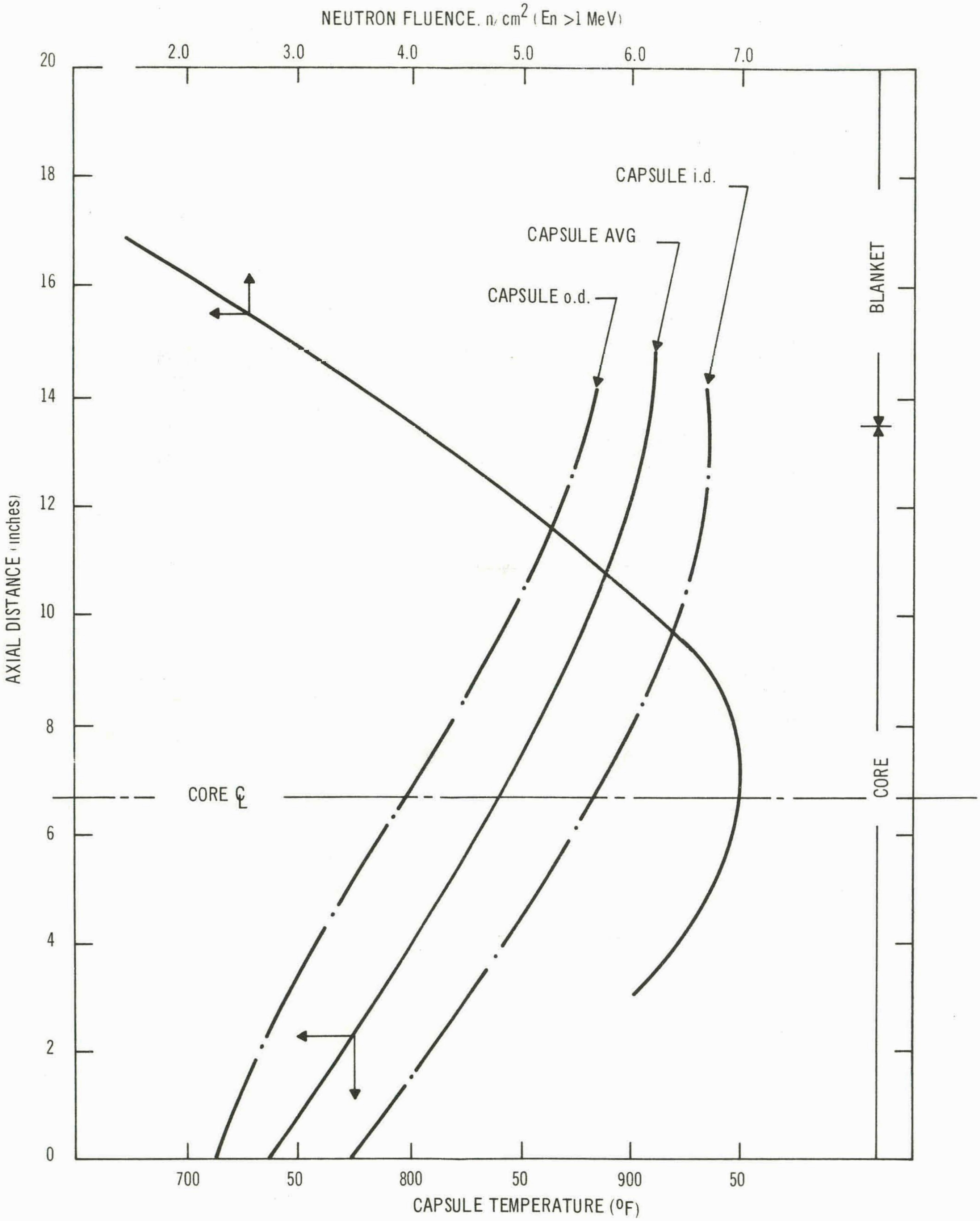

Figure 5-5. Exposure History of F2 Capsule Tubes in EBR-II

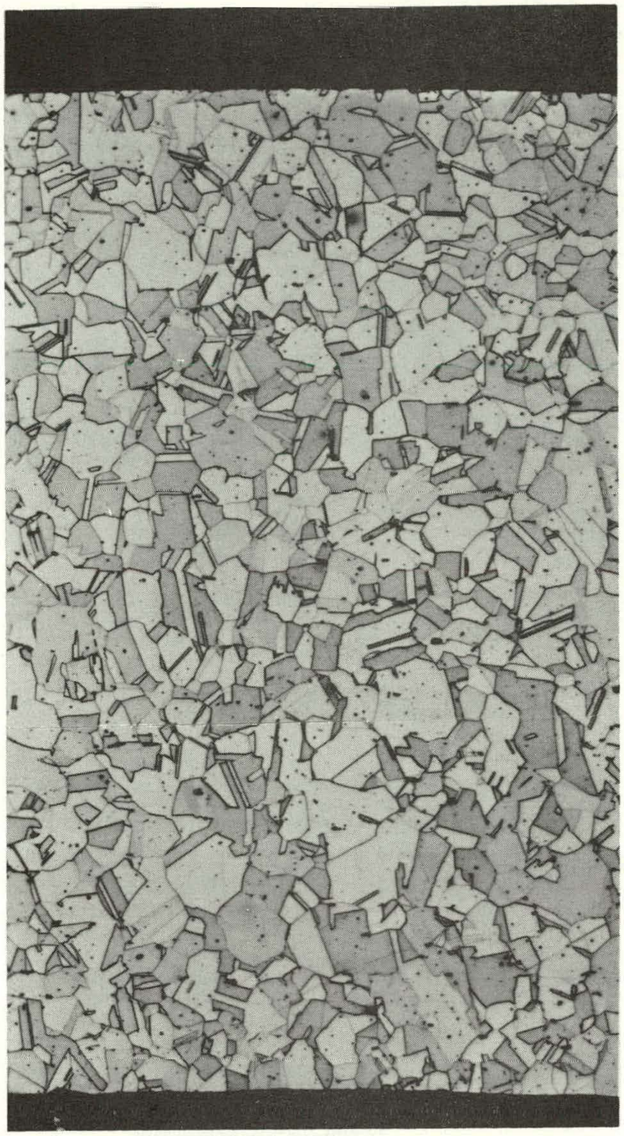

AS—RECEIVED TUBING,
MODIFIED GLYCEREGIA ETCH, 250X

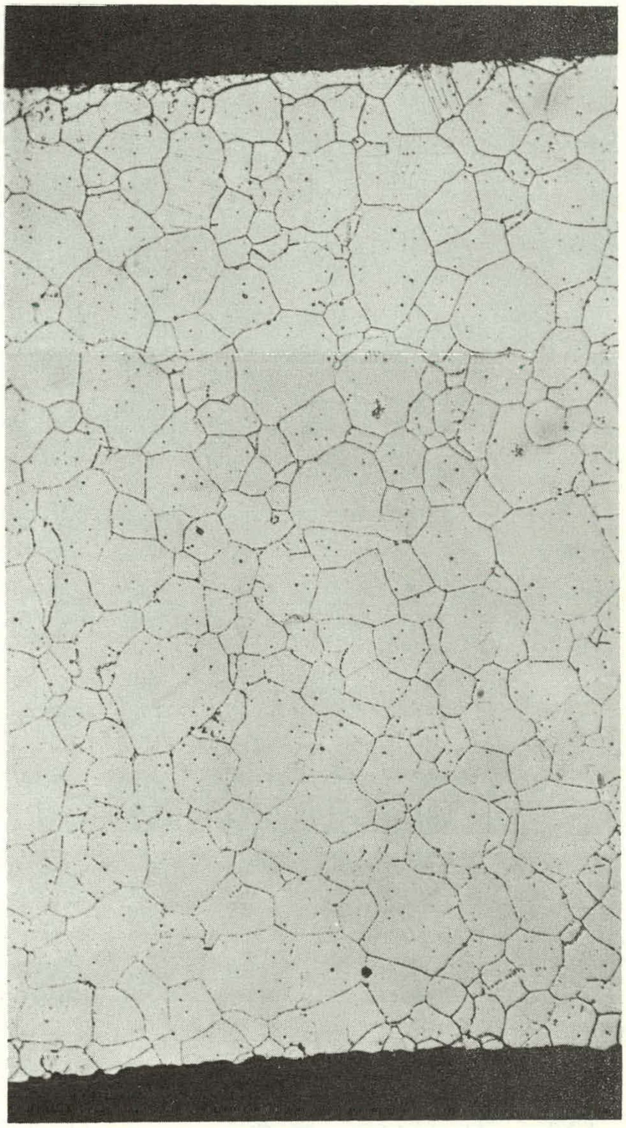

IRRADIATED TUBING
OXALIC ACID ETCH, 250X

IRRADIATED SPECIMEN IS FROM THE
CAPSULE TUBE OF PIN F2Q

Figure 5-6. Microstructure of Type-304 Capsule Tubes Used in FCR Fuels Irradiation Capsule Series F2

TABLE 5-3
CERTIFIED CHEMISTRY OF TYPE-304 CAPSULE TUBE

HEAT NO. 136272

Carbon	0.07	Chromium	18.46
Manganese	1.55	Nickel	9.35
Phosphorus	0.027	Iron	Balance
Silicon	0.48	Sulfur	0.019

In view of the calculated time-temperature history of the specimen during the irradiation test, the degree of sensitization observed is somewhat surprising. However, the fact that the capsule was stored for an extended period of time in reactor ambient sodium (~ 700°F) could account for such an occurrence.

5.2.1 Test Procedure

Test specimens were selected from two locations on the capsule tubes, representing regions of fairly uniform fluence over the length of the specimen: the mid-core or peak flux region, and the blanket region. Additional specimens were selected from the upper and lower core, as necessary to strengthen the data for a given test parameter.

The burst test apparatus used in this investigation is shown schematically in Figure 5-7. It was designed to provide a linear increase in pressure with time, pressure being monitored by recording the output signal of a transducer. The unit is capable of attaining a pressure of 10,000 psi.

Each test specimen was loaded with a solid rod (nominally, 0.325-inch diameter) to reduce the internal volume of the piece, thereby reducing the energy release on failure. The specimens were attached to the pressure line and sealed with "Swagelok" fittings. Specimens were heated in air in a resistance furnace, and stabilized at temperature prior to pressurization.* Specimens were run at a pressurizing rate of 200 psi/min. Burst-testing was performed at 900, 1100, 1300 and 1500°F.

5.2.2 Results and Discussion

Macroscopic examination of the sections after testing revealed that the failures in irradiated tubing, some of which are shown in Figure 5-8, were predominantly lenticular in shape, with crack propagation occurring longitudinally. This configuration suggests that failure occurred along the seam weld. The burst region on unirradiated specimens, on the other hand, was characterized by a severe transverse tearing which, in most cases, completely severed the tube section, as can be seen in Figure 5-9. Detailed metallographic examination of these control tubes showed that failure was not associated with the seam weld. Cross sections of a representative test specimen are shown in Figure 5-10.

The experimental and analytical burst data are listed in Table 5-4 and plotted in Figure 5-11. Thin wall analysis (hoop strength = PD/2t) was applied to convert burst pressure P to hoop or tangential rupture strength. The data show a marked increase in hoop strength with decreasing test temperature, relative to that of the unirradiated controls. In all cases, the specimens irradiated in the core region of EBR-II exhibited higher hoop strength than those exposed in the blanket. Extrapolation of the data shows that the hoop strength of irradiated and control specimens converge at approximately 1600°F, indicating complete recovery at this temperature. This work is in close agreement with that of Holmes and Irvin (Ref. 7), who observed that hardening of Type-304 stainless steel in a fast flux (measured by 0.2% offset yield stress) is stable to 0.67 T_m (~ 1600°F). Recent studies, performed at Argonne National Laboratory (ANL) on Type-304L stainless steel irradiated to 1.4×10^{22} n/cm^2 (total) in EBR-II (Ref. 8,9), show a similar change in rupture strength with test temperature and indicate that irradiation-induced strengthening in this modified alloy is completely removed at approximately 1400°F. This lower recovery temperature may be associated with the higher temperature achieved by the ANL cladding specimens. A comparison of ANL and GE data is shown in Figure 5-12.

The effect of irradiation on the elevated temperature ductility of Type-304 stainless steel is indicated in Figure 5-13. Diametral fracture strain values, calculated from micrometer measurements adjacent to the fracture tip, are listed in Table 5-5. Although the spread in the data is somewhat large, the measurements show a very definite reduction in elevated-temperature ductility with irradiation. The data further show an increase in ductility with test temperature to 1300°F, with an apparent reduction above 1300°F. Although the range of test temperatures was insufficient to establish a minimum ductility temperature, previous work (Ref. 8,9) has shown a minimum ductility at approximately 900°F for irradiated Type-304 stainless steel, with a slight recovery above this temperature. It is

* The time at temperature prior to pressurization was approximately 30 minutes.

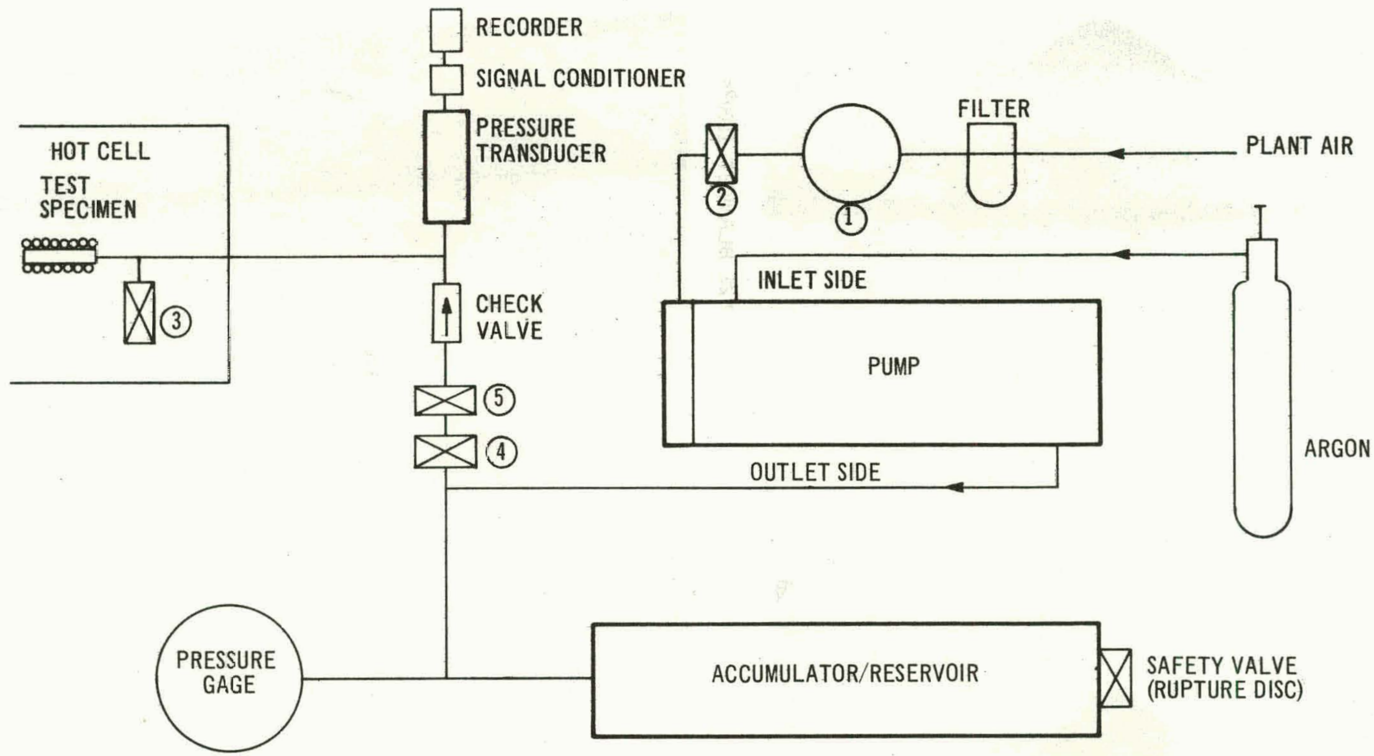

(1) PLANT AIR REGULATOR AND GAGE
(2) PLANT AIR SHUTOFF VALVE
(3) SYSTEM VENT VALVE
(4) SYSTEM SHUTOFF VALVE
(5) METERING VALVE

Figure 5-7. Dynamic Burst Apparatus

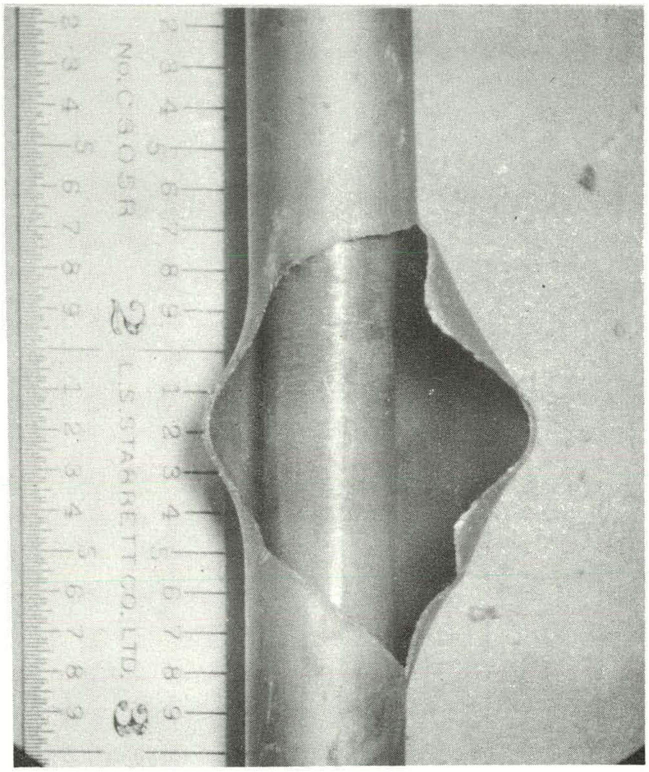

F2E, BLANKET, 1300°F

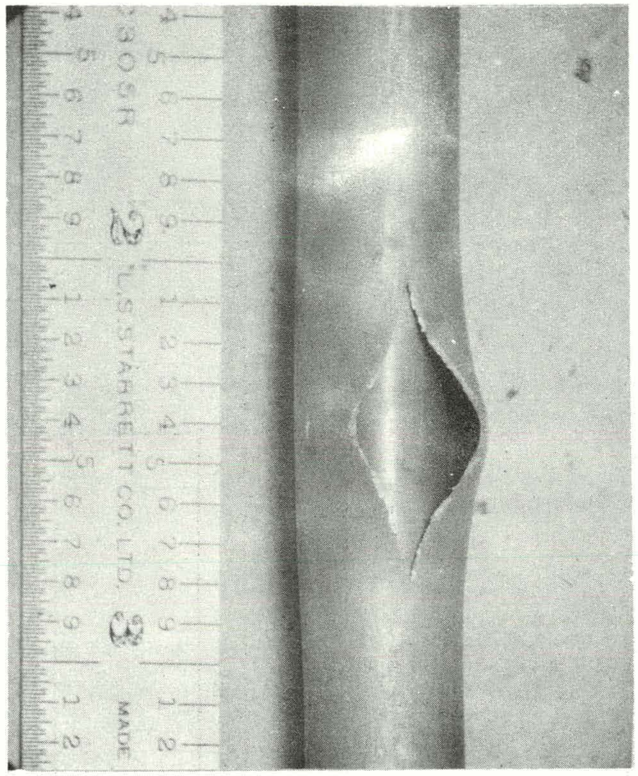

F2S. BLANKET. 1500°F

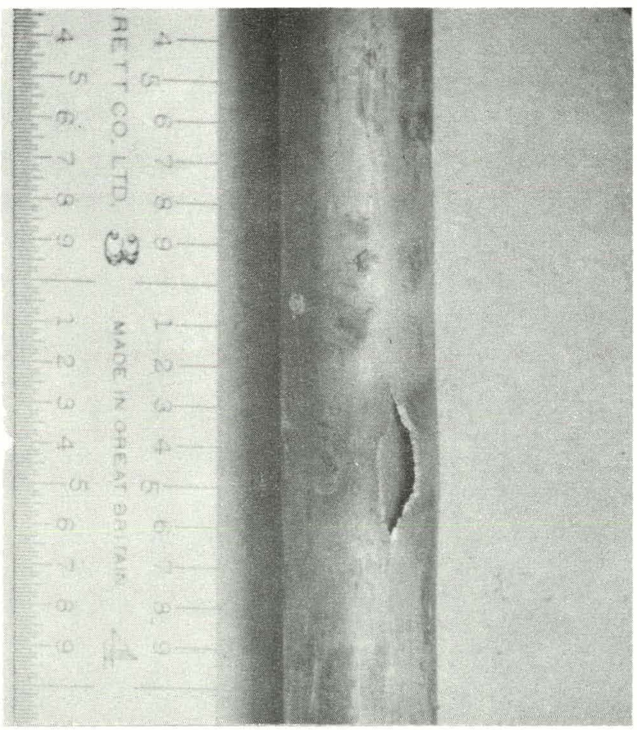

F2E, CORE, 1300°F

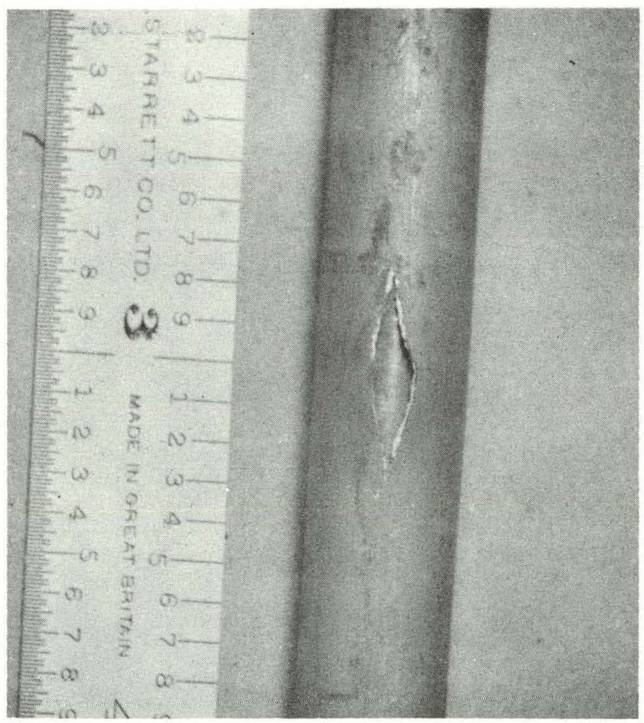

F2S, CORE, 1500°F

Figure 5-8. Rupture Characteristics of Irradiated Type-304 Burst Specimens

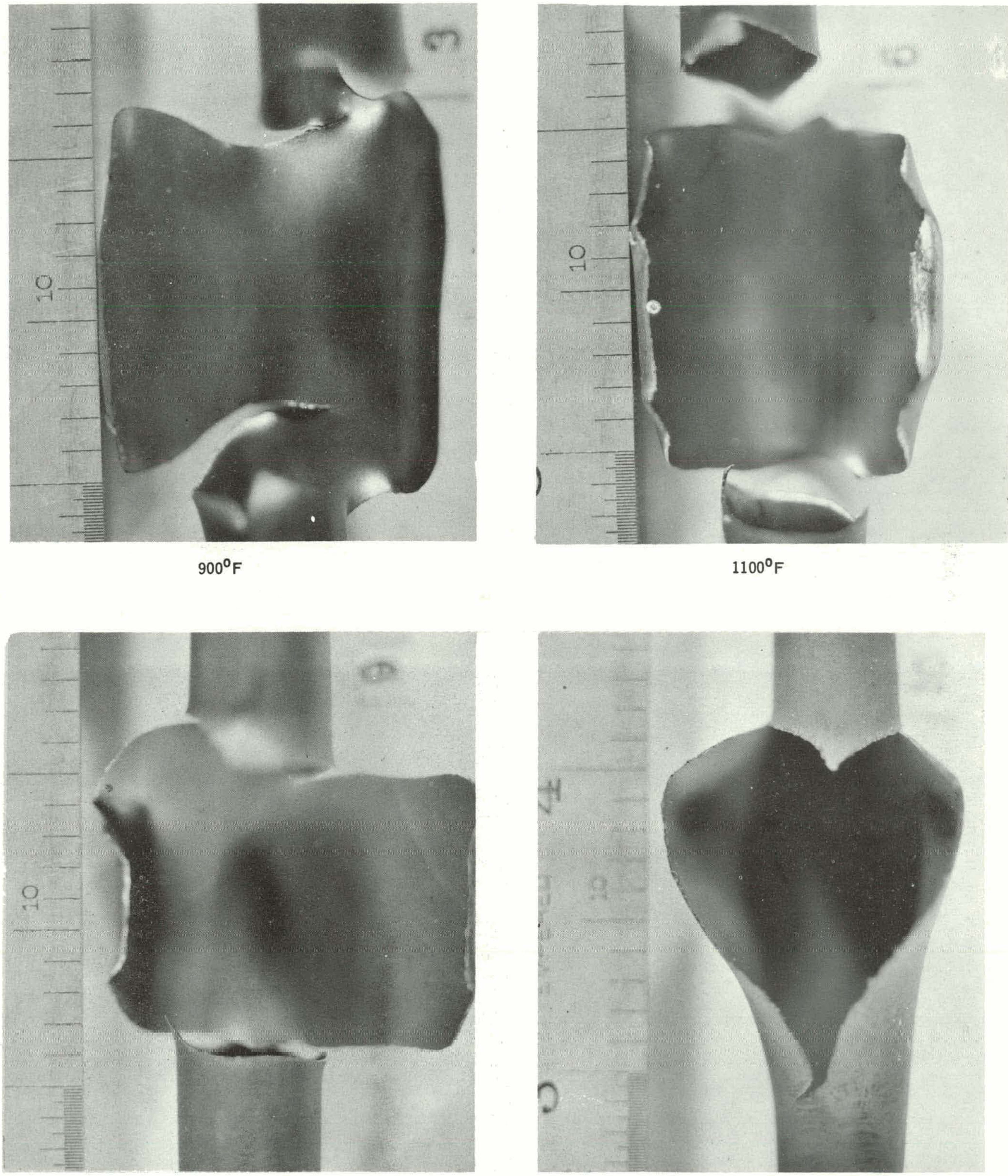

900°F

1100°F

1300°F

1500°F

Figure 5-9. Rupture Characteristics of Unirradiated Type-304 Burst Specimens

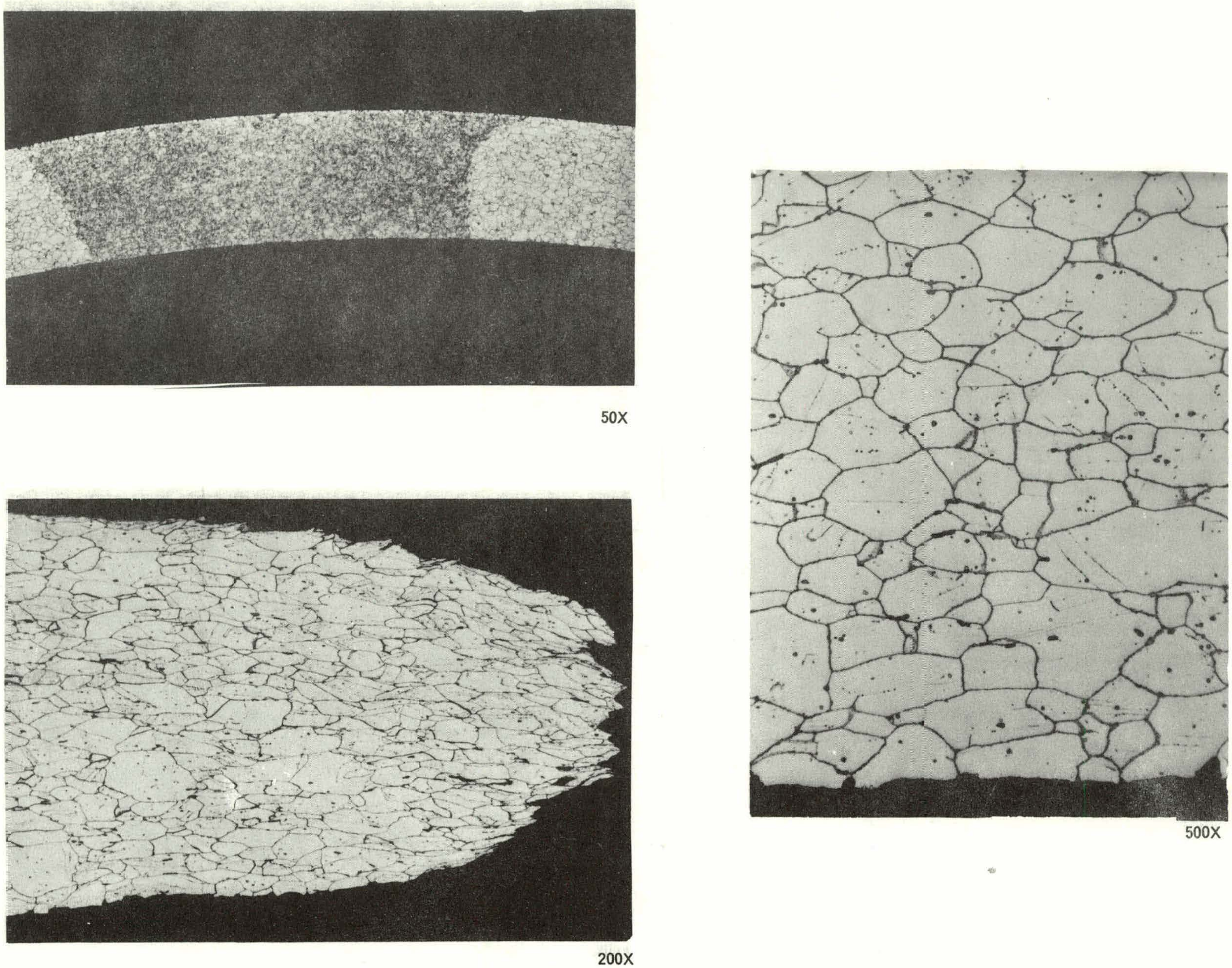

Figure 5-10. Microstructure of Representative Control Specimens, Annealed. Burst Temperature was 900°F

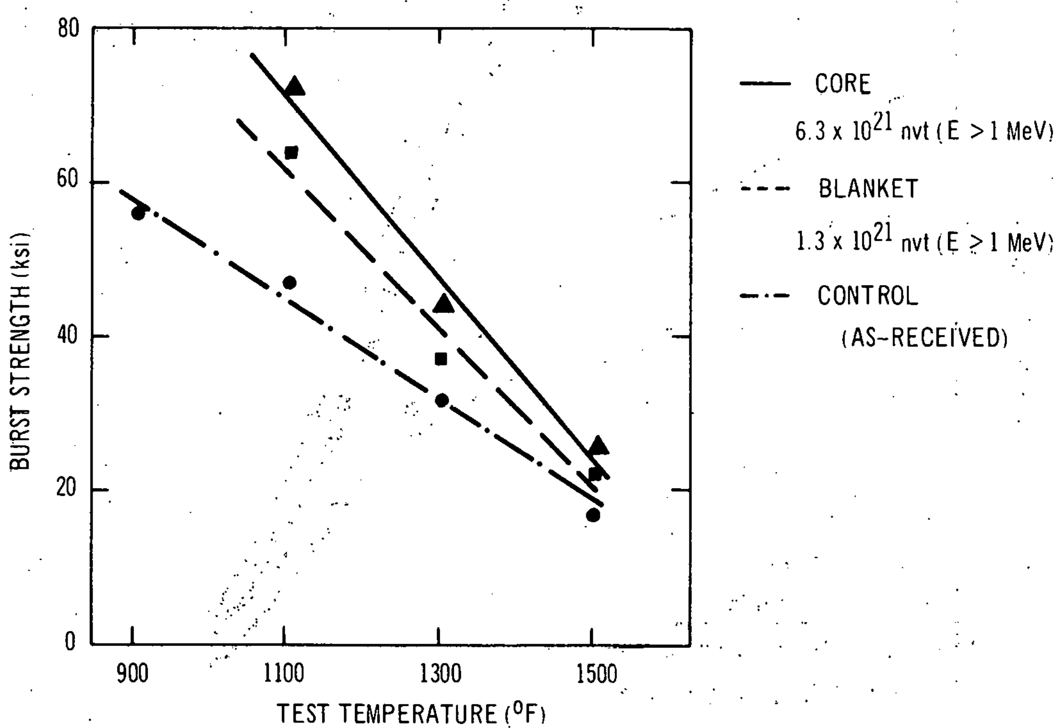

Figure 5-11. Effect of Post-Irradiation Test Temperature on Burst Strength of Type-304 Tubing

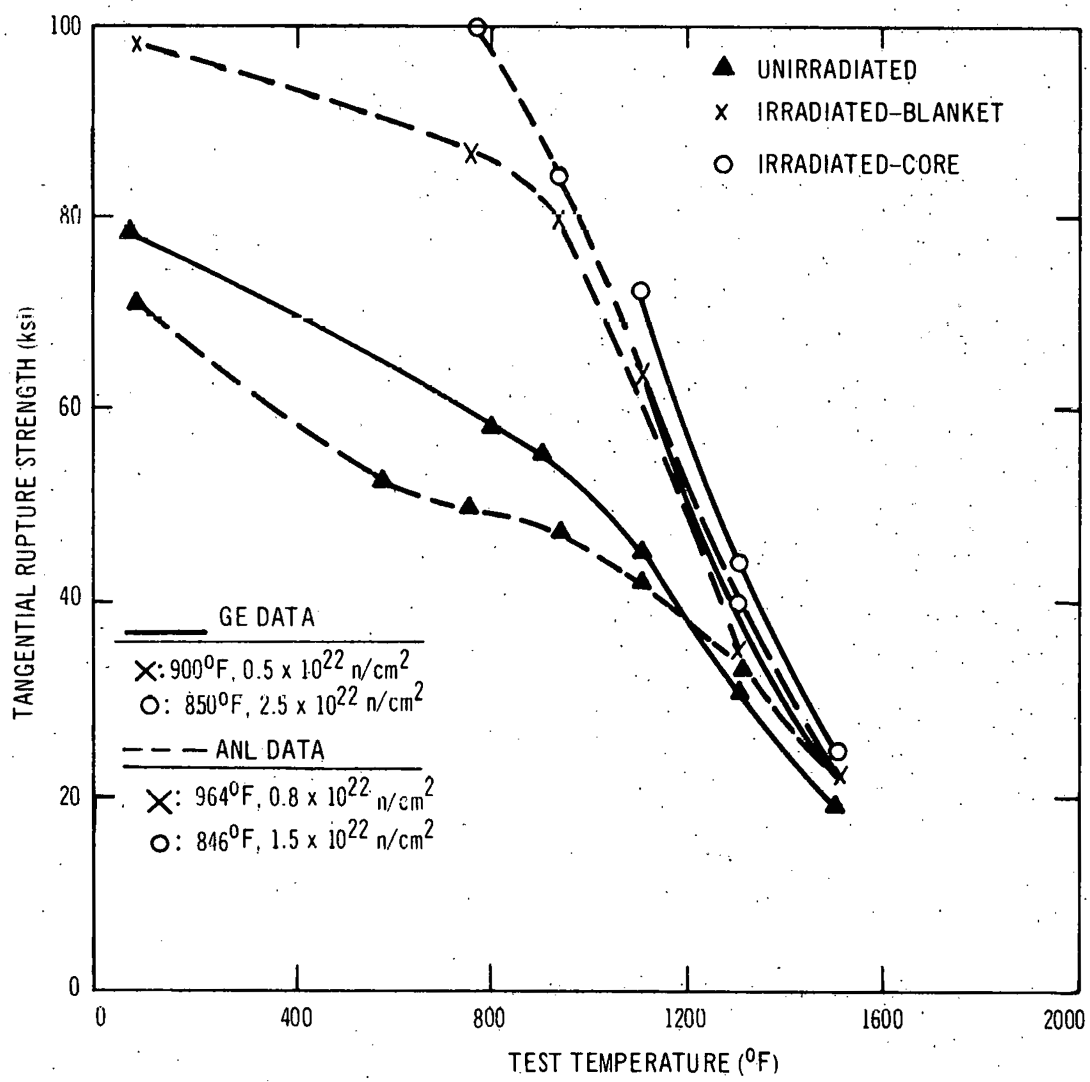

Figure 5-12. Effect of Irradiation on High Temperature Rupture Strength of Type-304 Tubing. Comparison with other data.

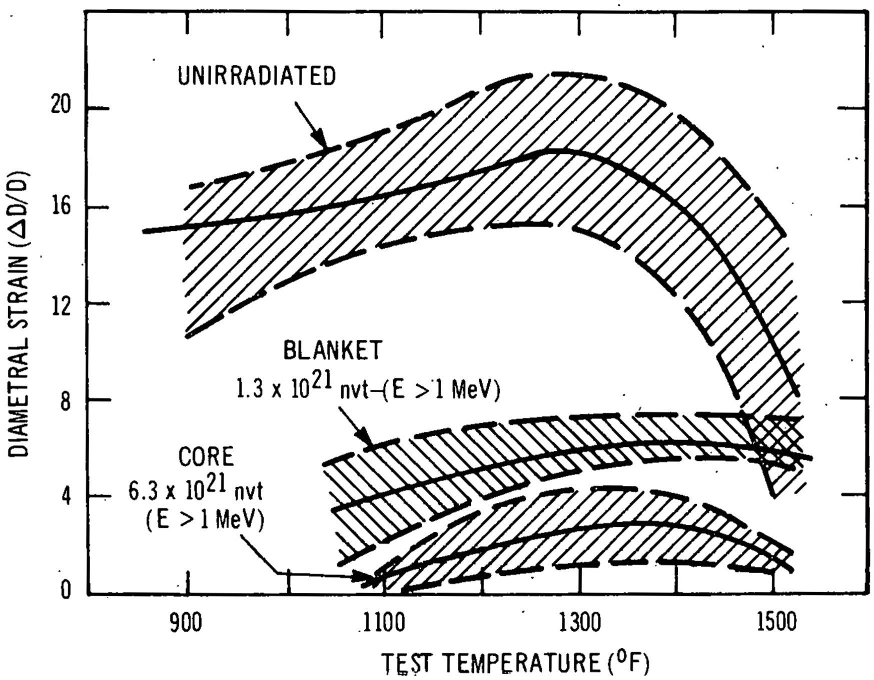

Figure 5-13. Effect of Irradiation on the High-Temperature Ductility of Type-304 Tubing

TABLE 5-4
BURST DATA ON F2 CAPSULE TUBES—IRRADIATED AND CONTROL

Specimen No.	Condition	Test Temperature (°F)	Time to Rupture (min) Core	Time to Rupture (min)	Time to Rupture (min) Blanket	Burst Pressure (psi) Core	Burst Pressure (psi)	Burst Pressure (psi) Blanket	Hoop Strength (psi) Core	Hoop Strength (psi)	Hoop Strength (psi) Blanket
Control 1	As-received	900		28.8			6450			57,000	
Control 2	As-received	900		28.9			6250			55,400	
Control 3	As-received	900		32.3			6250			55,400	
Control A1	Annealed*	900		32.6			6450			57,212	
Control A2	Annealed	900		28.9			5800			51,446	
F2P-X	Irradiated	900	>57.9**			>9235			>81,800		
Control 4	As-received	1100		27.0			5300			47,000	
Control 5	As-received	1100		27.3			5170			45,900	
Control 6	As-received	1100		25.2			5300			47,000	
Control A3	Annealed	1100		19.0			4550			40,358	
Control A4	Annealed	1100		22.0			4800			42,576	
Control 44	As-received	1100		–			5100			45,237	
Control 45	As-received	1100		–			5300			47,011	
Control 46	As-received	1100		–			5300			47,011	
Control 47	As-received	1100		–			5700			50,559	
F2A	Irradiated	1100	25.2		38.5	8020		7000	71,100		62,000
F2B	Irradiated	1100	30.4		42.8	8210		7025	72,800		62,300
F2Y	Irradiated	1100	43.1		21.5	8195		7435	72,700		65,900
Control 7	As-received	1300		16.7			3530			31,300	
Control 8	As-received	1300		17.0			3440			30,500	
Control 9	As-received	1300		18.0			3700			32,800	
Control A5	Annealed	1300		16.7			3300			29,271	
Control A6	Annealed	1300		18.2			3560			31,557	
F2E	Irradiated	1300	23.3		21.1	4735		4060	42,000		36,000
F2U	Irradiated	1300	22.1		21.7	5020		4125	44,500		36,600
F2Z	Irradiated	1300	20.8		22.7	5175		4300	45,900		38,100
Control 10	As-received	1500		9.4			1820			16,100	
Control A7	Annealed	1500		11.5			2300			20,401	
Control A8	Annealed	1500		10.9			2280			20,224	
Control 48	As-received	1500		–			2380			21,106	
Control 49	As-received	1500		–			1950			17,296	
F2N	Irradiated	1500	10.5		15.2	2910		2530	25,800		22,400
F2P	Irradiated	1500	16.3		12.2	2860		2435	25,400		22,000
F2S	Irradiated	1500	11.0		14.2	2660		2535	23,600		23,000

* 74 days at 1000°F in air.
** Specimen did not burst at pressure limit of equipment.

TABLE 5-5
POST-BURST DIAMETRAL CHANGES IN CONTROL AND IRRADIATED TYPE-304 TUBING

Specimen No.	Position(a)	Temperature (°F)	D_{Top}(b) (in.)	D_{Bottom} (in.)	D_{Avg} (in.)	ΔD (in.)	$\Delta D/D_o$ (%)
1	Control	900	0.433	–			
2	Control		0.438	–			
3	Control		0.432	–	0.431	0.056	14.9
A1	Annealed Control		0.436	–			
A2	Annealed Control		0.433	0.415			
F2A-2	Core	1100	–	0.380			
F2B-2	Core		–	0.376	0.377	0.002	0.5
F2Y-2	Core		0.375	0.376			
F2A-4	Blanket		0.396	0.400			
F2B-4	Blanket		–	0.389	0.390	0.015	4.0
F2Y-4	Blanket		0.386	0.379			
4	Control		0.447	0.431			
5	Control		0.442	0.442			
6	Control		0.432	–	0.437	0.062	16.5
A3	Annealed Control		0.428	–			
A4	Annealed Control		0.438	–			
F2E-2	Core	1300	–	0.383			
F2U-1B	Core		–	0.391			
F2Z-2	Core		0.388	0.379	0.385	0.010	2.7
F2E-4	Blanket		0.397	0.406			
F2U-4B	Blanket		0.394	–	0.397	0.022	5.9
F2Z-4	Blanket		0.394	0.392			
7	Control		0.437	-			
8	Control		0.451	0.443	0.443	0.068	18.1
9	Control		0.442	0.456			
A5	Annealed Control		0.440	–			
A6	Annealed Control		0.431	–			
F2N-2	Core	1500	–	0.378			
F2P-2	Core		0.380	0.380	0.380	0.005	1.3
F2S-2	Core		0.378	0.383			
F2N-4	Blanket		0.389	0.400			
F2P-4	Blanket		0.395	0.395	0.397	0.022	5.9
F2S-4	Blanket		0.402	0.402			
10	Control		0.434	–	0.414	0.039	10.4
A7	Annealed Control		0.400	0.425			
A8	Annealed Control		0.412	0.390			

(a) Core fluence was 2.5×10^{22} total n/cm^2.
Blanket fluence was 0.5×10^{22} total n/cm^2.

(b) Diametral measurements were made above and below the fracture region, at a point ½-inch from the crack tip.

perhaps significant, in this regard, that no substantial radiation damage recovery could be detected in these tests, although all specimens were held at the test temperature for 30 minutes prior to the application of pressure.

The bulk of the fast flux radiation damage work to date is restricted to a narrow band, roughly encompassing an exposure level of 10^{21} to 10^{22} nvt (E ⩾ 1 MeV), but is sufficient to indicate trends in the effect of accumulated fast neutron irradiation on the strength of Type-304 stainless steel. This effect is shown graphically in Figure 5-14. The three curves represent data collected at the three given post-irradiation test temperatures. The reduction in slope of the curves with increasing test temperature is further evidence of the trend toward recovery.

5.3 TENSILE EVALUATION

The irradiated tensile coupons described in subsection 4.2 were uniaxially tested on a universal testing machine at temperatures from 900 to 1500°F at strain rates from 0.0002 inch/inch-min to 0.02 inch/inch-min. The tensile results are included in Table 5-6 for the five austenitic stainless steels in both pre-irradiation conditions, annealed at 1800°F for 15 minutes, and annealed at 1800°F for 15 minutes plus 1650°F for 24 hours. Tensile tests were generally performed in duplicate, subsequent to a 15-minute soak at temperature. The data are graphically presented in Figures 5-15 to 5-26.

5.3.1 Properties of Alloys in the Mill-Annealed Condition

Within the fluence range investigated (1.3-6.3 X 10^{21} n/cm^2; En ⩾ 1 MeV), irradiation-induced strengthening, measured by 0.2% offset yield strength, increases from a low of 40% (Type 321) to as high as 147% (Type 304) (Figure 5-15). Type 304 showed the greatest amount of strengthening at elevated temperature followed, in decreasing order, by Types 316, 321, 347, and Incoloy-800.

The degree of strengthening is reduced with increasing test temperatures, with full recovery of unirradiated properties at 1500 to 1600°F (Figures 5-17 through 5-20). An anomalous behavior was observed with Incoloy-800 (Figure 5-21).

Irradiation-induced embrittlement, monitored by percent reduction in total tensile strain, is similar for all candidate cladding alloys (Figure 5-16). The percentage loss in ductility ranges from 70 to 83% at the lower fluence, to 82 to 98% at 6.7 X 10^{21} n/cm^2 (En > 1 MeV). (Irradiation embrittlement of 100% indicates nil ductility.)

All alloys showed a general loss in post-irradiation ductility with increasing test temperature (Figures 5-17 through 5-21), while comparable data for unirradiated materials generally increase over the temperature range of 900 to 1500°F. Note that while recovery of yield stress was obtained at test temperatures of 1500 to 1600°F, no such restoration of ductility occurred.

Reducing the strain rates produces a corresponding reduction in total tensile strain and yield strengths of these irradiated alloys (Figures 5-22 through 5-26). Unirradiated material shows this general behavior at strain rates below 0.02 min^{-1}. For the limited strain rate range investigated on irradiated alloys (0.02 to 0.0002 min^{-1}), Type 316L was least sensitive to strain rate effects within experimental error. The response of ductility to strain-rate changes was similar for Types 304, 321, 347, and Incoloy-800. Types 304 and 316L indicated higher ductilities than the other candidate alloys, but the differences are not statistically supported at present.

Both optical and electron metallographic techniques have been used to elucidate differences observed in the mechanical properties of Type-304 tensile specimens irradiated in these capsules. Two tensile specimens, tested at 1300°F, were selected for examination. Both were mill-annealed (1800°F for 15 min) prior to irradiation but tested at different strain rates (0.02 and 0.0002 min^{-1}). The examination showed that incipient cracking occurred with the tensile specimen tested at 0.002 min^{-1} (Figure 5-27a). Both surface and internal grain-boundary cracking was observed throughout the gage section as far away from the fracture surface as 0.4 inch. The failure was intergranular, and it appeared that two opposite surface cracks, located near each other, converged, causing fracture. The general structure was sensitized, with no grain growth anywhere along the sample. The specimen tested at 0.02 min^{-1} (Figure 5-27b) also showed edge cracking at grain boundaries, as well as internal triple-point cracking which was localized near the failure. Again, no grain growth was observed, and the structure was sensitized.

These observations are consistent with the expected deformation behavior of this material at comparable strain rates. As shown in Figure 5-28, at 0.02 min^{-1} the stress increases beyond plastic yielding until failure occurs. However, at 0.0002 min^{-1} the yield stress and ultimate stress coincide; the stress then continuously decreases with strain, until the fracture strain is attained. Time-dependent propagation of these cracks, in effect, reduces the sample's load-bearing capacity, resulting in reduced loads with further deformation. However, the stress at the crack's tip or at the reduced internal section is increasing slowly.

Recent transmission electron microscopy studies at GE (Ref. 10,11) showed evidence of polyhedral cavities in irradiated austenitic stainless steels; these cavities were correlated with measured density changes in these materials. In Figure 5-29 is a transmission electron micrograph from the gage length of a failed tensile coupon of mill-annealed and irradiated Type 304 which shows similar cavities. Also visible in the figure are dislocations which have interacted with the cavities, forming jogs and intersections. There appears to be a slight denudation of cavities near the grain boundary. Other micrographs show dislocations interconnected with cavities. It is believed that the observed

TABLE 5-6
POST-IRRADIATION TENSILE PROPERTIES OF AUSTENITIC STAINLESS STEEL

Alloy	Structure	Fluence, E>1 MeV ($n/cm^2 \times 10^{21}$)	Temperature (°F)	Strain Rate (min^{-1})	Uniform[a] Strain (%)	Total[a] Strain (%)	Yield Stress (0.2%, ksi)	Ultimate Stress (ksi)
Type 304	Mill-Annealed[b]	1.3	1300	0.01	4.4–6.8	4.9–7.0	19.4–26.9	34.3–35.8
		1.3	1300	0.02	7.1–7.8	12.6–12.9	27.8–28.4	34.3–34.7
		6.7	1300	0.02	3.3–3.8	5.2–8.3	36.0–38.4	40.7–41.0
		6.2	1300	0.0002	0.4–0.5	4.1–5.6	24.0–27.2	24.2–27.2
		6.7	1100	0.02	3.3–3.4	4.2–4.4	54.8–54.9	57.1–58.6
		6.7	1500	0.02	1.2–1.5	3.6–4.8	19.3–19.3	19.9–20.1
Type 304	Carbide-Agglomerated[c]	0.22	1300	0.02	7.6–9.0	15.1–15.6	25.3–27.8	32.6–33.8
		0.76	1300	0.02	7.7–8.0	10.5–11.0	26.4–28.7	35.6–37.9
		2.4	1300	0.02	10.7–12.4	12.1–14.2	16.4–16.7	26.8–28.6
		3.0	1300	0.02	13.4	18.0	16.2	26.4
		2.5	1100	0.02	22.2	23.0	15.3	39.5
		3.0	1100	0.02	15.5	16.8	17.5	39.2
Type 316L	Mill-Annealed	1.3	1300	0.02	4.0–7.1	6.4–9.1	30.1–39.2	39.5–44.3
		1.3	1300	0.02	4.6–9.4	7.6–12.3	22.5–32.0	32.6–37.5
		6.7	1300	0.02	3.1–4.6	4.4–7.7	39.9–41.7	44.1–47.3
		6.7	1300	0.02	3.8	6.4	35.1	39.7
		6.2	1300	0.0002	0.1–0.4	5.2–7.3	25.7–28.3	26.0–28.3
		6.7	1100	0.02	5.4–6.5	6.1–7.4	49.4–56.7	62.0–67.0
		6.7	1100	0.02	8.8	10.9	36.1	53.9
		6.2	1500	0.02	1.3	6.0	24.1	24.5
Type 316	Carbide-Agglomerated	0.30	1300	0.02	6.1–6.3	8.9–11.2	21.4–27.3	35.5–36.3
		0.96	1300	0.02	5.5–6.7	9.9–11.0	38.1–38.7	43.1–43.4
		3.10	1300	0.01	1.9–3.7	2.1–3.9	30.7–32.7	36.7–37.3
		3.30	1300	0.02	5.7	7.1	19.0	31.2
		3.90	1300	0.01	1.6	2.1	43.8	49.0
		3.90	1300	0.02	1.7	2.1	29.8	41.1
		3.30	1300	0.0002	0.4–1.0	12.5–14.3	20.6–24.2	20.9–24.2
		3.10	1100	0.02	11.6–20.9	15.4–22.1	15.9–51.3	43.0–62.7
		3.30	1100	0.02	11.3	15.0	18.5	52.7
Type 321	Mill-Annealed	1.3	1300	0.02	4.6–4.7	9.1–9.4	34.7–35.1	37.7–38.0
		1.3	1300	0.02	1.9–2.4	5.8–7.1	32.0–34.5	33.1–35.4
		6.7	1300	0.02	1.2–1.5	1.6–2.5	35.1–36.6	36.6–38.0
		6.7	1300	0.0002	0.2–0.3	0.2–0.4	21.5–24.3	21.5–24.3
		6.7	1100	0.02	2.0–4.4	2.2–5.4	59.8–62.0	63.0–68.0

TABLE 5-6, (Continued)
POST-IRRADIATION TENSILE PROPERTIES OF AUSTENITIC STAINLESS STEEL

Alloy	Structure	Fluence, E>1 MeV ($n/cm^2 \times 10^{21}$)	Temperature (°F)	Strain Rate (min^{-1})	Uniform[(a)] Strain (%)	Total[(a)] Strain (%)	Yield Stress (0.2%, ksi)	Ultimate Stress (ksi)
Type 321	Carbide-Agglomerated	0.76	1300	0.02	6.6–6.9	14.8–15.2	23.8–25.2	28.9–30.4
		3.0	1300	0.02	2.2–2.7	5.3–5.8	27.4–31.9	29.3–34.6
		2.5	1100	0.02	1.7–1.7	2.6–3.1	57.4–57.7	59.8–60.3
		2.4	1500	0.02	2.0–2.4	9.8–10.1	14.1–14.4	15.2–15.6
Type 347	Mill-Annealed	1.3	1300	0.02	4.0–4.1	6.8–7.3	33.1–33.5	39.2–40.7
		6.2	1300	0.02	0.7	1.4	43.8	44.2
		6.7	1300	0.01	0.9	1.0	40.5	44.5
		6.2	1300	0.0002	0.5–0.6	0.7–1.1	24.8–28.8	25.8–29.0
		6.2	1100	0.02	1.4–1.5	2.2–2.6	60.1–62.1	61.4–63.4
		6.2	1500	0.02	0.9	4.3	18.2	18.8
Type 347	Carbide-Agglomerated	0.22	1300	0.02	11.2–11.4	26.6–32.2	22.4–23.1	31.6–31.9
		0.76	1300	0.02	2.0–8.2	5.0–10.0	19.9–31.1	29.9–32.2
		3.0	1300	0.02	8.1–8.6	10.3–11.8	21.4–21.9	29.4–29.8
		2.5	1100	0.02	8.1–8.3	9.4–10.5	39.6–41.3	47.6–48.1
		2.4	1500	0.02	3.8–4.1	8.9–10.2	13.0–13.2	15.4–15.7
Incoloy-800	Mill-Annealed	1.3	1300	0.02	3.2–4.5	6.6–8.8	34.8–42.0	39.0–43.3
		1.3	1300	0.02	3.0–3.8	4.3–4.9	41.0–44.3	45.1–48.5
		6.2	1300	0.01	0.7–0.8	0.8–1.3	–	–
		6.2	1300	0.02	0.7–2.7	4.5–5.8	38.7–40.7	40.3–41.0
		6.7	1300	0.01	2.0–3.3	2.2–3.9	–	–
		6.2	1300	0.0002	0.2–0.4	1.6–3.2	25.7–27.3	26.1–27.7
		6.7	1100	0.01	2.1–2.2	2.3–2.6	23.3–25.3	50.1–50.7
		6.7	1500	0.01	1.1–1.1	3.5–5.4	8.5–9.2	9.0–10.9
Incoloy-800	Carbide-Agglomerated	0.76	1300	0.02	2.6–3.2	5.3–8.9	35.3–38.6	37.8–41.0
		3.0	1800	0.02	1.6–2.8	3.6–4.4	35.9–36.1	37.5–42.8
		2.4	1300	0.0002	0.4–0.9	6.3–7.9	19.6–34.9	19.6–36.9
		3.0	1300	0.0002	0.5	8.2	31.0	31.3
		3.0	900	0.02	9.2	10.7	53.1	74.5
		2.5	1100	0.02	2.4–2.5	2.7–3.1	60.4–63.1	67.5–70.2
		2.4	1500	0.02	1.0–1.6	9.6–10.5	15.4–16.5	15.8–17.0

(a) Original gage length: 1 inch.
(b) Annealed at 1800°F for 15 minutes, air quenched.
(c) Annealed at 1800°F for 15 minutes, air quenched; heat-treated at 1650°F for 24 hours, air quenched.

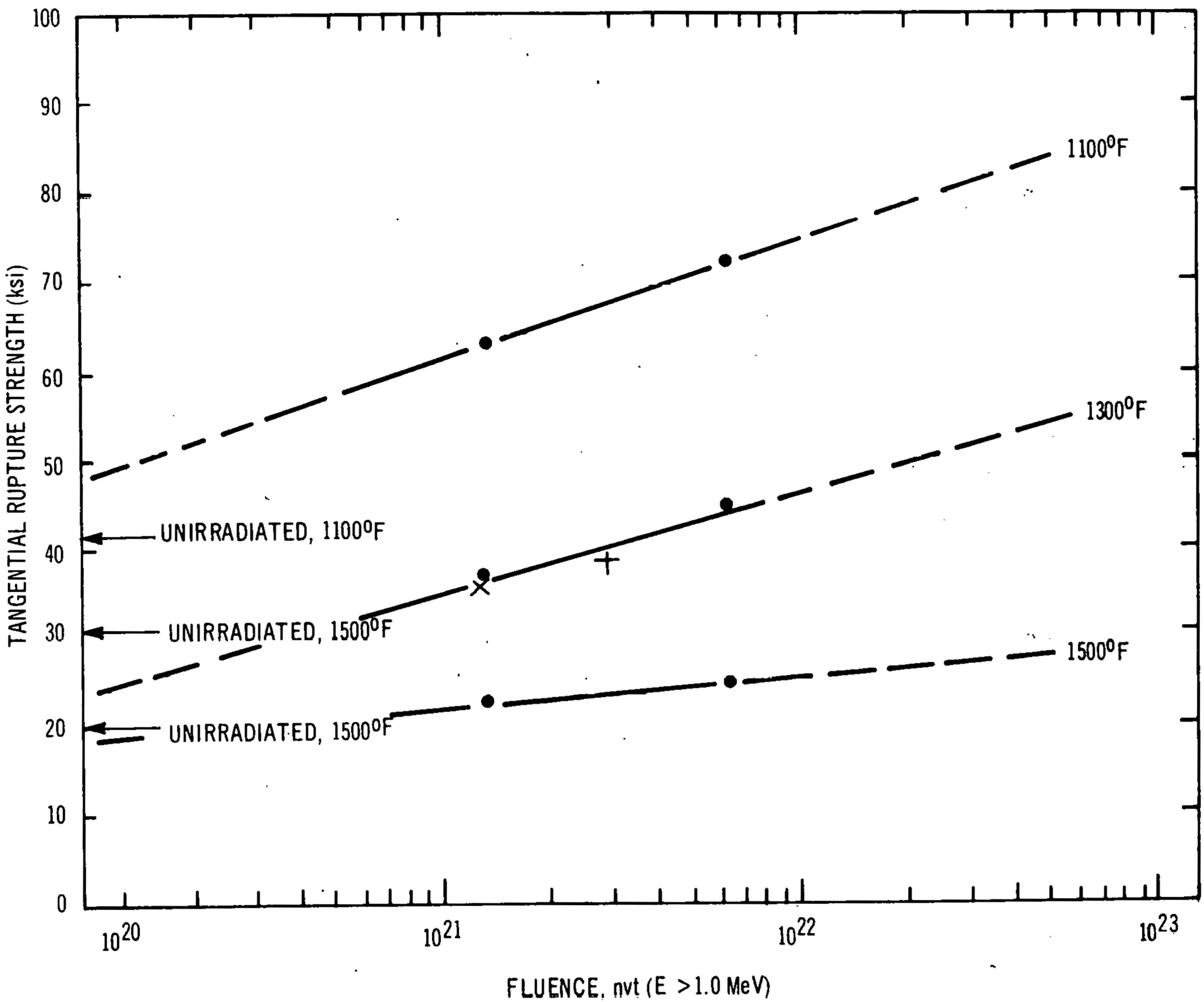

Figure 5-14. Effect of Fluence and Test Temperature on Rupture Strength of Type-304 Tubing

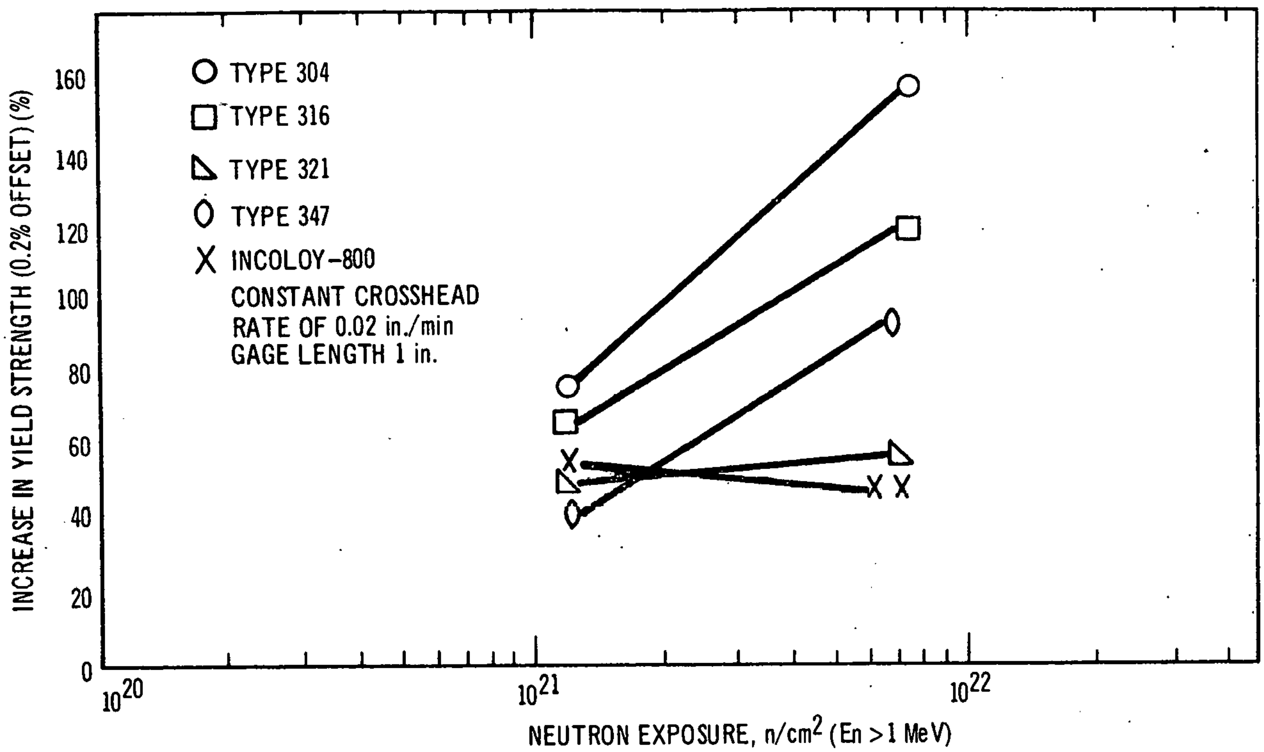

Figure 5-15. Radiation Strengthening of Austenitic Stainless Steel at 1300°F versus Fluence

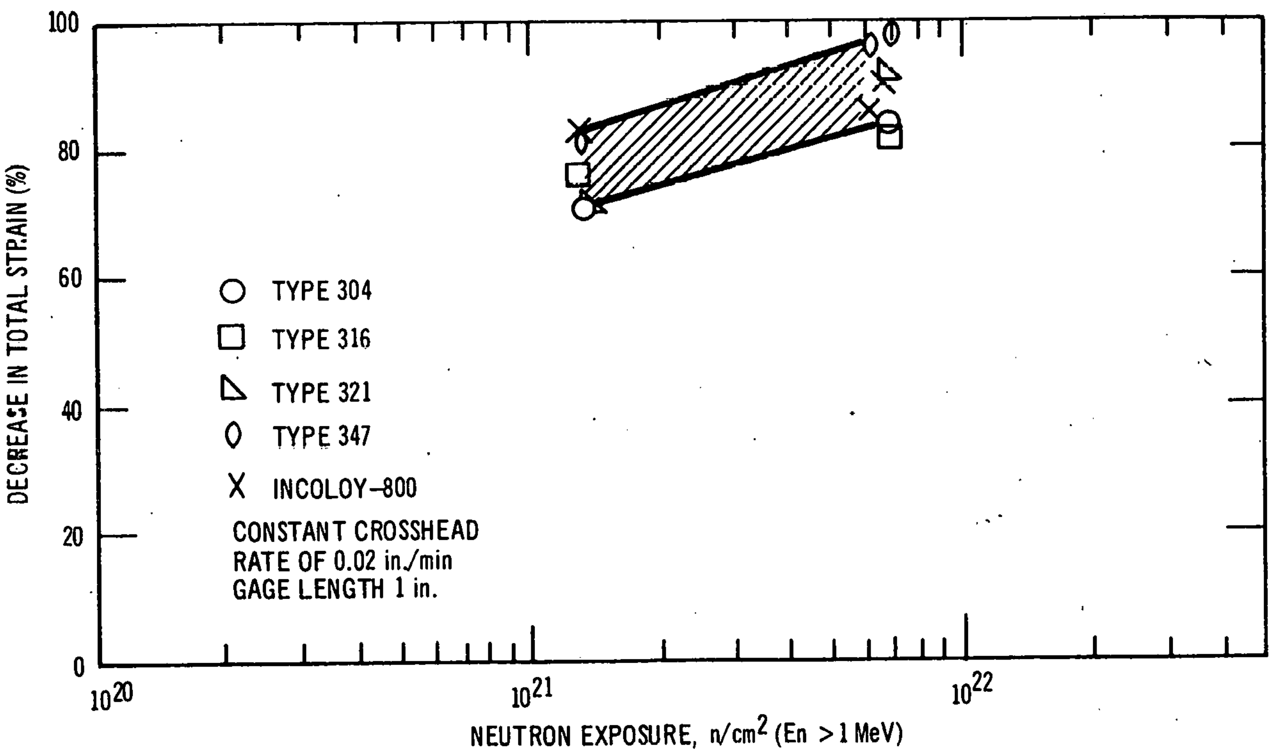

Figure 5-16. Radiation Embrittlement of Austenitic Stainless Steel at 1300°F versus Fluence

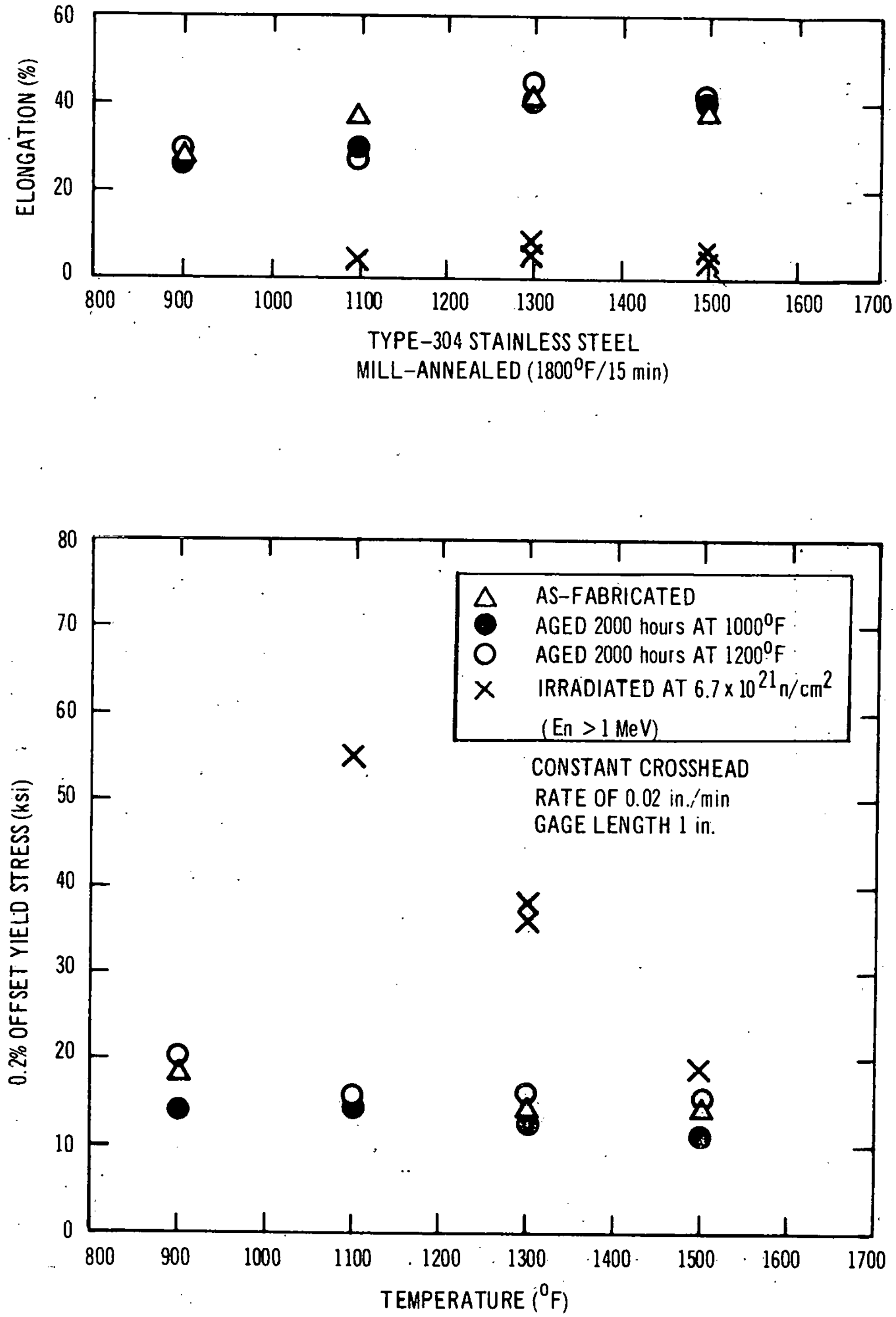

Figure 5-17. Temperature Dependence of Type 304 Tensile Properties

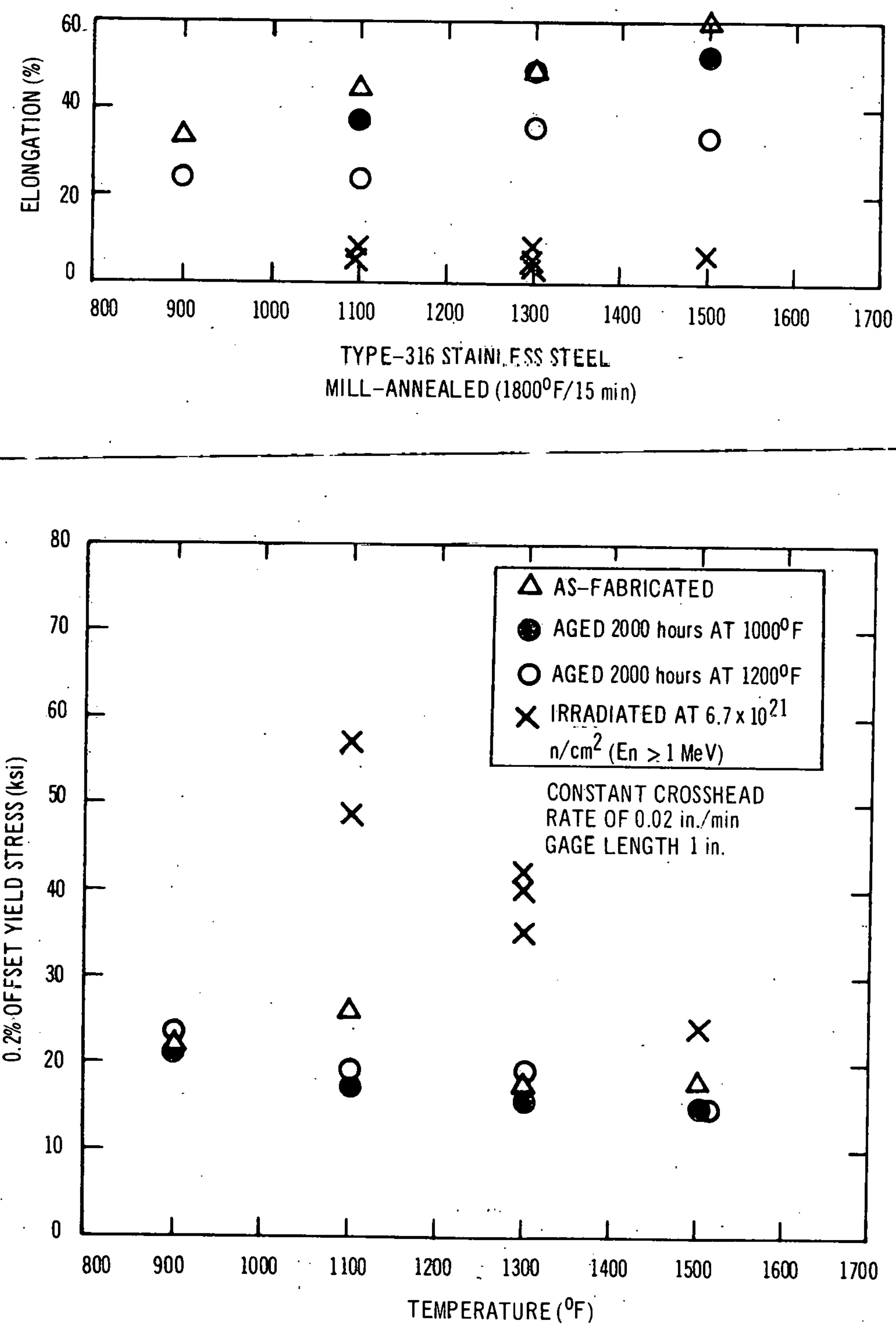

Figure 5-18. Temperature Dependence of Type 316L Tensile Properties

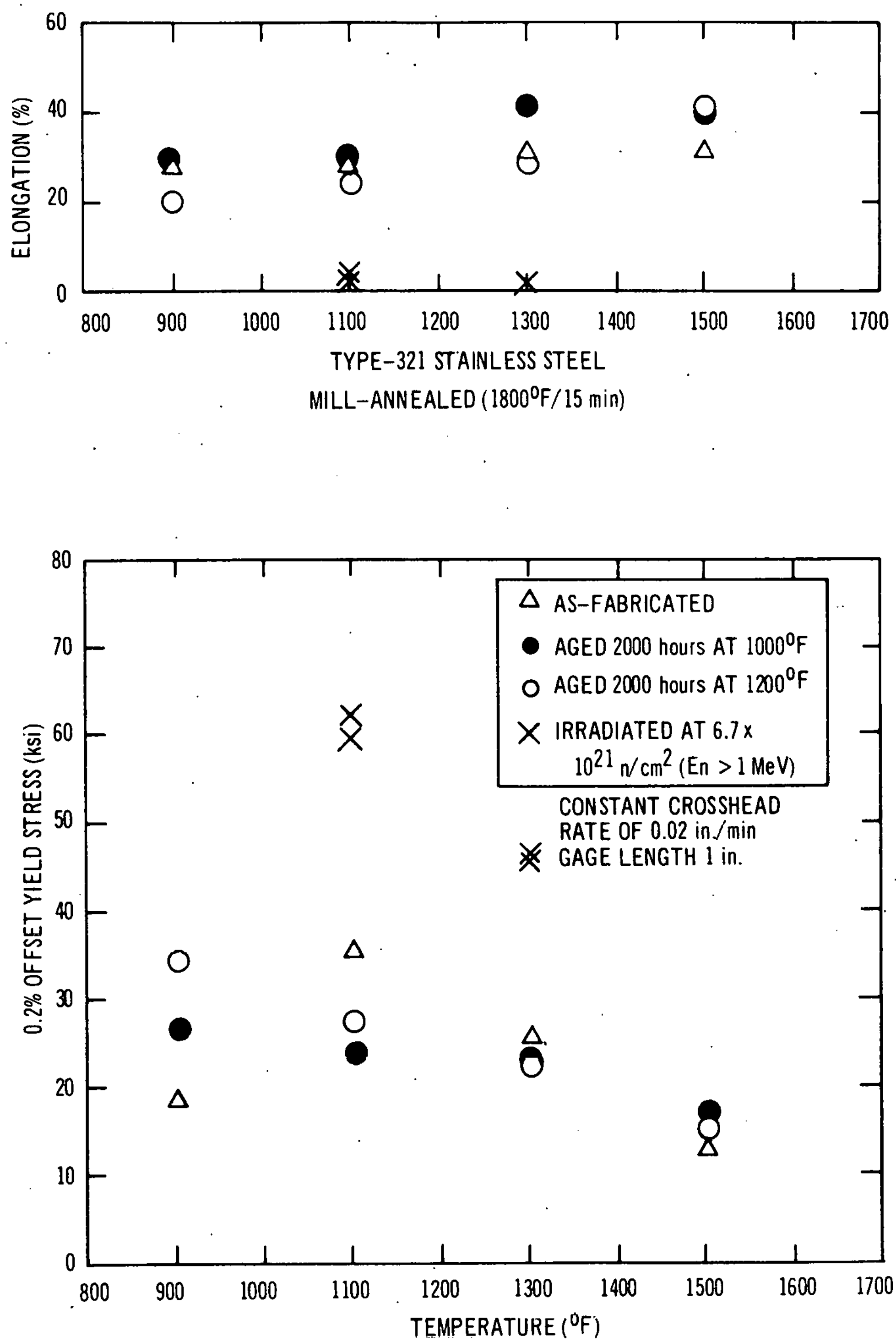

Figure 5-19. Temperature Dependence of Type 321 Tensile Properties

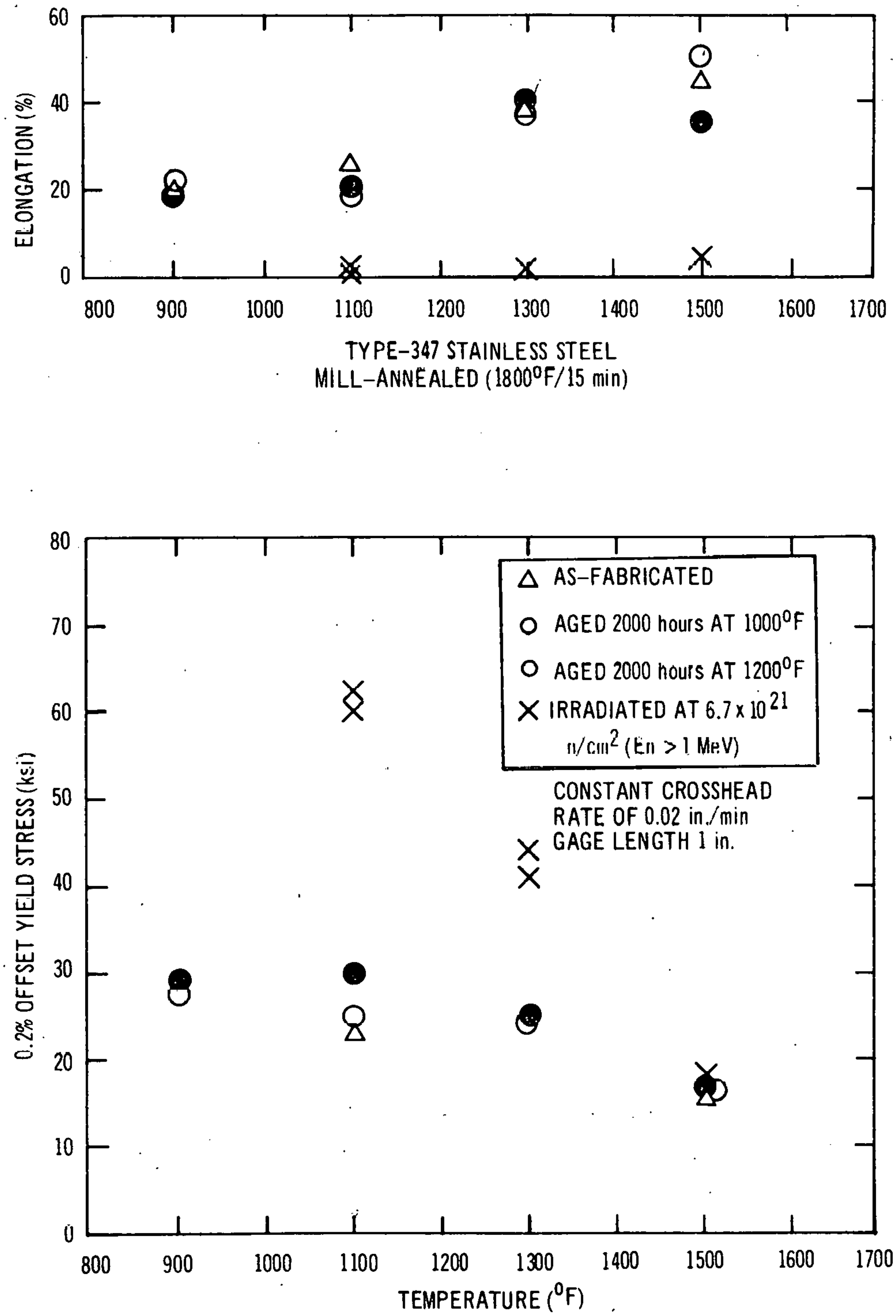

Figure 5-20. Temperature Dependence of Type 347 Tensile Properties

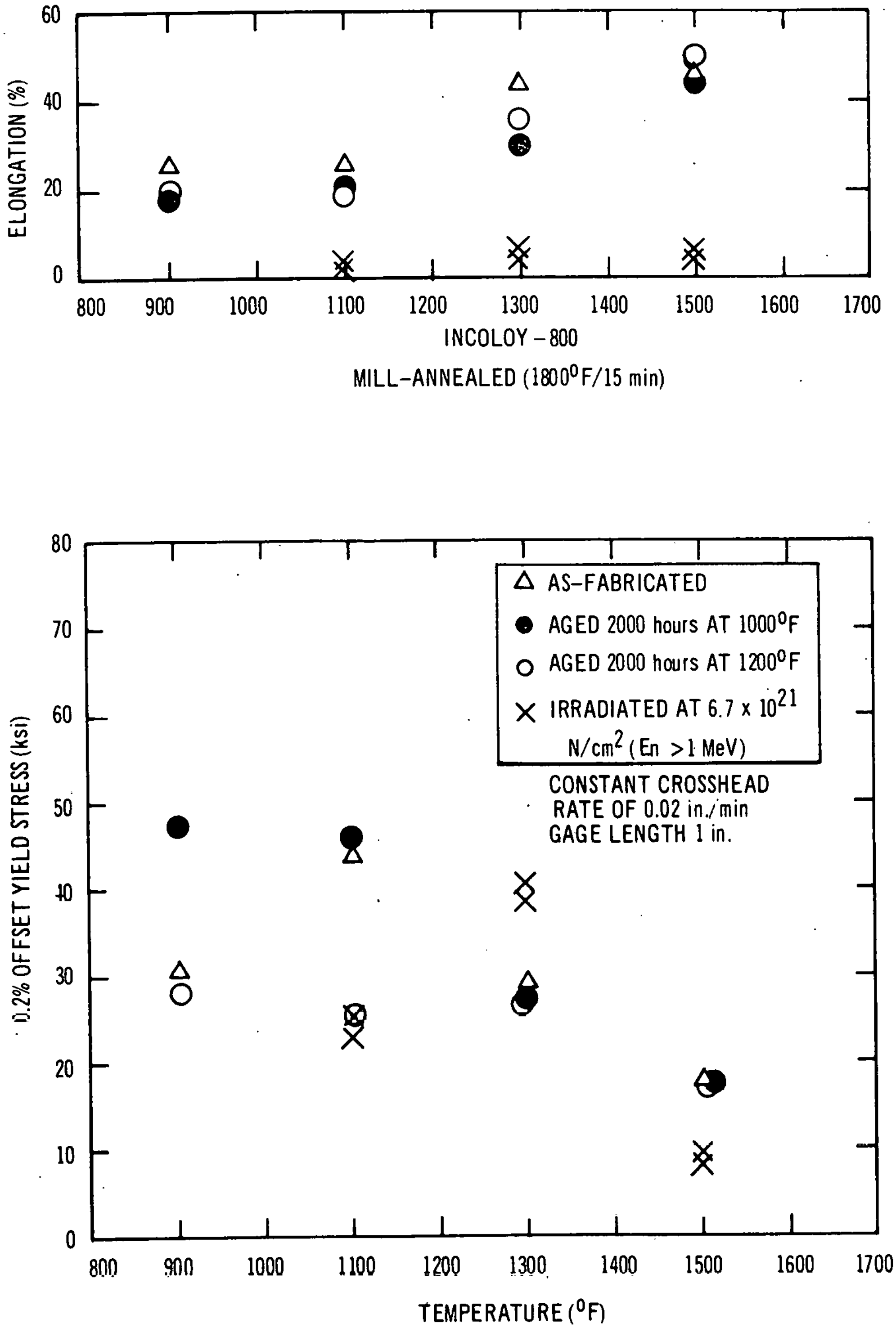

Figure 5-21. Temperature Dependence of Incoloy-800 Tensile Properties

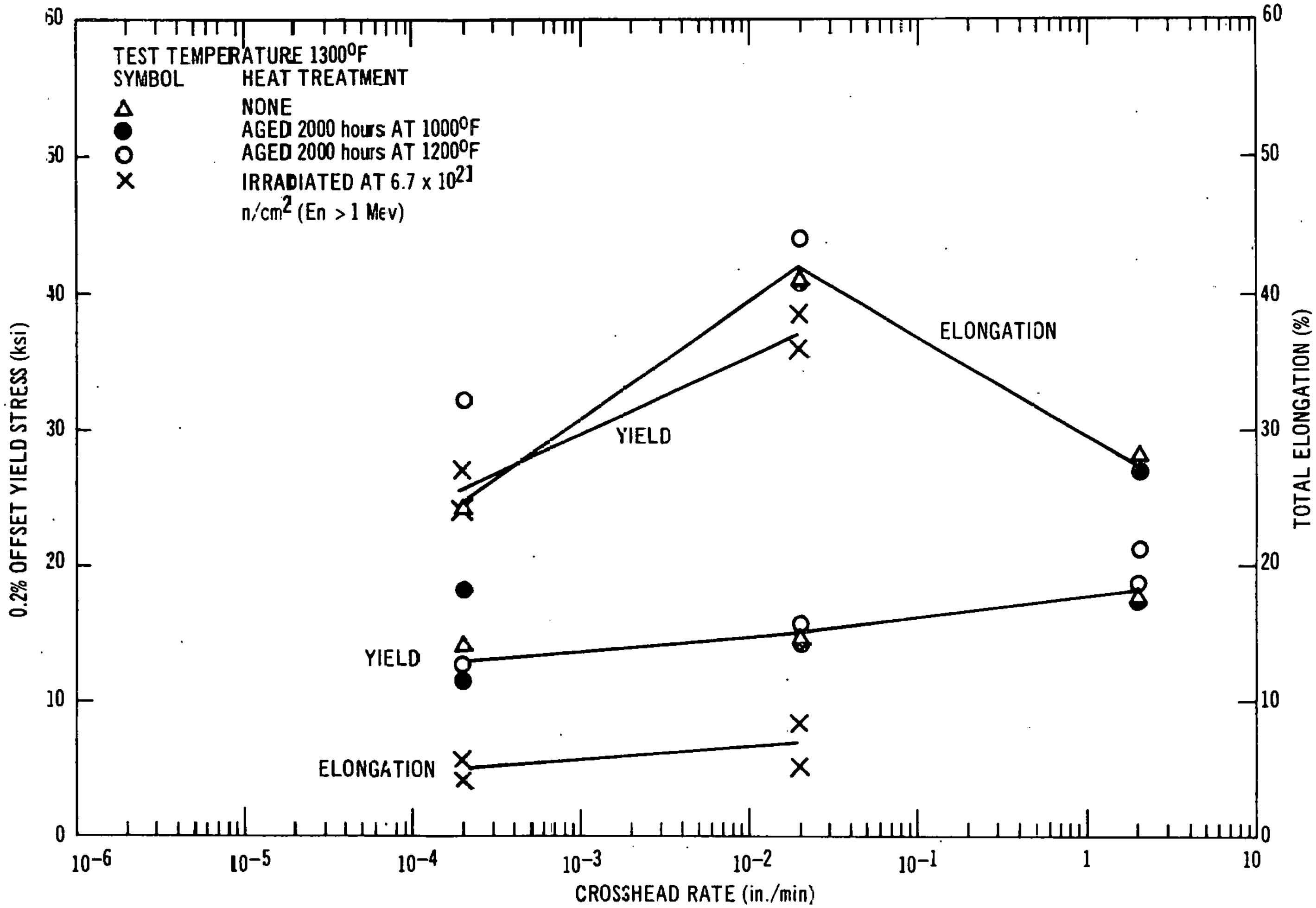

Figure 5-22. Rate Dependence of 1300 °F Tensile Properties for Type 304

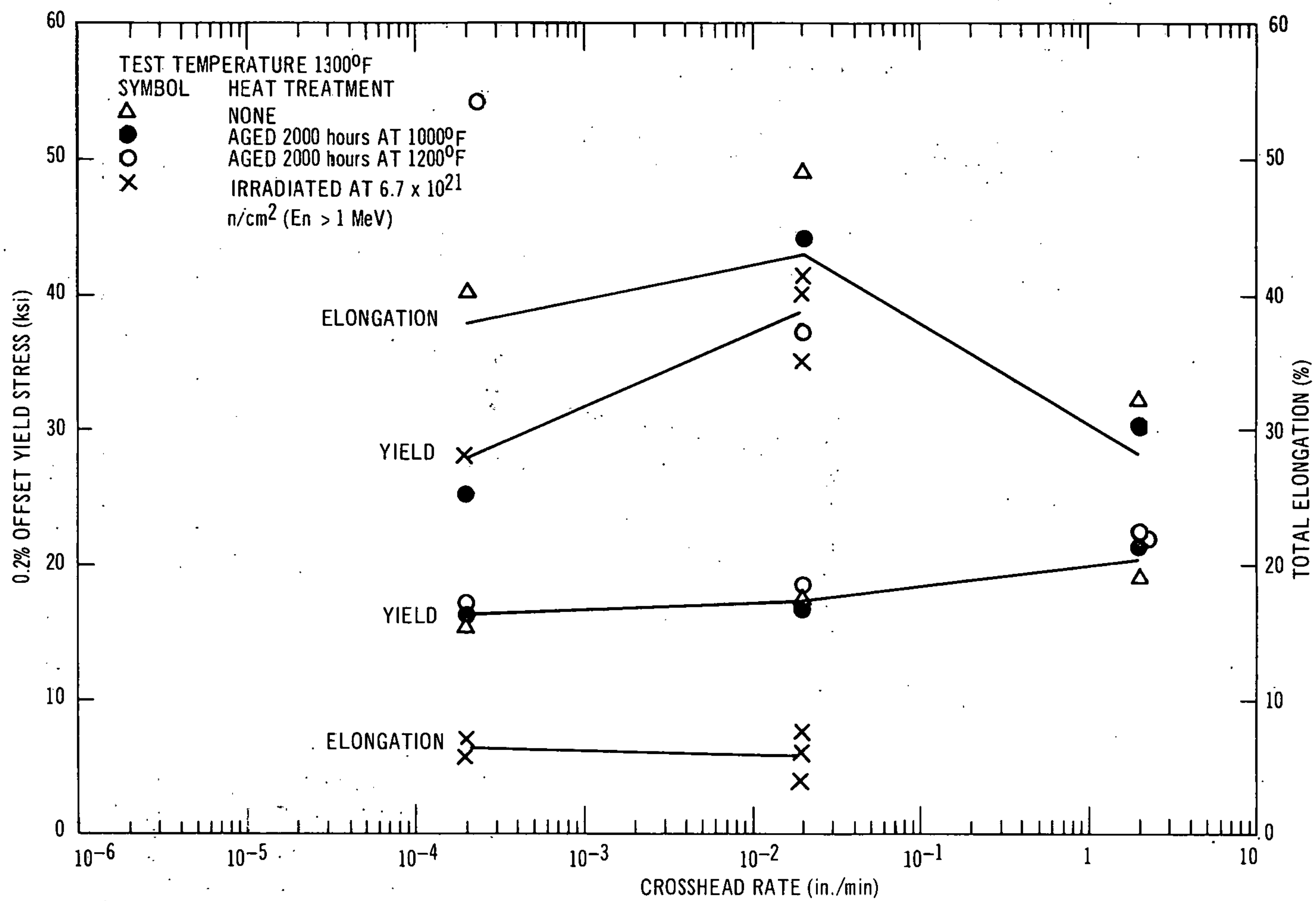

Figure 5-23. Rate Dependence of 1300° F Tensile Properties for Type 316L

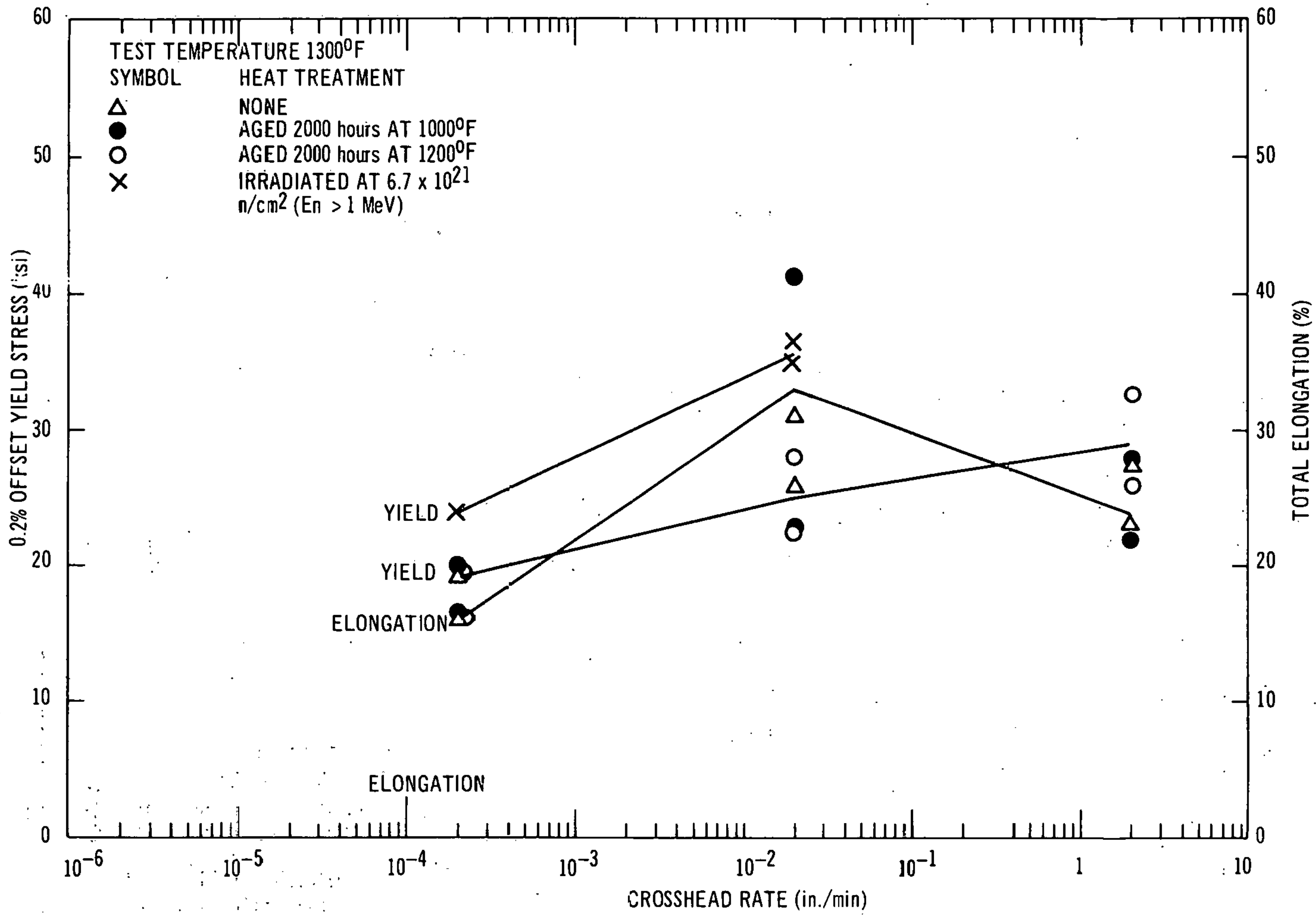

Figure 5-24. Rate Dependence of 1300°F Tensile Properties for Type 321

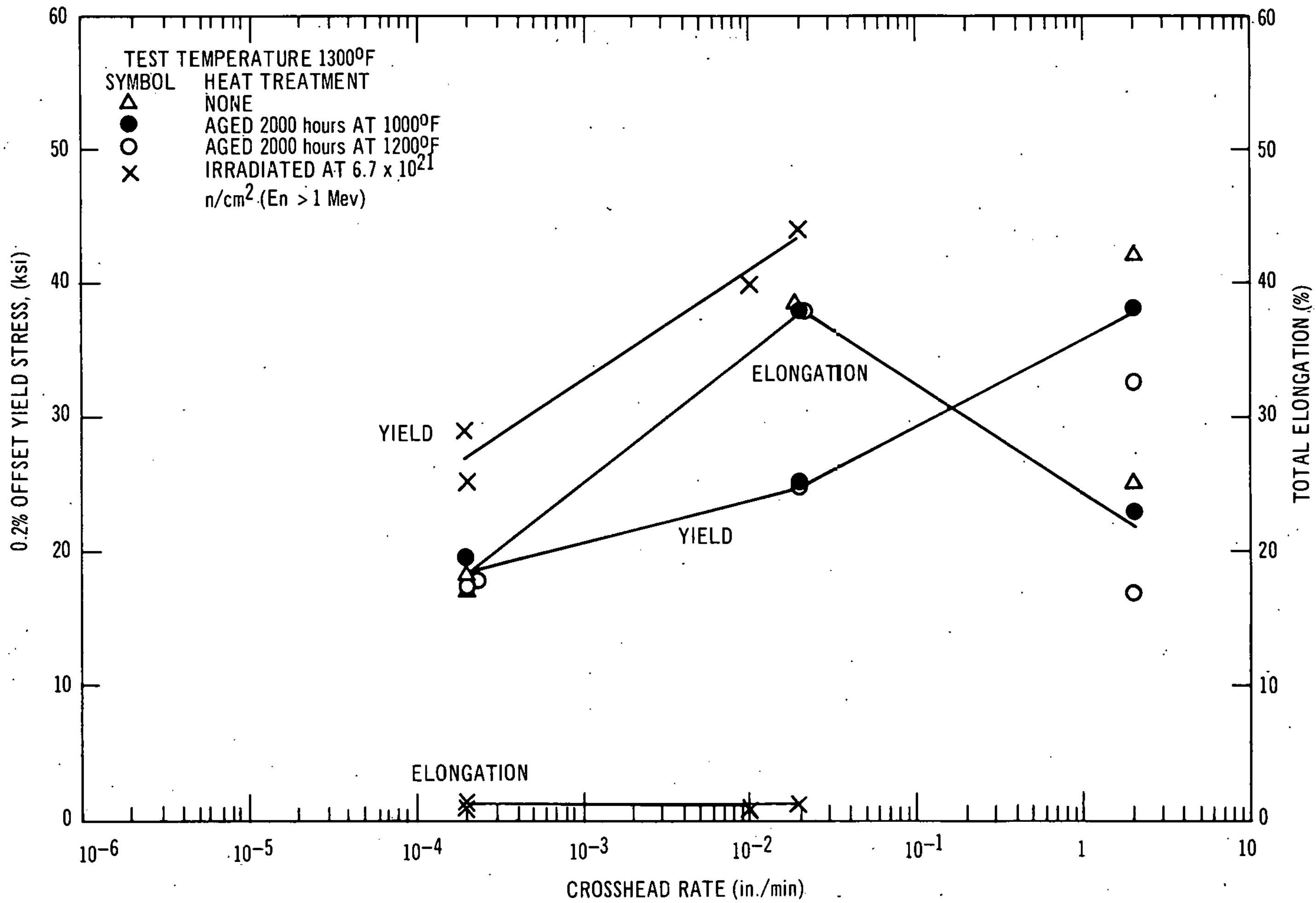

Figure 5-25. Rate Dependence of 1300°F Tensile Properties for Type 347

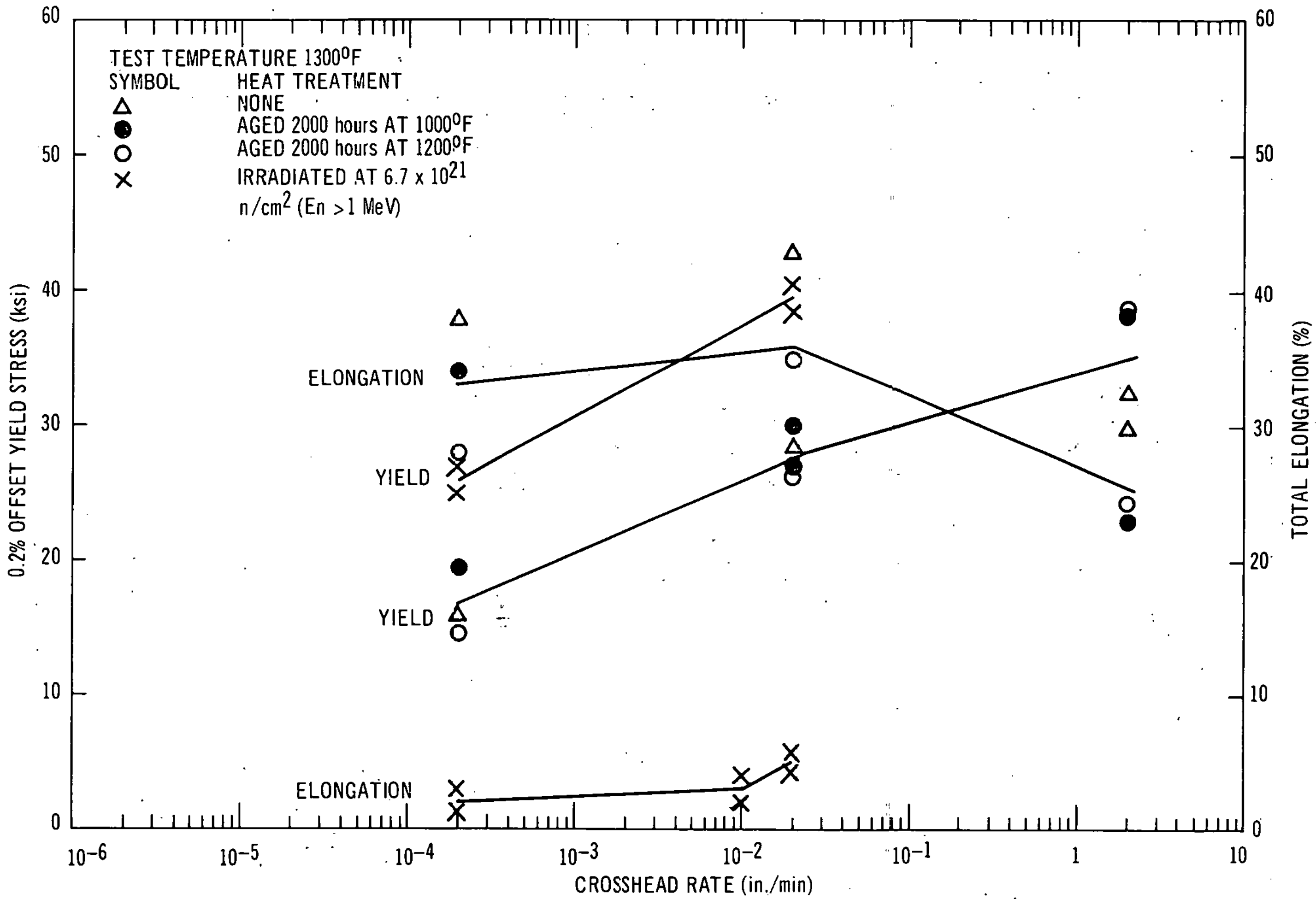

Figure 5-26. Rate Dependence of 1300°F Tensile Properties for Incoloy-800

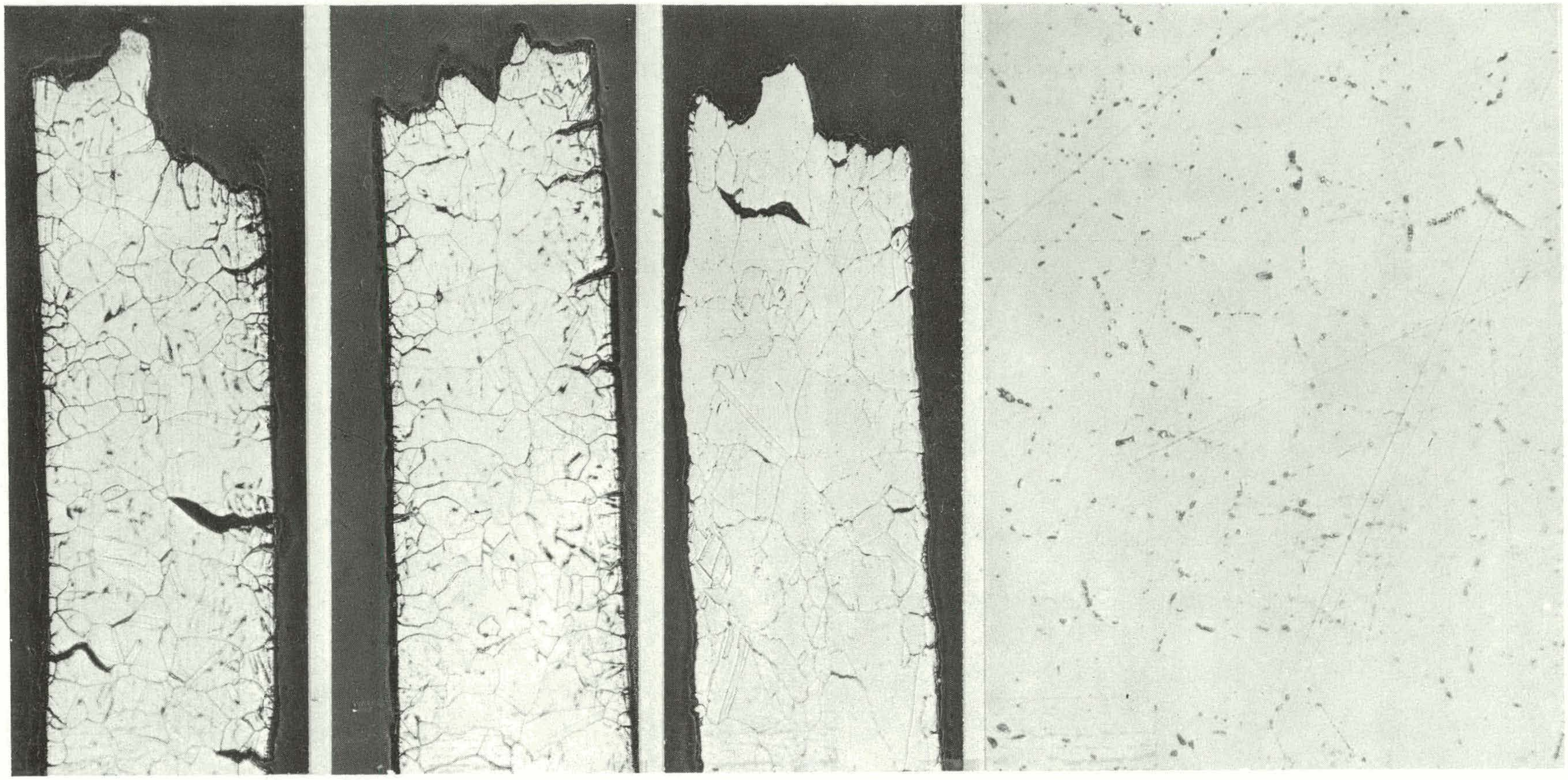

(a) 100X (b) 100X (c) 100X (d) 500X

(a) MILL–ANNEALED STRUCTURE, IRRADIATED TO 6.7×10^{21} n/cm^2 (En > 1 MeV) AND TESTED AT 0.0002 min^{-1}

(b) MILL–ANNEALED STRUCTURE, IRRADIATED TO 6.7×10^{21} n/cm^2 (En > 1 MeV) AND TESTED AT 0.02 min^{-1}

(c) and (d) CARBIDE–AGGLOMERATED STRUCTURE, IRRADIATED TO 3×10^{21} n/cm^2 (En > 1 MeV) AND TESTED AT 0.02 min^{-1}

Figure 5-27. Microstructures of Irradiated Type 304 Tensile Tested at 1300°F

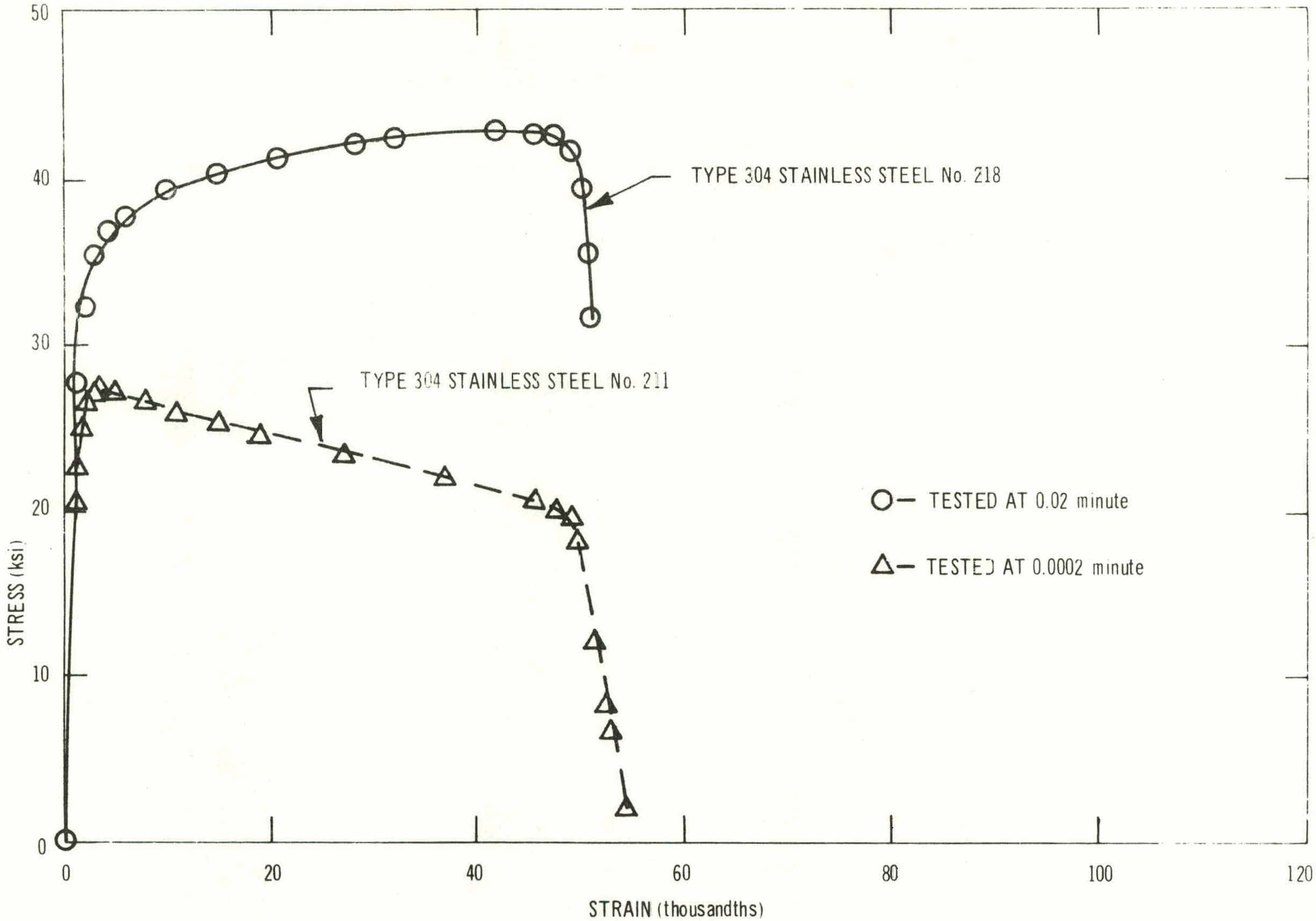

Figure 5-28. Effect of Strain Rate on the 1300°F Flow Curves of Mill-Annealed Type 304, Irradiated at $> 6.2 \times 10^{21}$ ($E_n >$ 1 MeV)

radiation strengthening (as measured by increases in the 0.2% offset yield strength) arises from the interaction of cavities with dislocations (cavities modify the dislocation mobility).

Other transmission electron micrographs show that the gage section of the coupon tested at the strain rate of 0.0002 min^{-1} had a much lower dislocation density than the corresponding high strain rate specimen. However, the total deformation in the sample tested at 0.0002 min^{-1} was much lower than the deformation in the sample tested at 0.02 min^{-1}. Deformation at low strain rates generally occurs in the grain boundaries, leading to incipient grain-boundary cracking, whereas the grains are relatively undeformed.

Chromium-shadowed carbon replicas were made of the optical metallographic surfaces examined previously (Ref. 10). The specimen, which was in a mill-annealed condition prior to irradiation and tested at 0.02 min^{-1}, is shown in Figure 5-30. A continuous carbide network is present in grain boundaries, with short intergranular cracks in some of the surface grain boundaries. No cracks were observed to be greater than one grain deep. Other micrographs show similar carbide precipitation in coherent and incoherent twin boundaries but no crack formation was noted.

Another specimen, in the same pre-irradiated condition but tested at 0.0002 min^{-1}, shows the same general carbide distribution (Figure 5-31) as the more rapidly tested sample. However, because of the slow strain rate during the tensile test, surface cracks were found in every grain boundary. These cracks were much deeper than those observed in Figure 5-30, and often extended for several grains. As previously suggested, the differences in the stress strain curves for Type 304 may be associated with time-dependent propagation of incipient cracks in the slowly-strained sample, whereas localized and rapid propagation of cracks occurred in the sample tested at faster rates.

5.3.2 Properties of Alloys in the Carbide-Agglomerated Condition

The heat-treatment of as-received materials at 1650°F for 24 hours appears to have promise as a method to improve resistance to irradiation damage. The results for Type 304 in this carbide-agglomerated condition (Figure 5-32) suggest that some improvement in fracture strain may be realized at the higher fluence levels when compared with material in the mill-annealed condition. This trend is presently suggested by a singular set of data, and further confirmation is required for statistical significance.

The pre- and post-irradiation optical microstructures shown in Figure 5-33 provide some evidence to explain the differing tensile behavior of mill-annealed versus carbide-agglomerated material. In the mill-annealed condition, the alloy was free of grain boundary carbides before irradiation but had a continuous grain boundary precipitation after irradiation. In the carbide-agglomerated condition, the microstructure consisted of large, discrete, intergranular carbides both before and after irradiation.

Chromium-shadowed carbon replicas were prepared from metallographic surfaces of irradiated tensile coupons and examined by electron microscopy techniques (Figure 5-34). The heat-treated specimen retained the pre-irradiation morphology and distribution of rounded discrete carbides in the grain boundary. These large carbides did not seem to have a detrimental effect on surface crack formation. The annealed material had a nearly continuous network of carbides in grain and twin boundaries, and short surface cracks were found intermittently. Thus, the detailed metallographic examinations shows that agglomerated carbides are retained in Type 304 after irradiation exposure, while the mill-annealed material developed a sensitized microstructure as expected in this temperature range.

The following thoughts are suggested to explain the apparent improvement in irradiation performance of carbide-agglomerated material:

a. As the matrix of the alloy is strengthened through the formation of voids, a greater share of the deformation must be borne by the grain boundaries through sliding. The existence of large, discrete particles in the boundary may act as a key between adjacent grains to reduce or minimize the initiation and growth of wedge-type cracks which normally occur under these circumstances.

b. A heat-treatment of this type has been shown (Ref. 1) to reduce effectively the concentration of undesirable tramp elements at the grain boundaries by providing preferred sites in the structure for the complex carbide. This would effectively increase the surface energy for fracture at the grain boundaries, thereby increasing the minimum shear stress required to initiate a crack, as defined by the Stroh relationship (Ref. 12).

c. The effective removal of supersaturated carbon from the lattice prior to irradiation may have beneficial effects, if the movement of carbon and the kinetics of carbide precipitation are intimately associated with the grain boundary embrittlement phenomenon (helium generation and movement).

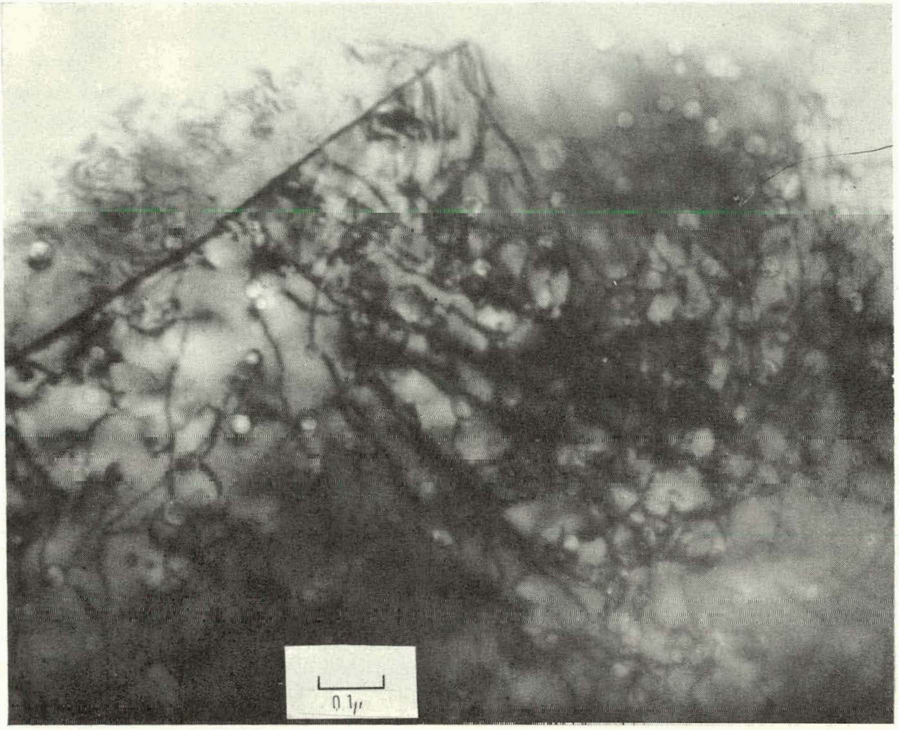

Figure 5-29. Transmission Electron Micrograph from Gage Section of Failed Specimen No. 218 (Mill-Annealed Type 304)

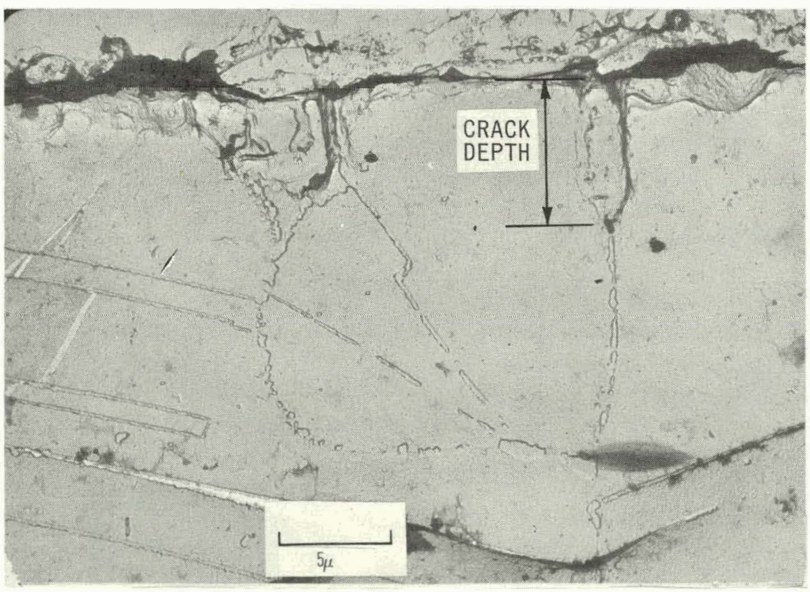

Figure 5-30. Surface Microstructure of Failed Specimen No. 218 (Mill-Annealed Type 304)

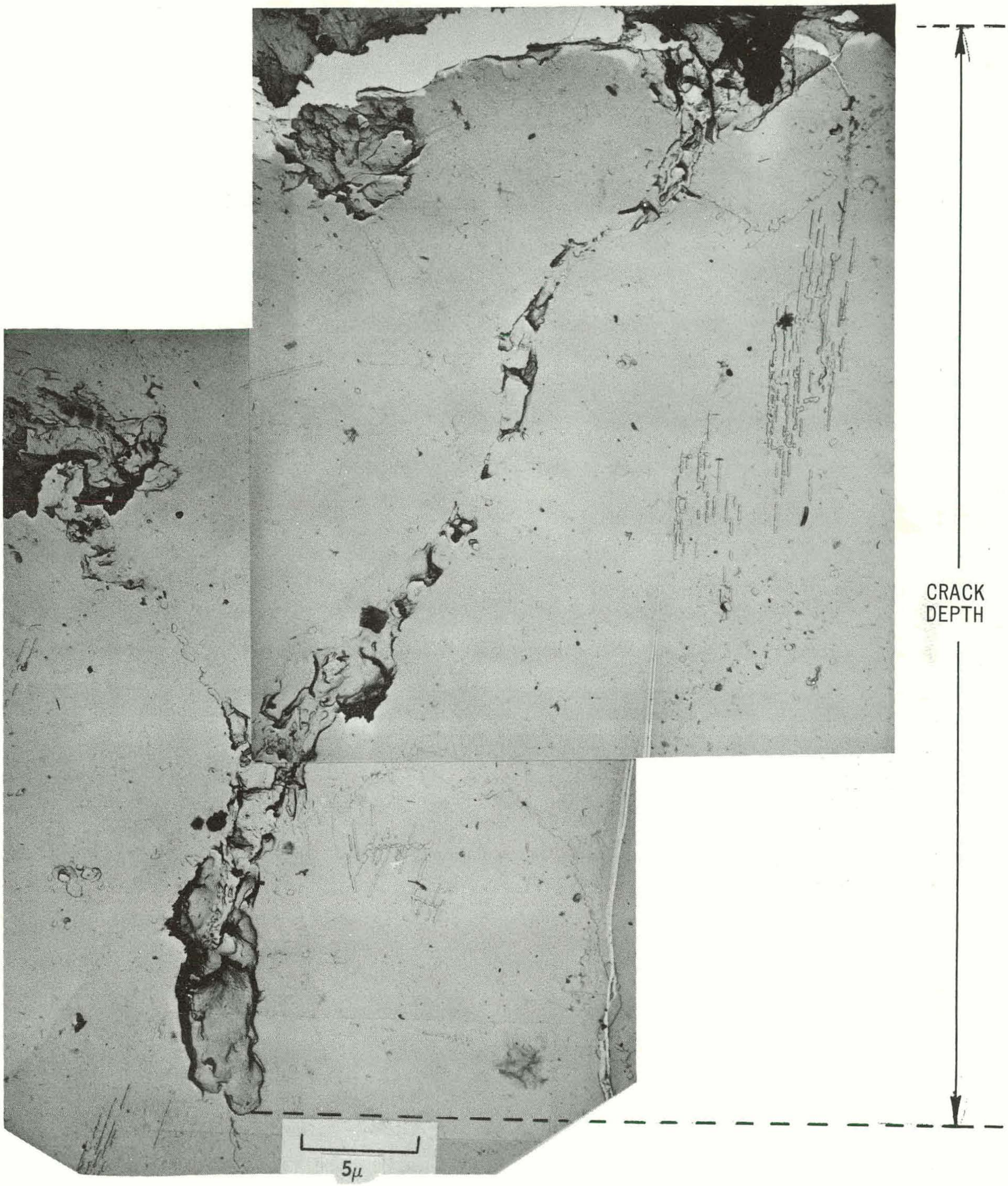

Figure 5-31. Surface Microstructure of Failed Specimen No. 211 (Mill-Annealed Type 304)

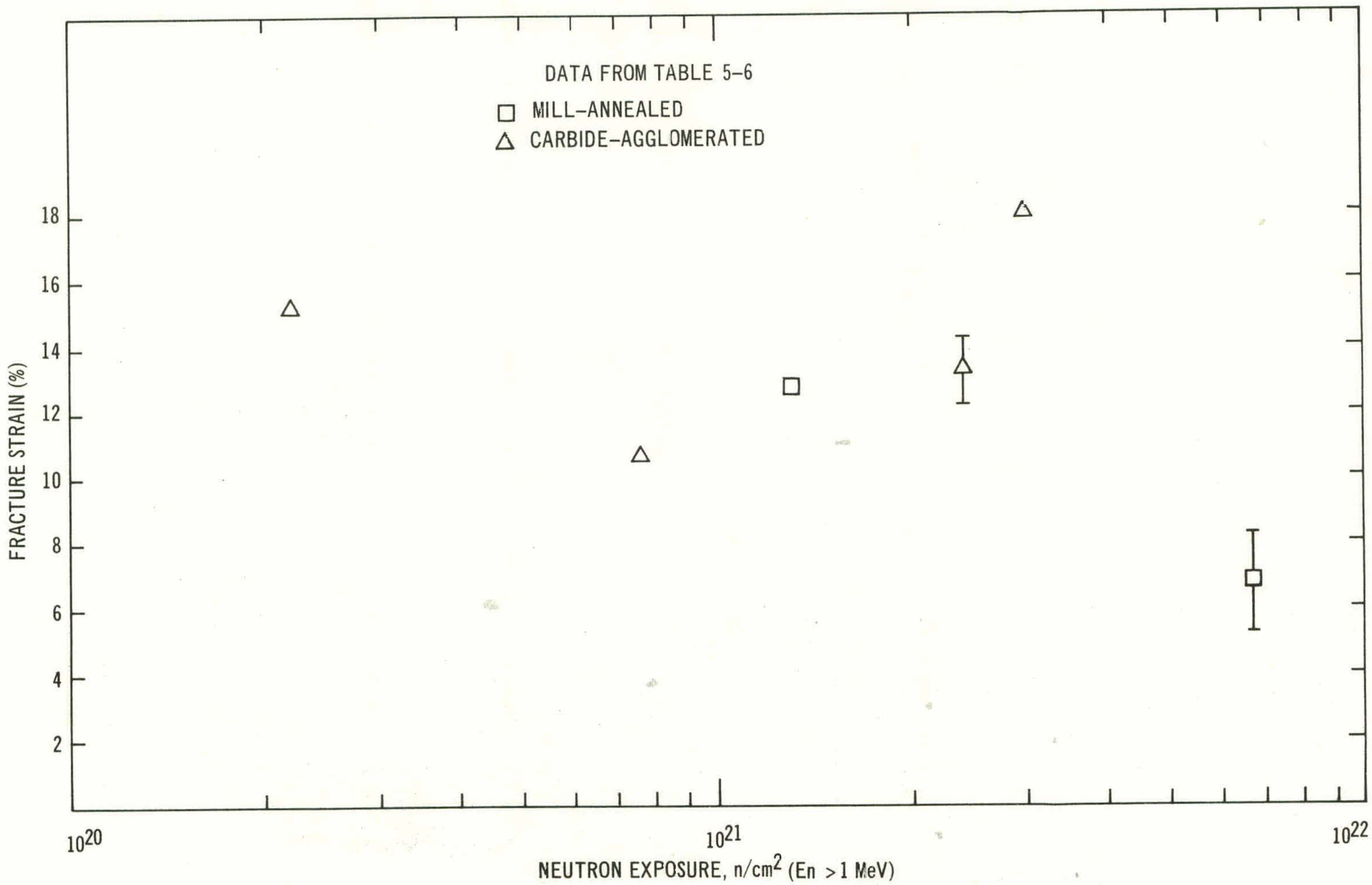

Figure 5-32. Post-Irradiation Strain Properties of Type 304 at 1300°F versus Fluence

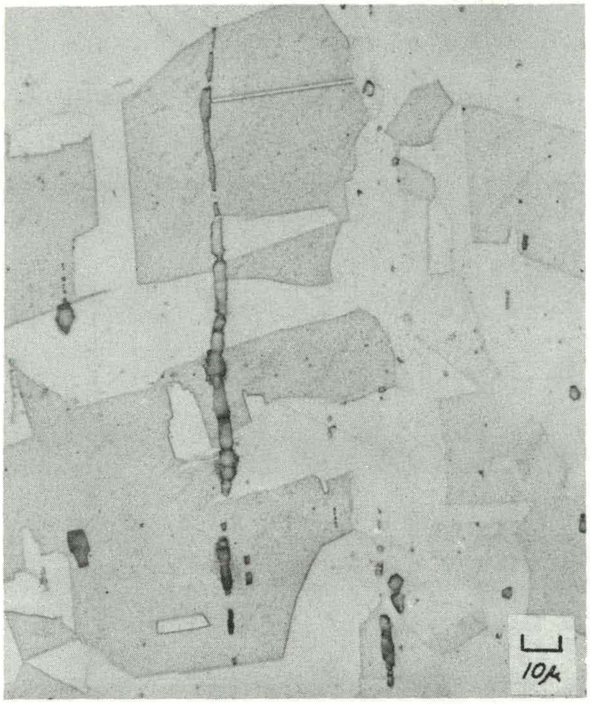

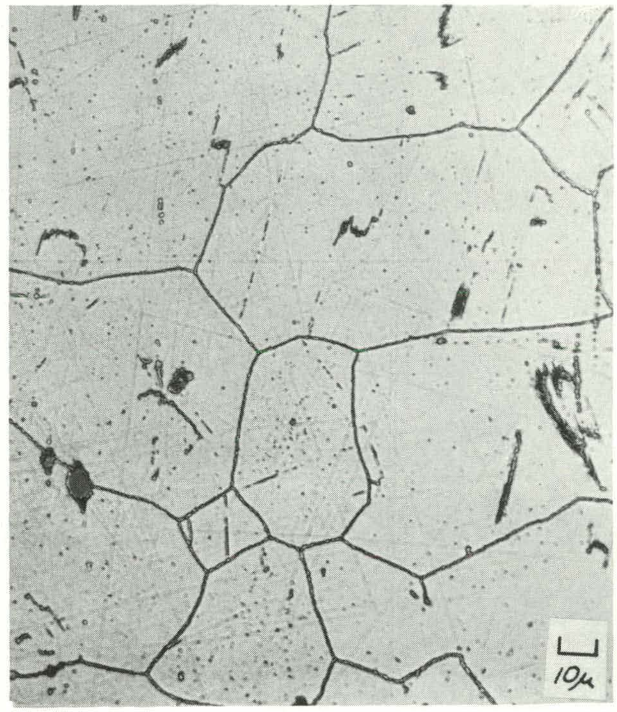

UNIRRADIATED (a) IRRADIATED

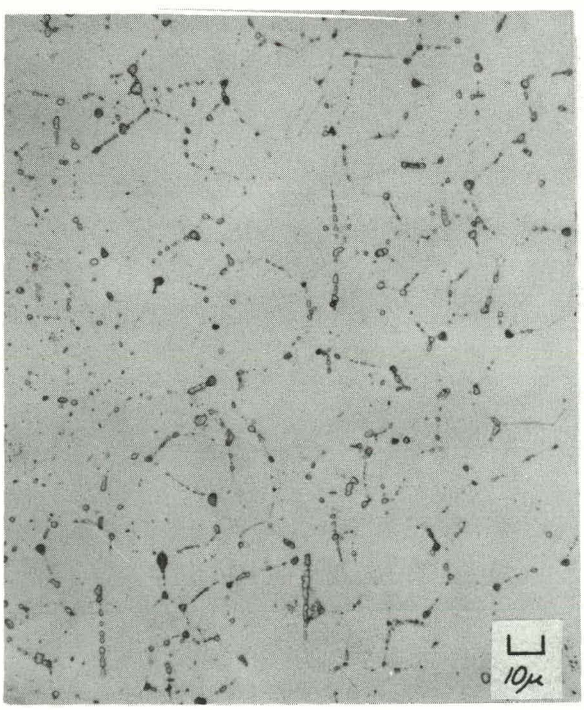

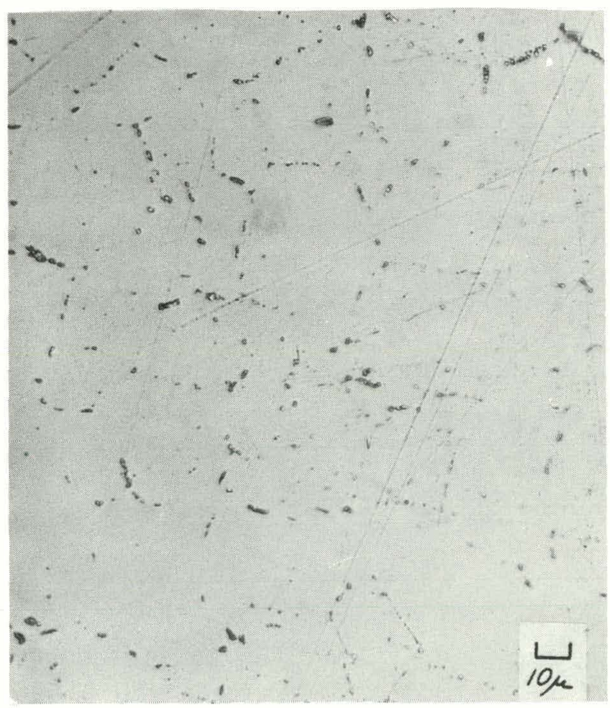

UNIRRADIATED (b) IRRADIATED

Figure 5-33. Comparison of Microstructure for (a) Mill-Annealed, and (b) Carbide-Agglomerated Type 304 in both Unirradiated and Irradiated Conditions

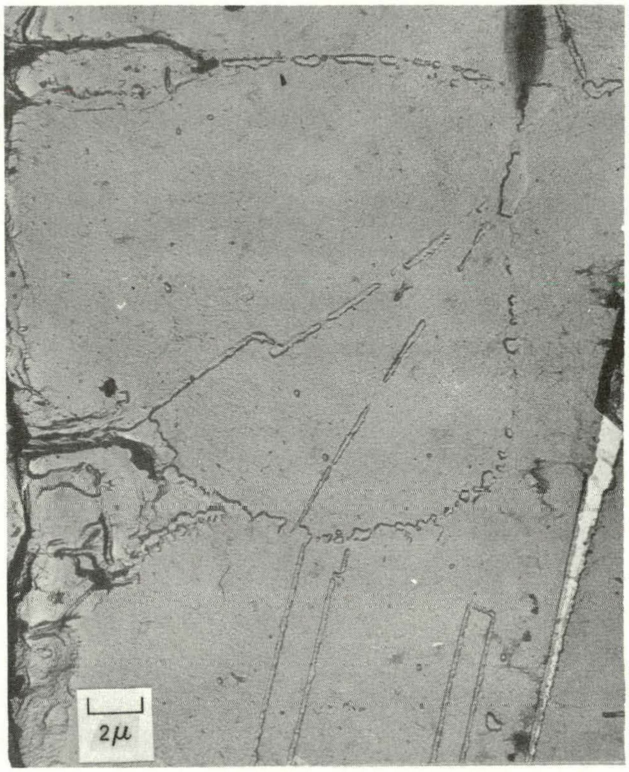

(a)

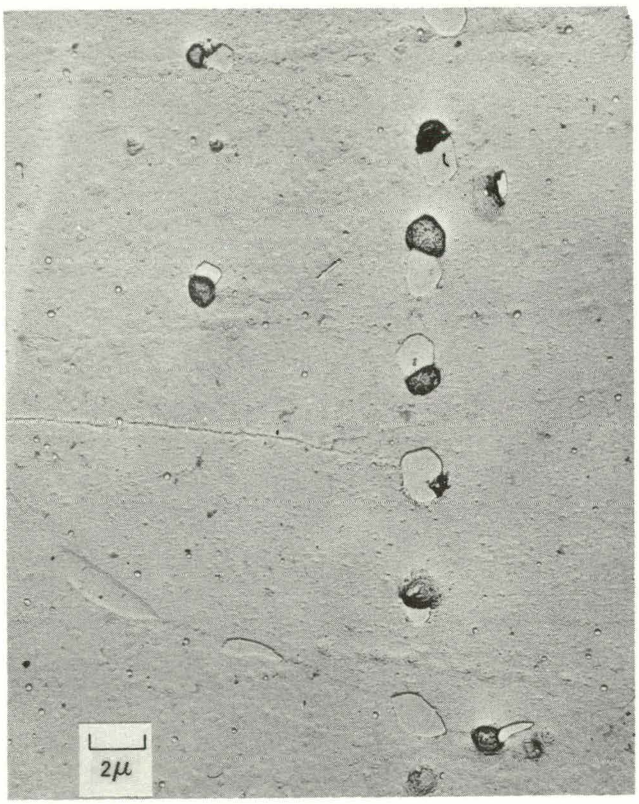

(b)

Figure 5-34. Replica Electron Micrographs of (a) Annealed, and (b) Carbide-Agglomerated Type 304 Irradiated in EBR-II

APPENDIX

To establish base mechanical properties from which the effects of irradiation could be determined, control samples were given thermal treatments out-of-reactor to establish the effect of temperature exposure. The results of these studies are listed in the following table, for each of the alloys in the program.

TENSILE PROPERTIES OF MILL-ANNEALED AUSTENITIC STAINLESS STEEL BEFORE AND AFTER THERMAL EXPOSURE

Alloy	Heat Treatment	Test Temperature (°F)	Crosshead Rate (min^{-1})	0.2% Yield Stress (ksi)	Ultimate Stress (ksi)	Total* Elongation (%)
Type 304	Mill-Annealed (+800°F for 15 min)	75	0.02	33.3	86.8	57
		900	0.02	18.6	65.9	28
		1100	0.02	–	53.0	37
		1300	2.0	17.9	43.3	28
		1300	0.02	14.6	31.1	41
		1300	0.0002	14.0	17.5	24
		1500	0.02	14.1	18.2	37
	Mill-Annealed and Aged 1000°F for 2000 h	75	0.02	30.3	84.6	58
		900	0.02	14.2	56.6	28
		1100	0.02	13.1	50.2	30
		1300	2.0	17.5	40.7	27
		1300	0.02	13.8	29.5	41
		1300	0.0002	11.5	20.2	18
		1500	0.02	11.5	17.3	38
	Mill-Annealed and Aged 1200°F for 2000 h	75	0.02	39.0	87.6	48
		900	0.02	20.9	65.3	28
		1100	0.02	15.5	47.8	27
		1300	2.0	18.6	37.9	21
		1300	0.02	15.8	30.9	44
		1300	0.0002	12.8	19.6	32
		1500	0.02	11.8	17.8	41
Type 316	Mill-Annealed (+800°F for 15 min)	75	0.02	33.9	80.0	56
		900	0.02	21.7	75.7	34
		1100	0.02	26.4	57.2	45
		1300	2.0	18.4	47.0	32
		1300	0.02	17.7	38.7	49
		1300	0.0002	15.3	24.4	40
		1500	0.02	18.0	23.5	60
	Mill-Annealed and Aged 1000°F for 2000 h	75	0.02	36.3	87.3	45
		900	0.02	21.2	74.0	–
		1100	0.02	17.2	61.6	37
		1300	2.0	21.1	49.1	30
		1300	0.02	16.5	38.2	44
		1300	0.0002	16.3	27.0	25
		1500	0.02	15.3	23.0	52

TENSILE PROPERTIES OF MILL-ANNEALED AUSTENITIC STAINLESS STEEL BEFORE AND AFTER THERMAL EXPOSURE

Alloy	Heat Treatment	Test Temperature (°F)	Crosshead Rate (min^{-1})	0.2% Yield Stress (ksi)	Ultimate Stress (ksi)	Total* Elongation (%)
	Mill-Annealed and Aged 1200°F for 2000 h	75	0.02	36.3	84.9	38
		900	0.02	23.6	70.8	24
		1100	0.02	19.1	55.8	24
		1300	2.0	22.6	47.2	22
		1300	0.02	18.5	38.6	37
		1300	0.0002	17.2	23.6	54
		1500	0.02	15.1	23.2	34
Type 321	Mill-Annealed (+800°F for 15 min)	75	0.02	34.4	79.0	59
		900	0.02	18.6	65.8	28
		1100	0.02	35.6	51.5	28
		1300	2.0	27.2	40.3	23
		1300	0.02	26.5	32.2	31
		1300	0.0002	19.4	23.6	16
		1500	0.02	13.2	16.2	32
	Mill-Annealed and Aged 1000°F for 2000 h	75	0.02	40.4	85.5	48
		900	0.02	26.6	55.5	24
		1100	0.02	23.3	47.1	29
		1300	2.0	27.3	41.6	22
		1300	0.02	23.6	33.0	41
		1300	0.0002	18.3	20.9	17
		1500	0.02	17.3	19.1	39
	Mill-Annealed and Aged 1200°F for 2000 h	75	0.02	39.7	84.2	38
		900	0.02	34.6	60.5	20
		1100	0.02	27.6	47.1	24
		1300	2.0	32.3	40.4	26
		1300	0.02	22.5	30.8	28
		1300	0.0002	19.1	20.2	16
		1500	0.02	15.5	17.8	40
Type 347	Mill-Annealed (+800°F for 15 min)	75	0.02	30.3	80.2	40
		900	0.02		67.5	20
		1100	0.02	23.5	46.2	26
		1300	2.0	42.2	44.6	25
		1300	0.02		36.1	38
		1300	0.0002	18.1	26.1	17
		1500	0.02	16.4	18.8	45

TENSILE PROPERTIES OF MILL-ANNEALED AUSTENITIC STAINLESS STEEL BEFORE AND AFTER THERMAL EXPOSURE

Alloy	Heat Treatment	Test Temperature (°F)	Crosshead Rate (min^{-1})	0.2% Yield Stress (ksi)	Ultimate Stress (ksi)	Total* Elongation (%)
	Mill-Annealed and Aged 1000°F for 2000 h	75	0.02	44.4	106.3	42
		900	0.02	29.0	66.0	19
		1100	0.02	29.3	59.5	20
		1300	2.0	38.1	55.7	23
		1300	0.02	25.0	39.1	38
		1300	0.0002	19.3	20.2	34
		1500	0.02	16.7	19.9	34
	Mill-Annealed and Aged 1200°F for 2000 h	75	0.02	41.1	111.5	36
		900	0.02	27.9	64.5	20
		1100	0.02	25.2	57.2	19
		1300	2.0	32.7	48.8	17
		1300	0.02	24.6	35.7	38
		1300	0.0002	17.5	23.6	18
		1500	0.02	17.2	23.6	50
Incoloy-800	Mill-Annealed (+800°F for 15 min)	75	0.02	53.2	92.9	27
		900	0.02	30.0	78.2	26
		1100	0.02	44.8	64.1	27
		1300	2.0	32.6	51.7	30
		1300	0.02	28.6	37.8	43
		1300	0.0002	16.0	18.4	38
		1500	0.02	18.2	21.4	47
	Mill-Annealed and Aged 1000°F for 2000 h	75	0.02	49.8	103.5	24
		900	0.02	47.2	82.2	18
		1100	0.02	46.5	71.1	22
		1300	2.0	38.1	55.7	23
		1300	0.02	27.0	39.6	30
		1300	0.0002	19.3	20.2	34
		1500	0.02	18.7	20.9	46
	Mill-Annealed and Aged 1200°F for 2000 h	75	0.02			
		900	0.02	27.9	64.5	20
		1100	0.02	25.2	57.2	19
		1300	2.0	38.8	52.1	24
		1300	0.02	26.2	37.4	35
		1300	0.0002	14.8	21.2	28
		1500	0.02	17.2	23.6	50

* Original Gage Length - 1 inch.

REFERENCES

1. Holmes, J. J., Robbins, R. E., Brimhall, J. L., and Mastel, B., "Elevated Temperature Irradiation Hardening in Austenitic Stainless Steel," *Acta Met.*, 7, 16 (July 1968) 955.
2. Stiegler, J. O., Bloom, E. E., and Weir, J. R., "Electron Microscopy of Irradiated EBR-II Fuel Cladding," *Trans. ANS*, 1, 11 (June 1968) 146.
3. Cawthorne, C., and Fulton, E. J., *Nature*, 216 (November 11, 1967) 575.
4. Brager, H., and Robbins, R. E., "Stabilized Cavities in Irradiated Austenitic Stainless Steel," BNWL-SA-1701 (February 1968).
5. Rossin, A. D., "Dosimetry for Radiation Damage Studies," ANL-6828 (March 1964).
6. Withop, A., Hutchins, B. A., and Martin, G. C., "Analytical Procedures and Application of Fluence Determinations from EBR-II Flux Wires," GEAP-5744, (March 1969).
7. Holmes, J. J., and Irvin, J. E., *Trans. ANS*, **10**, 2 (1967).
8. Kittel, J. H., BNWL-609, December 1967.
9. Murphy, W. F., and Strohm, H. E. *Nuclear Applications*, **4**, 4, 1968.
10. "Sodium-Cooled Reactor, Fast Ceramic Reactor Development Program, Task L, May–July 1968," GEAP-5677.
11. "Sodium-Cooled Reactor, Fast Ceramic Reactor Development Program, Task L, August–October 1968," GEAP-5700.
12. Stroh, A. N., *Proc. Royal Society, Ser A*, **223**, (1954) 404.

ACKNOWLEDGMENTS

The following individuals have made significant contributions to this report and are accorded special recognition: R. E. Smith and D. S. Vash of Vallecitos Nuclear Center (VNC), for optical metallography and mechanical testing of irradiated materials; U. E. Wolff of VNC, for electron microscopy; W. J. Wagner and A. Montes, for optical metallography of unirradiated alloys; D. H. Frisby, for mechanical testing of unirradiated materials; and H. Saethre, for heat-transfer analysis. In addition, the constructive review of this report by C. N. Spalaris, and the contribution of N. I. Brown toward computations and graphical analysis, are gratefully acknowledged.

DISTRIBUTION LIST

Director, Contracts Division — 2
U. S. Atomic Energy Commission
San Francisco Operations Office
2111 Bancroft Way
Berkeley, California 94704

Chief, California Patent Group — 1
U. S. Atomic Energy Commission
San Francisco Operations Office
P. O. Box 808
Livermore, California 94551

Division of Reactor Development and Technology — 2
U. S. Atomic Energy Commission
Washington, D. C. 20545
Attn: Asst. Director for Reactor Engineering

Division of Reactor Development and Technology — 1
U. S. Atomic Energy Commission
Washington, D. C. 20545
Attn: M. J. Whitman
Asst. Director for Program Analysis

Division of Reactor Development and Technology — 3
U. S. Atomic Energy Commission
Washington, D. C. 20545
Attn: A. Giambusso
Asst. Director for Project Mgmt
(Attn: R. Sweek, G. Wensch, J. Morabito)

Division of Reactor Development and Technology — 1
U. S. Atomic Energy Commission
Washington, D. C. 20545
Attn: J. A. Lieberman
Asst. Director for Nuclear Safety

DISTRIBUTION LIST (Continued)

Division of Reactor Development and Technology U. S. Atomic Energy Commission Washington, D. C. 20545 Attn: J. A. Lieberman Asst. Director for Nuclear Safety	1
Division of Reactor Development and Technology U.S. Atomic Energy Commission Washington, D. C. 20545 Attn: J. W. Crawford Asst. Director for Plant Engineering	1
Division of Reactor Development and Technology U.S. Atomic Energy Commission Washington, D. C. 20545 Attn: R. H. Steel Division of Naval Reactors	1
Division of Reactor Development and Technology U.S. Atomic Energy Commission Washington, D. C. 20545 Attn: E. E. Sinclair Asst. Director for Reactor Tech. (Attn: J. M. Simmons; I. Zartman)	2
RDT Site Office U.S. Atomic Energy Commission c/o General Electric Company 310 DeGuigne Drive Sunnyvale, California Attn: J. V. Levy	2
LMFBR Program Office Argonne National Laboratory 9800 South Cass Avenue Argonne, Illinois 60439 Attn: A. Amorosi, Director	1
LMFBR Program Office Argonne National Laboratory 9800 South Cass Avenue Argonne, Illinois 60439 Attn: L. R. Kelman	1
Atomics International P.O. Box 309 Canoga Park, California 91304 Attn: S. Golan	2
Director Liquid Metals Information Center P. O. Box 309 Canoga Park, California 91305	2
The Babcock & Wilcox Company Atomic Energy Division Lynchburg, Virginia 24501 Attn: M. W. Croft	2
Mr. L. W. Fromm, Manager 1000 MWe LMFBR Follow-On Study Project Building 208 Argonne National Laboratory 9800 South Cass Avenue Argonne, Illinois 60439	2
Mr. C. A. Anderson, Project Mgr 1000 MWe LMFBR Follow-On Study Westinghouse Electric Corporation Advanced Reactors Division Waltz Mill Site P. O. Box 158 Madison, Pennsylvania 15663	2
FFTF Project P. O. Box 220 Richland, Washington 99352 Attn: Configuration & Data Management	8
W. P. Staker, Project Manager 1000 MWe LMFBR Follow-On Study Combustion Engineering, Inc. P. O. Box 500 Windsor, Connecticut 06095	2
RDT Senior Site Representative Canoga Park Area Office P. O. Box 2325 San Diego, California 92112	1
RDT Senior Site Representative Canoga Park Area Office P. O. Box 591 Canoga Park, California 91305	1
RDT Senior Site Representative U.S. Atomic Energy Commission Argonne National Laboratory 9800 South Cass Avenue Argonne, Illinois 60439	1

DISTRIBUTION LIST (Continued)

RDT Site Office — 1
U.S. Atomic Energy Commission
Atomic Power Development Associates, Inc.
1911 First Street
Detroit, Michigan 48226

RDT Senior Site Representative — 1
Oak Ridge National Laboratory
P. O. Box X
Oak Ridge, Tennessee 37830

The Babcock & Wilcox Company — 1
Atomic Energy Division
Lynchburg, Virginia 24501
Attn: S. H. Esleeck

RDT Senior Site Representative — 1
U.S. Atomic Energy Commission
P. O. Box 550
Richland, Washington 99352

RDT Site Representative — 1
U.S. Atomic Energy Commission
Post Office Box 2108
Idaho Falls, Idaho 83401

RDT Site Representative — 1
U.S. Atomic Energy Commission
United Nuclear Corporation
Grasslands Road
Elmsford, New York 10523
Attn: M. Napack

RDT Site Representative — 1
U.S. Atomic Energy Commission
United Nuclear Corporation
Grasslands Road
Elmsford, New York 10523
Attn: A Strasser

Argonne National Laboratory — 3
9800 South Cass Avenue
Argonne, Illinois 60439
Attn: J. H. Kittel

Argonne National Laboratory — 1
9800 South Cass Avenue
Argonne, Illinois 60439
Attn: R. C. Vogel

Pacific Northwest Laboratory — 1
P. O. Box 999
Richland, Washington 99352
Attn: E. A. Eschbach

Pacific Northwest Laboratory — 2
P.O. Box 999
Richland, Washington 99352
Attn: E. A. Evans

University of California — 1
Lawrence Radiation Laboratory
P. O. Box 808
Livermore, California 94551
Attn: A. Rothman

Los Alamos Scientific Laboratory — 1
P. O. Box 1663
Los Alamos, New Mexico 87544
Attn: R. D. Baker

Los Alamos Scientific Laboratory — 1
P. O. Box 1663
Los Alamos, New Mexico 87544
Attn: D. B. Hall

Los Alamos Scientific Laboratory — 1
P. O. Box 1663
Los Alamos, New Mexico 87544
Attn: J. C. Clifford

Scientific Laboratory — 1
P. O. Box 1663
Los Alamos, New Mexico 87544
Attn: Reports Librarian

Westinghouse Electric Corporation — 1
Bettis Atomic Power Laboratory
P. O. Box 79
West Mifflin, Pennsylvania
Attn: E. J. Kreh

Oak Ridge National Laboratory — 1
P. O. Box X
Oak Ridge, Tennessee 37830
Attn: J. E. Cunningham

Brookhaven National Laboratory — 1
Upton, New York 11973
Attn: O. E. Dwyer

DISTRIBUTION LIST (Continued)

Battelle Memorial Institute
Columbus Laboratories
505 King Avenue
Columbus, Ohio 43201
Attn: D. Keller — 1

Atomics International
P. O. Box 309
Canoga Park, California 91304
Attn: H. Pearlman — 1

Atomics International
P. O. Box 309
Canoga Park, California 91304
Attn: FBR Project Manager
(R. J. Beeley) — 1

Dow Chemical Company
Rock Flats Division
P. O. Box 888
Golden, Colorado 80401
Attn: R. D. Forest — 1

Scientific Representative
U.S. Atomic Energy Commission
American Embassy
APO San Francisco 96503 — 1

U.S. AEC Scientific Representative
United States Embassy
Paris, France
APO New York 09777 — 1

Senior U.S. AEC Representative
U.S. Mission to the European Communities
United States Embassy
Brussels, Belgium — 1

Division of Technical Information Ext.
U.S. Atomic Energy Commission
P. O. Box 62
Oak Ridge, Tennessee 37831 — 50

Dr. John C. Woodhouse
1 Guest Lane
Wilmington, Delaware 19809 — 1

Power Reactor Development Corp.
1911 First Street
Detroit, Michigan 48226
Attn: W. J. McCarthy — 1

Argonne National Laboratory
Idaho Division
P. O. Box 1096
Idaho Falls, Idaho 83401
Attn: F. W. Thalgott — 1

Detroit Edison Company
1911 First Street
Detroit, Michigan 48226
Attn: A. S. Griswold — 1

Atomic Power Development Associates
1911 First Street
Detroit, Michigan 48226
Attn: A. A. Shoudy — 1

Combustion Engineering, Inc.
Nuclear Division
Prospect Hill Road
Windsor, Connecticut 06095
Attn: W. P. Chernock — 1

The Babcock & Wilcox Company
Atomic Energy Division
Lynchburg, Virginia 24501
Attn: H. S. Barringer — 1

General Atomic
P. O. Box 608
San Diego, California 92112
Attn: D. B. Coburn — 1

The Babcock & Wilcox Company
Alliance Research Center
Alliance, Ohio 44601
Attn: D. Koch — 1

Westinghouse Electric Corporation
Advance Reactors Division
P. O. Box 217
Cheswick, Pennsylvania 15024
Attn: W. E. Ray — 1

Nuclear Materials & Equipment Corp.
Plutonium Laboratory
Leechburg, Pennsylvania 15656
Attn: William J. Ross — 1

U. S. AEC Scientific Representative
United States Embassy
London, England — 1

DISTRIBUTION LIST (Continued)

S. F. Stachura
Villa Plein Ciel
Quartier Roussier
Aix-en-Provence
13 - France 1

S. Visner
Nuclear Division
Combustion Engineering, Inc.
P. O. Box 500
Windsor, Connecticut 06095 2

W. B. Cottrell, Director
Nuclear Safety Program
Oak Ridge National Laboratory
P. O. Box Y
Oak Ridge, Tennessee 37830 1